THEORETICAL STUDIES OF BOUND EXCITON DECAY

AND OF TRANSPORT ACROSS SEMICONDUCTOR INTERFACES

Thesis by

Gordon C. Osbourn

In Partial Fulfillment of the Requirements

for the Degree of

Doctor of Philosophy

California Institute of Technology

Pasadena, California

1979

(submitted May 7, 1979)

To my Parents

ACKNOWLEDGEMENTS

I would like to express my appreciation and thanks to Dr. Darryl L. Smith and Dr. Thomas C. McGill for their valuable guidance and assistance. I have profited greatly from their encouragement and advice.

I had many useful discussions with Dr. M. Chen, K. R. Elliott, Dr. S. A. Lyon, Dr. D. S. Pan, and J. N. Schulman. I would also like to thank Y. C. Chang, M. Daw, A. Hoffmeister, A. Hunter, R. James, and G. Mitchard for providing a stimulating research environment. I am indebted to V. Snell for providing friendly assistance and for typing this thesis.

I am thankful for financial support received from the California Institute of Technology, the Schlumberger Co., and the Department of the Air Force.

Finally, I would like to express my deepest appreciation to my wife Pat for her constant support and encouragement.

ABSTRACT

This thesis presents theoretical studies of three topics in solid state physics. Chapters 2 and 3 are concerned with the Auger and radiative decay properties of excitons bound to acceptors in indirect and direct band semiconductors, respectively. Chapter 4 deals with the transport properties of carriers across semiconductor heterojunctions. Chapter 5 treats the effect of a heterojunction on carrier impact ionization (the inverse of a free carrier Auger process).

In Chapter 2, we present calculations of the phononless Auger and radiative transition rates for excitons bound to the four common shallow acceptors (B, Al, Ga and In) in Si and Ge. The calculated Auger rates for the bound excitons in Si vary significantly for the different acceptors, increasing rapidly as the acceptor binding energy increases. This is in agreement with the rapid decrease with increasing acceptor binding energy of measured acceptor bound exciton lifetimes in Si. Numerically, the calculated Auger rates are within about a factor of three of the measured recombination rates for the different acceptors. The dependence of the Auger rates on acceptor binding energy is due to an increased spreading in momentum space of the bound exciton wavefunction. In Ge, the calculated Auger rates are orders of magnitude less than the measured free exciton recombination rate in undoped Ge, suggesting that the phononless Auger

transition is not important for acceptor bound excitons in Ge. This is consistent with the experimental observation that light doping with shallow acceptors has little effect on the lifetimes of photo-excited carriers at low temperatures in Ge; whereas, in Si the carrier lifetimes can be decreased by orders of magnitude. The principle difference between Si and Ge is that the acceptor binding energies are much greater in Si than they are in Ge. The calculation of radiative transition rates is compared to estimates obtained from absorption experiments. Results of the calculation agree with experiment to within a factor of two.

In Chapter 3, we present calculations of the Auger and radiative recombination rates for acceptor bound excitons in the HgCdTe alloy system and in GaAs. The transition rates are computed as a function of band gap in the HgCdTe alloy and as a function of the acceptor binding energy. The Auger rate is found to increase and the radiative rate to decrease with increasing acceptor binding energy. The radiative recombination rate is found to increase with increasing band gap. The Auger rate decreases with increasing band gap except: when the band gap first exceeds the spin-orbit splitting in the valence band and for band gaps less than about 0.2 eV where the density of final hole states and the electron-hole overlap becomes small. We find that Auger recombination is dominant for hydrogenic acceptors in HgCdTe for materials with a band gap less than about

0.35 eV and radiative recombination is dominant for larger gap materials. For deeper acceptors, this crossover occurs at larger band gaps. For GaAs, we find that radiative recombination dominates for all reasonably shallow acceptors.

In Chapter 4, we present calculations of reflection and transmission coefficients for electrons and holes at abrupt and graded (100) interfaces for the GaAs-$Ga_{1-x}Al_xAs$ system. We consider semi-infinite crystals of the two semiconductors joined at an abrupt or compositionally graded interface. The calculations are performed using the empirical tight binding approximation. The transport coefficients were computed as a function of the components of the incident carrier wavevector normal and parallel to the interface. We have investigated the transport coefficients for incident states near various band minima into different final state channels. The transmission into states with qualitatively similar character to the incident state is found to be much greater than transmission into states of different character. For example, an electron near the X minimum normal to the interface in $Ga_{1-x}Al_xAs$ transmits into the X valley of GaAs with much greater probability than it transmits into the Γ minimum of GaAs. The dependence of the transport coefficients on the alloy composition has been investigated. The effect of the distance over which the interface is graded on the transport coefficients has also been investigated.

In Chapter 5, we present a theoretical study of impact ionization in heterojunction systems. We find that impact ionization by electrons near the conduction band minimum of the larger band gap material can occur in two ways: the electron can transmit into the smaller gap material and undergo essentially bulk impact ionization; the electron can impact ionize at the interface. We concentrate on the second process, which leads to a probability for impact ionization at the interface. We find a general formula for the first order contribution to this probability. For a simple model we find a simple expression for the interface impact ionization probability which demonstrates the dependences of this probability on the incident electron wavevector component normal to the interface, the conduction band offsets, and the energy gap of the smaller gap material.

Parts of this thesis either have been or will be published under the following titles:

Chapter 2:

Bound Exciton Lifetimes for Acceptors in Si, S. A. Lyon, G. C. Osbourn, D. L. Smith, and T. C. McGill, Solid State Commun. 23, 425 (1977).

Auger Transition Rates for Excitons Bound to Acceptors in Si and Ge, G. C. Osbourn and D. L. Smith, Phys. Rev. B16, 5426 (1977).

Bound Exciton Absorption in Si:Al, Si:Ga, and Si:In, K. R. Elliott, G. C. Osbourn, D. L. Smith, and T. C. McGill, Phys. Rev. B17, 1808 (1978).

Chapter 3:

Auger and Radiative Recombination of Acceptor Bound Excitons in Semiconductors, G. C. Osbourn, S. A. Lyon, K. R. Elliott, D. L. Smith, and T. C. McGill, Solid State Electron. 21, 1339 (1978).

Auger and Radiative Transition Rates for Acceptor Bound Excitons in Direct Gap Semiconductors, G. C. Osbourn and D. L. Smith, (submitted to Physical Review)

Chapter 4:

Transmission and Reflection Coefficients of Carriers at an Abrupt GaAs-GaAlAs (100) Interface, G. C. Osbourn and D. L. Smith, Phys. Rev. B __, (1979).

Carrier Transport Across GaAs-GaAlAs (100) Interfaces, G. C. Osbourn and D. L. Smith, (to appear in J. Vac. Sci. Technol.)

Chapter 5:

Impact Ionization in Heterojunctions, G. C. Osbourn and D. L. Smith, (in preparation)

TABLE OF CONTENTS

ACKNOWLEDGEMENTS iii

ABSTRACT iv

TABLE OF CONTENTS x

CHAPTER 1. INTRODUCTION 1

I. Background 2

II. Outline of Thesis 12

III. Summary of Main Results 18

REFERENCES 21

CHAPTER 2. AUGER AND RADIATIVE TRANSITION RATES OF ACCEPTOR BOUND EXCITONS IN INDIRECT GAP SEMICONDUCTORS 23

I. Introduction 24

II. Qualitative Physics of the Auger and Radiative Transition Rates 27

III. Calculation of Auger and Radiative Transition Rates 31

IV. Results of Calculation 49

V. Summary and Conclusion 59

APPENDIX: DIELECTRIC FUNCTION CONTRIBUTION TO SHORT RANGE POTENTIAL 61

REFERENCES 62

CHAPTER 3. AUGER AND RADIATIVE TRANSITION RATES OF ACCEPTOR BOUND EXCITONS IN DIRECT GAP SEMI-CONDUCTORS 66

I. Introduction 67

II. Qualitative Behavior of Auger and Radiative Transitions 68

III. Calculation of Auger and Radiative Transition Rates 72

IV. Results 80

V. Summary and Conclusions 86

REFERENCES 87

CHAPTER 4. TRANSMISSION AND REFLECTION COEFFICIENTS FOR CARRIERS AT ABRUPT AND COMPOSITIONALLY GRADED GaAs-GaAlAs (100) INTERFACES 89

I. Introduction 90

II. Theoretical Approach 91

III. Evanescent States 104

IV. Qualitative Features of Carrier Transport Coefficients 108

V. Numerical Results 113

VI. Summary and Conclusions 128

APPENDIX: Reciprocity Theorem 132

REFERENCES 135

CHAPTER 5. IMPACT IONIZATION IN HETEROJUNCTIONS 137

I. Introduction 138

II. Theoretical Calculation 139

III. Qualitative Dependences 147

IV. Summary and Conclusions 151

REFERENCES 152

CHAPTER 1

I. BACKGROUND

The study of periodic crystals has led to substantial understanding of the bulk electronic properties of solids. Theoretically, the use of Bloch's theorem in the Hartree-Fock approximation has greatly simplified the problem leading to a qualitative and reasonably good quantitative description of the electronic states of periodic solids. There is great current interest in extending this treatment to include electronic states not described in the Hartree Fock approximation and to describe the electronic states of solids with periodicity in less than three dimensions.

The exciton is a state not described in the Hartree Fock approximation, consisting of an electron bound to a hole by their mutual Coloumb interaction. The exciton can move freely through the solid, and in this case is referred to as a free exciton (FE) [1]. An exciton can also become captured by an impurity, and is then called a bound exciton (BE) [2]. In Si, the binding energy of the electron and hole in the FE is 14.7 meV [3]. For the common shallow acceptor impurities in Si, the binding energy of the exciton on the impurity ranges from 5 meV to 16 meV [2]. At low temperatures, FE and BE can be created by exciting excess electron hole pairs with a laser. These states can be directly studied experimentally by observing the characteristic luminescence produced by their decay. The energy of the emitted photons can be used to obtain binding

energies of the states. The intensity of the luminescence is proportional to the number of states present in the solid. By observing the time decay of the luminescence of a particular state after turning off the laser source, the decay time of the state is directly obtained. The decay time and the decay mechanisms of the BE are important because at low temperatures BE decay can be the dominant route by which excess electrons and holes excited in a solid ultimately decay. For example, carriers created in Si by laser excitation rapidly bind to form FE. The cross section for the binding of an electron to a hole has been theoretically estimated to be $\sim 10^{-13}cm^2$ (5). The FE can decay (with a lifetime of 2.6 μsec (6)) or bind to an impurity. The capture cross section for an exciton on an In acceptor has recently been found experimentally to be greater than $10^{-13}cm^2$ for temperatures less than $10^{o}K$ (7). For concentrations of In greater than $10^{16}cm^{-3}$, the capture time of the exciton on an impurity is less than the decay time of the BE after it has been captured. BE lifetimes have been measured for the common acceptors in Si, and range from 1 μsec (4) to 2.7 nsec (8). For the above range of impurity concentrations and temperatures, the formation and decay of BE therefore provides the most rapid decay mechanism for excess carriers, with the rate limiting step being the decay of the BE. It is therefore interesting to study the possible decay mechanisms of the BE. The major decay modes are radiative (no phonon assistance), Auger (no phonon assistance), and phonon assisted radiative and Auger.

In radiative decay, the electron recombines with a hole and the energy released is emitted as a photon. In Auger decay, the energy released is given off to the remaining hole so that the acceptor is ionized. Phonon assisted transitions involve the accompanying emission of a phonon. Phonon assisted decay is typically slow, so that the important decay mechanisms are no phonon radiative and no phonon Auger (hereafter referred to as simply radiative and Auger). The relative importance of radiative and Auger decay depends on whether the band gap of the semiconductor is direct or indirect. Direct band gap materials are those in which the conduction band minimum occurs at the same wavevector as the valence band maximum, while indirect gap materials are those in which the conduction band minimum occurs at a different wavevector than the valence band maximum. In Figure 1, the band structure on the left has a direct band gap while the one on the right is indirect. BE radiative decay involves recombination of electrons and holes at the same wavevector in k-space. The electron in the acceptor BE tends to be near the conduction band minimum, and the holes are near the valence band maximum. This leads to: fast radiative transitions in direct gap materials because the electron and holes are in the same region of k-space; slow radiative transitions in indirect gap materials because the electrons and holes tend to be widely separated in k-space. As a result, Auger transitions of acceptor BE are usually fast

Fig. 1. The band structure on the left is for a direct band gap material, while the one on the right is for an indirect band gap material.

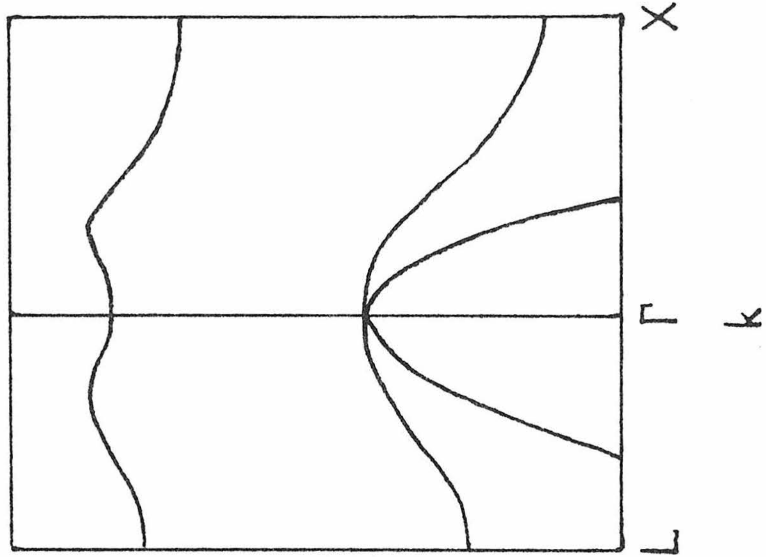
X
Γ
L
k

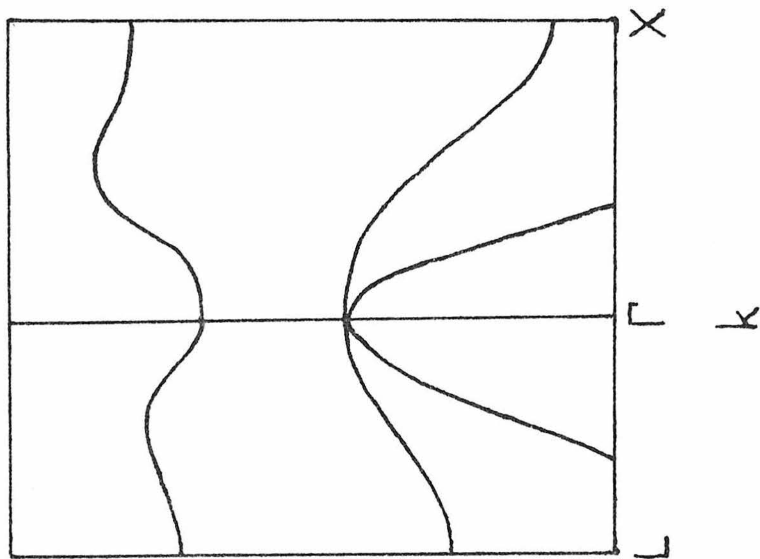
X
Γ
L
k
E(k)

relative to radiative transitions in indirect gap materials [4,9-12], while in direct gap materials the reverse is typically true [13-15]. In this thesis calculations of radiative and Auger transition rates for acceptor BE are presented. The motivation for the work is to (i) identify the decay mechanism of the BE by comparing computed lifetimes with experiment, (ii) understand the qualitative dependence of the transition rates on acceptor type and semiconductor material type. The indirect gap and direct gap cases are treated separately in Chapters 2 and 3 because, as discussed above, the qualitative physics of BE decay is completely different for these cases.

One of the simplest systems with periodicity in less than three dimensions is the heterojunction. The ideal heterojunction consists of two different crystals with the same lattice structures and the same lattice constants joined at an interface. Semiconductor heterojunctions have recently attracted a great deal of theoretical and experimental interest [16]. Theoretically, the study of the Hartree Fock electronic states is greatly simplified by the periodicity of the heterojunction in the plane parallel to the interface. These states can be constructed as eigenstates of wavevectors in the plane parallel to the interface ($k^{||}$). Experimentally, a new crystal growing technique called molecular beam epitaxy has made possible the construction of well characterized semiconductor heterojunctions which are very nearly abrupt on the atomic scale [17-25]. An interesting feature of heterojunction systems that can

be studied theoretically by constructing the one electron states of these systems is the possibility of quantum mechanical reflection of electrons and holes at the interface. Although quantum mechanical reflection of carriers has an important effect on the transport properties of the carriers in the heterojunction system, no realistic studies of this effect have been made. A nearly ideal heterojunction system for studying quantum mechanical reflection is the GaAs-$Al_xGa_{1-x}As$ interface. These semiconductors have a very small lattice mismatch and are chemically similar. In addition, the alloy $Al_xGa_{1-x}As$ provides a continuous range of different materials to study. Finally, this system has been frequently studied experimentally. As the alloy composition x is varied from 0 to 1, the alloy changes from the direct band gap material GaAs to the indirect band gap material AlAs. The GaAs conduction band minimum is at the wavevector $\frac{2\pi}{a}$ (0,0,0) (called the Γ point) and the AlAs minimum is at $k = \frac{2\pi}{a}$ (1,0,0) (called the X point). In the range of x for which the alloy band gap is indirect (direct) electrons incident in the interface from the alloy side start out in the conduction band near the X(Γ) point. For the indirect alloy case, incident electrons in the alloy that transmit can do so into the GaAs conduction band near either the X point or the Γ point. The possibility of transport into more than one transmission state is an interesting aspect of heterojunction systems without analogy in simple one-dimensional models of quantum mechanical transmission and reflection of electrons.

In Chapter 4, calculations of reflection and transmission coefficients for carriers incident on abrupt and compositionally graded GaAs-$Al_xGa_{1-x}As$ (100) interfaces are presented. The motivation of the work was to understand the dependence of the quantum mechanical transmission and reflection coefficients on: (i) the wavevector of the incident state; (ii) the alloy composition x of $Al_xGa_{1-x}As$; (iii) the distance over which the interface is compositionally graded. In addition, it was desired to understand the relative importance of electron transmission from states near X in the alloy into GaAs states near either X or Γ.

Impact ionization, in which a high energy carrier relaxes to a lower energy state in the same band by exciting an electron hole pair, is a process of great interest in bulk materials because it is usually the cause of avalanche breakdown of reverse biased diodes. This process has been studied frequently both experimentally and theoretically [12,26]. Impact ionization in heterojunction systems can also produce interesting effects. The threshold current of an infrared heterojunction laser might be reduced by the impact ionization of carriers injected from a high band gap material into a smaller band gap active region of the laser. It has been suggested that impact ionization of carriers in the base region of a heterojunction transistor might lead to an $\alpha > 1$ [16]. An example of a heterojunction system that could exhibit such impact ionization processes is the CdTe-$Hg_{1-x}Cd_xTe$ interface. The CdTe material has

a band gap of 1.5 eV and the alloy $Hg_{1-x}Cd_xTe$ has a band gap that can be varied from 1.5 eV to 0 eV by increasing the HgTe content. Until now, the mechanism for impact ionization in the heterojunction has been considered to be essentially a bulk effect occurring in the smaller gap material. The bulk impact ionization process is the inverse of free carrier Auger recombination, and both processes require total wavevector conservation [11,12]. However, in the heterojunction system k is not conserved in the direction normal to the interface, so that the k conservation requirement can be relaxed. As a result, impact ionization by electrons near the conduction band minimum of a larger band gap material can occur in two ways in the heterojunction system: the carrier can cross the interface into the smaller gap material and undergo essentially bulk impact ionization; the carrier can impact ionize at the interface. The first process is the one usually considered as the impact ionization mechanism in the heterojunction system. To the author's knowledge, this is the first suggestion in the literature of the existence of the second process, which produces a nonzero probability for carriers to impact ionize at the interface. In Chapter 5, we present a theoretical study of impact ionization in the heterojunction system. We concentrate on the interesting case of impact ionization at the interface. The qualitative dependence of this process on the normal component of the incident carrier wavevector, the conduction band

offsets, and the energy gap of the smaller gap material have been determined.

II. OUTLINE OF THESIS

In Chapter 2, calculations are presented for Auger and radiative transition rates for excitons bound to acceptors in the indirect gap materials Si and Ge. In Si, acceptor BE lifetimes have been measured for the common acceptors B, Al, Ga, and In. The observed lifetimes vary over almost three orders of magnitude from 1 μsec for B to 2.7 nsec for In. Estimates of radiative lifetimes obtained from optical absorption measurements are several orders of magnitude longer than the longest observed BE lifetime (for B), so that the decay mechanism of the acceptor BE in Si is nonradiative. By comparing observed BE lifetimes with calculated Auger lifetimes, we conclude that the acceptor BE in Si decays by the Auger transition. In addition, the strong dependence of the BE lifetimes on acceptor type is understood qualitatively in terms of the dependence of the Auger transition rate on the k-space spreading of the BE wavefunction. The Auger transition requires a large amplitude for the BE k-space wavefunction to have the same wavevector as the final state ionized hole. In indirect band gap materials, the BE wavefunction is peaked in a region of k space away from the final state hole wavevector, so that spreading out of the BE wavefunction is necessary to have fast Auger rates. Spreading of the BE wavefunction in k-space corresponds to localization of the BE holes tightly about the acceptor. Acceptors with large acceptor binding energies tightly

bind the BE holes, so that the k-space spreading of the BE wavefunction is large and the Auger rates are fast. The situation for Ge is qualitatively different than that for Si. Measured BE lifetimes for B, Al, Ga, and In in Ge are all essentially equal to the FE lifetime which is 7 μsec. The calculation of the acceptor BE Auger lifetimes in Ge produces results that are orders of magnitude longer than the experimental lifetimes, demonstrating that the qualitatively different behavior of the BE decay in Ge occurs because the Auger rate is unimportant in Ge. Acceptor BE Auger transition rates are slow in Ge because the acceptors have small binding energies so that the k-space spreading of the BE wavefunction is small. Radiative transitions are also quite slow (the oscillator strengths are too weak to measure experimentally) so that acceptor BE lifetimes in Ge are not determined by Auger or radiative transitions.

In Chapter 3, calculations are presented for Auger and radiative transition rates for excitons bound to acceptors in the direct gap materials $Hg_{1-x}Cd_xTe$ and GaAs. In direct gap materials, it is found that for a fixed acceptor type the Auger transition rate generally decreases for larger energy gap materials while the radiative rate increases. For direct gap materials with large band gap the radiative transition determines the acceptor BE lifetimes, while for sufficiently small gaps the Auger transition dominates. The alloy $Hg_{1-x}Cd_xTe$ is a good system in which to study the dependence of the

transition rates in the small gap regime because the band gap can be varied from 0 eV to 1.5 eV by varying the alloy composition x from 0 to 1. It is found for shallow acceptors that the BE Auger rate becomes equal to the radiative rate in $Hg_{1-x}Cd_xTe$ at a gap of about .35 eV. In the relatively large gap material GaAs, the acceptor BE decays radiatively, and the calculated radiative BE lifetime for the shallow acceptor Zn is consistent with the experimentally observed BE lifetime. The dependence of the BE transition rates on acceptor type has also been examined. In the large gap regime in which radiative decay dominates, the BE lifetime increases for acceptors with larger acceptor binding energies. For the small gap regime in which the Auger decay dominates, the BE lifetime decreases with increasing acceptor binding energies. As a result of these dependences, the crossing point of Auger and radiative rates in $Hg_{1-x}Cd_xTe$ moves to higher energy gaps with increasing acceptor binding energies.

In Chapter 4, calculations are presented for carrier reflection and transmission coefficients at GaAs-$Al_xGa_{1-x}As$ (100) abrupt and graded interfaces. The calculations were performed in a linear combination of atomic orbitals (tight binding) scheme. It is found from the results of the calculation that there is large carrier transport into outgoing (reflection or transmission) Bloch states that have qualitatively similar state character to the incident Bloch state. For example, incident states in AlAs with wavevectors

near the X point transmit almost totally into transmission states in GaAs near the X point rather than into states near the Γ point. The states near the X point in GaAs are qualitatively similar to the X point states in AlAs, while the states near the Γ point in GaAs are not similar to the AlAs X point states. It is found that the total reflection coefficient is exactly 1 for the incident states at a band extrema and drops off for incident states away from the extrema. This drop in reflection is most rapid in the direction normal to the interface, because the dependence of the transport coefficients on wavevector components parallel to the interface is weak. As the AlAs content of the $Al_xGa_{1-x}As$ alloy is increased, the alloy material is made more different from GaAs. This leads to larger changes in the crystal potential at the interface, so that the total reflection coefficient increases for a given incident state as the alloy composition x is increased. If the GaAs-$Al_xGa_{1-x}As$ interface is graded linearly over sufficiently many atomic planes, the effect on the transport coefficients is to increase the total transmission coefficient of a given incident state. This occurs because the change in crystal potential from GaAs to $Al_xGa_{1-x}As$ is smoothed out over a large region, so that reflection is reduced. Increasing the grading distance further results in further increases in the total transmission coefficient.

In Chapter 5, we present a theoretical study of impact ionization in the heterojunction system. As a result of the breakdown in wavevector conservation in the direction normal to the interface, impact ionization by an electron near the conduction band minimum in the larger gap material can occur in two ways: the incident carrier can transmit into the smaller band gap material and undergo essentially bulk type impact ionization; the incident carrier can impact ionize at the interface. The first process determines the bulk type impact ionization rate in the smaller gap material, while the second process leads to a finite probability that the incident carrier will impact ionize. We find the first order contribution, in which one electron hole pair is produced, for both the bulk type impact ionization rate and the probability of carrier impact ionization at the interface. For the second process, some simple qualitative dependences are determined for incident electrons with no component of wavevector parallel to the interface. These qualitative dependences are described by the following simple expression for the interface impact ionization probability (for $k'' = 0$ and small $k^{\perp}$)

$$P \propto k^{\perp}\left(\frac{\hbar^2 k^{\perp 2}}{2m^*_{e_1}} + E_{c_1} - E_{c_2} - E_{g_2}\right)^{5/2} . \qquad (1)$$

E_{c_1} and E_{c_2} are the energies of the conduction band minima in the two materials, E_{g_2} is the band gap of the smaller gap material, $k^{\perp}$ is the component of the incident electron wavevector normal to the

interface, and $m_{e_1}^*$ is the electron effective mass in the larger gap material. For fixed conduction band offset $E_{c_1}-E_{c_2}$ and fixed E_{g_2}, the impact ionization probability increases for incident electron states with increasing $k^{\perp}$. For fixed $k^{\perp}$, the probability increases with increasing conduction band offset for fixed E_{g_2}; and with decreasing E_{g_2} for fixed conduction band offset. For fixed $\frac{\hbar^2 k^{\perp 2}}{2m_{e_1}^*} + E_{c_1}$, the probability increases with: decreasing conduction band offsets for fixed (or decreasing) E_{c_2} and E_{g_2}; and with decreasing E_{g_2} for fixed (or decreasing) E_{c_2} and conduction band offsets. Finally, the additional electron energy threshold above $E_{c_2}+E_{g_2}$ that is required in the bulk type impact ionization process because both energy and total wavevector must be conserved is not required in the interface impact ionization process.

III. SUMMARY OF MAIN RESULTS

Chapter 2

1. The Auger transition determines the lifetimes of BE on the acceptors B, Al, Ga, and In in Si.
2. The strong dependence of the BE lifetimes on acceptor type in Si is due to the strong dependence of the Auger rate on acceptor binding energy.
3. The qualitatively different behavior of Ge acceptor BE decay occurs because both Auger and radiative transitions are unimportant in determining the BE lifetimes. BE Auger transitions are slow in Ge because B, Al, Ga, and In have small acceptor binding energies in this material.

Chapter 3

1. The calculation shows that acceptor BE decay occurs by radiative transition in the large gap direct materials and by Auger transition in the small gap materials. For the variable band gap alloy HgCdTe, the BE Auger rate crosses the radiative rate for shallow acceptors at a band gap of about 0.35 eV.
2. The BE radiative lifetimes increase and the Auger lifetimes decrease as the acceptor binding energy is increased.
3. For acceptors with larger binding energy, the crossing point

of the BE Auger and radiative rates moves to higher band gaps.

Chapter 4

1. Quantum mechanical transmission and reflection coefficients are large for outgoing Bloch states that are qualitatively similar to the incident Bloch state. For example, X valley to X valley transport is large, while X valley to Γ valley transport is small.
2. Transmission is zero for incident states at band extrema points and turns on away from those points. The transport coefficients are less sensitive to the component of incident k parallel to the interface than to the perpendicular component.
3. As the alloy composition x is increased, the reflection coefficient for a given incident state increases.
4. As the interface is linearly graded over a sufficiently large number of atomic layers, the transmission coefficient of a given incident state is increased over the abrupt interface value. As the grading distance is further increased the transmission coefficient continues to increase.

Chapter 5

1. Wavevector nonconservation normal to the interface in heterojunction systems leads to two mechanisms for impact ionization: a bulk type process; impact ionization at the interface.
2. The probability that an electron in a larger gap material will impact ionize at the interface increases as the normal component of the incident electron wavevector increases.
3. For fixed component of incident electron wavevector normal to the interface, the probability of impact ionization at the interface increases: as the conduction band offset increases for fixed energy gap of the smaller gap material; as the energy gap of the smaller gap material decreases for fixed conduction band offset.
4. There is no additional energy threshold above $E_{c_2}+E_{g_2}$, where E_{c_2} is the energy of the conduction band minimum and E_{g_2} is the band gap of the smaller gap material, for impact ionization at the interface to occur. However, this additional energy threshold is still required for the bulk type process.

REFERENCES

1. R. S. Knox, Theory of Excitons, (Academic Press, New York, 1963).
2. J. R. Haynes, Phys. Rev. Lett. 4, 361 (1960).
3. K. L. Shaklee and B. Nahory, Phys. Rev. Lett. 24, 942 (1970).
4. S. L. Lyon, G. C. Osbourn, D. L. Smith, and T. C. McGill, Solid State Commun. 23, 425 (1977).
5. A. A. Lipnik, Soviet Physics - Solid State 3, 1683 (1962).
6. J. D. Cuthbert, Phys. Rev. B1, 1552 (1970).
7. K. R. Elliott, D. L. Smith, and T. C. McGill, Solid State Commun. 24, 461 (1977).
8. W. Schmid, Phys. Status Solidi(b), 84, 529 (1977).
9. D. F. Nelson, J. D. Cuthbert, P. J. Dean, and G. D. Thomas, Phys. Rev. Lett. 17, 1262 (1962).
10. P. J. Dean, R. A. Faulkner, S. Kimura, and M. Ilegems, Phys. Rev. B4, 1926 (1971).
11. P. T. Landsberg, Phys. Status Solidi 41, 457 (1970).
12. P. T. Landsberg and M. J. Adams, J. Lumin. 7, 3 (1973).
13. C. H. Henry and K. Nassau, Phys. Rev. B1, 1628 (1970).
14. C. J. Hwang and L. R. Dawson, Solid State Commun. 10, 443 (1972).
15. C. J. Hwang, Phys. Rev. B8, 646 (1973).
16. See, for example, A. G. Milnes and D. L. Feucht, Heterojunctions and Metal Semiconductor Junctions (Academic Press, New York, 1972).
17. L. L. Chang, L. Esaki, W. E. Howard, R. Ludeke, and G. Schul, J. Vac. Sci. Technol. 10, 655 (1973).

18. L. L. Chang, L. Esaki, and R. Tsu, Appl. Phys. Lett. 24, 593 (1974).

19. L. Esaki and L. L. Chang, Phys. Rev. Lett. 33, 495 (1974).

20. R. Ludeke, L. Esaki, and L. L. Chang, Appl. Phys. Lett. 24, 417 (1974).

21. R. Tsu, L. L. Chang, G. A. Sai-Halasy, and L. Esaki, Phys. Rev. Lett. 34, 1509 (1975).

22. L. L. Chang, A. Segmüller, and L. Esaki, Appl. Phys. Lett. 28, 39 (1976).

23. R. Dingle, A. C. Gossard and W. Wiegmann, Phys. Rev. Lett. 34, 1327 (1975).

24. R. Dingle, W. Wiegmann, and C. H. Henry, Phys. Rev. Lett. 33, 827 (1974).

25. J. P. van der Ziel and A. C. Gossard, J. Appl. Phys. 48, 3018 (1977).

26. See, for example, C. Todd, Zener and Avalanche Diodes, (Wiley-Interscience, 1970) and the references contained therein.

CHAPTER 2

I. INTRODUCTION

A bound exciton (BE) consists of three carriers (two holes and one electron for acceptor BE; two electrons and one hole for donor BE) bound to a charged impurity. There are a number of decay modes accessible to the BE. The BE can decay radiatively by emitting the electron hole recombination energy as a photon. However, in indirect gap materials the radiative transition is relatively slow. Because in a BE three carriers are localized in the same region of space, an Auger transition, in which an electron recombines with a hole and the energy is carried off by the third carrier, can occur. Auger transitions are believed to limit the lifetimes of bound excitons in many cases [1-5]. Auger transitions have also been shown to be important in band to band recombination and carrier capture at a trap site [4,5]. These processes have been studied theoretically [4,5], but to our knowledge, no quantitative calculations of BE Auger rates in semiconductors have been presented.

The bound exciton lifetimes for the four common shallow acceptors in Si (B, Al, Ga and In) have recently been measured [3]. The BE lifetime was found to be significantly shorter than the free exciton (FE) lifetime in undoped Si for each type of acceptor. The BE lifetime was strongly dependent on the type of acceptor, decreasing rapidly (at least a factor of 200 from Si:B to Si:In) as the acceptor binding energy increased. In addition, estimates

of the BE radiative lifetime in Si obtained from absorption measurements [8] indicate that the radiative rate is several orders of magnitude slower than the experimental BE lifetimes. The experimental lifetimes were interpreted as due to Auger transitions without phonon assistance. Qualitatively similar behavior has been observed for excitons bound to acceptors in GaP [2]. The lifetimes for the BE in GaP were also interpreted as limited by phononless Auger transitions.

Because the BE lifetimes are shorter than the FE lifetimes in undoped Si, the addition of small concentrations of shallow acceptors can greatly change the decay rate of photoexcited carriers in Si at low temperatures. For example, the free exciton lifetime in undoped Si is 2.6 μsec [6]. If Si is doped with In at the $10^{15}cm^{-3}$ level (or greater), the lifetime of photoexcited carriers (low excitation) is reduced to less than 5 nsec [3]. This dramatic reduction in carrier lifetime is most likely due to capture of a FE at the impurity to form a BE (the cross section for this process has recently been shown to be very large for Si:In at temperatures less than 10^oK [7]) followed by Auger recombination of the BE. The rate limiting step in the process is the Auger recombination rate (for doping in the $10^{16}cm^{-3}$ or greater level and temperatures less than 10^oK [7].)

In contrast to Si, doping Ge with shallow acceptors at the $10^{15}cm^{-3}$ level has little effect on the lifetime of photoexcited

carriers for temperature and excitation conditions at which electron-hole drops are not formed [8,9]. Both FE and BE are observed in the luminescence spectrum of Ge under these conditions and both decay with the lifetime of the FE in undoped Ge. Thus, it appears that Auger transitions for the BE in Ge are slow processes. Radiative transitions in Ge are also quite slow. The no phonon radiative oscillator strength is too weak to measure.

In this chapter, we present calculations of BE Auger transition rates and BE radiative transition rates for the common shallow acceptors in Si and Ge. The purposes of the calculation are: to establish that the Auger transition determines acceptor BE lifetimes in Si; and to understand the strong dependence of the Auger rate on acceptor type in Si and the qualitatively different effect doping with shallow acceptors has on the lifetime of photoexcited carriers in Si and Ge. The BE radiative oscillator strengths are computed and compared to experimentally measured radiative oscillator strengths to test the validity of the model BE wavefunction used to compute the Auger transition rates. The result of the calculation shows the observed dependence of the BE lifetime on acceptor type in Si and is within about a factor of three of the measured lifetime in absolute value. The computed BE Auger rates in Ge are found to be much slower than the measured free exciton lifetime in Ge. The important difference in the two materials is that the holes are much more strongly bound to the acceptors in Si than they are in Ge.

II. QUALITATIVE PHYSICS OF THE AUGER AND RADIATIVE TRANSITIONS

In their work on GaP, Dean and coworkers argued that the dependence of acceptor BE lifetimes on acceptor type could be understood as due to an increased localization (hence, an increased spreading in K-space) of the hole wavefunction in the BE for the more tightly bound acceptors [(2)]. (They did not, however, present quantitative calculations of the BE Auger rates to support their arguments.) We believe that the physical picture they suggest also applies to Si and can be used to understand the qualitatively different effect of doping with shallow acceptors on carrier lifetimes in photoexcited Si and Ge.

In the acceptor BE (initial state of the Auger transition) there are two holes near the valence band maximum and an electron near the conduction band minimum. The final state of the acceptor BE Auger transition has one hole in the valence band. The holes in the BE are spread in K-space because they are localized about the acceptor. The electron state will also be spread in K-space but the spreading will be small compared to that of the holes because the electron is not localized as much as the holes. The wavevector of the final state hole lies on a constant energy surface as required by energy conservation in the transition. Carrier-carrier scattering, which conserves total wavevector, is the dominant interaction responsible for an Auger transition. Thus, for the Auger transition to

take place, the initial BE state must have an amplitude to contain wavevectors which are accessible to the final state hole. The conduction band minimum is rather far in K-space from the constant energy surface of the final state hole. Since the BE wavefunction is peaked at the conduction band minimum, spreading of the BE wavefunction in K-space is essential for the Auger transition to occur. In Si, the holes in the acceptor BE are well localized, resulting in large hole wavefunction spreading and fast Auger rates. The dependence on acceptor type occurs because the acceptors with larger binding energy bind the holes in the BE more tightly leading to faster Auger rates. In Ge, the holes in the acceptor BE are not tightly bound, so that the hole wavefunction spreading is small and the Auger rates are slow.

In principle, the Auger transition could be phonon assisted. In contrast to the phononless Auger transition, an Auger transition involving a phonon should not be sensitive to the wavefunction spreading in the BE because the phonon would make up the difference in wavevector between the peak in K-space of the BE wavefunction and the final state hole. As a result the phonon assisted Auger transition rate should be insensitive to the acceptor type. Since the observed BE lifetimes in Si are, in fact, very sensitive to the acceptor type, the acceptor BE Auger transitions in Si most likely occur without phonon assistance. In Ge, it is very difficult to know whether the phonon assisted or no-phonon Auger transition is more

likely. Experimentally, neither process appears to be important. We will show that the no-phonon Auger process (which dominates in Si) is slow in Ge.

Radiative transitions involve the recombination of an electron and a hole with essentially the same wavevector K (the wavevectors of the electron and hole differ by the negligible wavevector of the emitted photon). Since the electron K-space wavefunction is peaked at the zone edge and the hole wavefunctions are peaked far away at the zone center, the amplitude for the electron and a hole in the BE to have the same wavevector is quite small. This results in very slow radiative transition rates for indirect gap materials. Because the radiative transition requires very large K space spreading of the BE hole wavefunctions, acceptors with larger acceptor binding energies (and therefore larger hole wavefunction spreading) have larger radiative rates. This dependence is similar to that of the Auger rate on acceptor type, and illustrates the similar sensitivities of the Auger and radiative transition rates on the large K region of the BE wavefunction.

In order to compute the BE Auger rate, it is necessary to know the BE wavefunction. It is very difficult to compute this wavefunction accurately, and we use an idealized model. In particular, we describe the interaction of the holes with the charged acceptor by a Coulomb potential and a short range square well. For Si:Al and Ge:Ga (the impurity has the same core structure as the host) the strength

of the short range well was taken to be due only to the wavevector dependence of the dielectric function. For the other impurities, it was adjusted to produce the observed acceptor binding energies for a simple hydrogenic model of the acceptor. In order to check the approximate validity of the model BE wavefunction, we used it to compute no-phonon oscillator strengths for BE absorption. For Si:Al, Si:Ga and Si:In, the results are within a factor of two of the measured values [10]. For Si:B, the computed oscillator strength is about a factor of four too large. We readjusted the strength of the square wells so as to give wavefunctions which produce the measured oscillator strengths. This procedure is appropriate because both the no-phonon oscillator strength and the Auger transition rate depend sensitively on the extent of K-space spreading of the hole wavefunction and hence on the strength of the short range potential. In contrast, the acceptor binding energy is not as strongly dependent on the strength of the short range potential. For Ge, the computed oscillator strengths were so small that they are probably not observable. This is consistent with the lack of no-phonon BE optical transitions for Ge doped with acceptors but is not of much help in the Auger rate calculations.

III. CALCULATION OF AUGER AND RADIATIVE TRANSITION RATES

From time dependent perturbation theory, the BE Auger transition rate is given by

$$\frac{1}{\tau} = \frac{2\pi}{\hbar} \sum_{F;\mathrm{Ave}\,I} |\langle F|H|I\rangle|^2 \ \delta(E_I - E_F) \tag{1}$$

here $|F\rangle$ is the final state which consists of a free hole, $|I\rangle$ is the BE initial state and H is the Hamiltonian for the solid. (The states $|I\rangle$ and $|F\rangle$ are only approximate eigenstates of H.) The BE wavefunction has the form

$$|I\rangle = \sum_{k_h, k_h', k_e, m_1 m_2} A^{JM}_{m_1 m_2}(k_h, k_h', k_e) \ \ \Psi(k_h m_1; k_h' m_2; k_e \sigma_e) \tag{2}$$

where $\Psi(k_h m_1; k_h' m_2; k_e \sigma_e)$ is a Slater determinant with the valence band states $(k_h m_1)$ and $(k_h' m_2)$ empty and the conduction band state $(k_e \sigma_e)$ occupied. Here m_1 and m_2 label the four hole bands degenerate at the valence band maximum and σ_e labels the electron spin. For simplicity, we neglect valley orbit splitting effects in the BE and restrict the electron to a particular conduction band minimum. $A^{JM}_{m_1 m_2}$ is the amplitude that a particular determinant is contained in the BE wavefunction; J is the total hole spin (2 or 0) with projection M along the Z axis. The final state is

$$|F\rangle = \Psi(k_f \sigma_f) \tag{3}$$

where $\Psi(k_f\sigma_f)$ is a Slater determinant with the valence band state $(k_f\sigma_f)$ empty and σ_f is the final state hole spin. (We neglect spin orbit splitting in the final state and the hole band index is included with σ_f.)

Using the wavefunctions given by Eqs. (2) and (3), the transition matrix element becomes [11]

$$<F|H|I> = \sum_{k_h k_h' k_e m_1 m_2} A^{JM}_{m_1 m_2}(k_h, k_h', k_e) \left[<\phi_{k_h m_1};\phi_{k_h' m_2}|V_{ee}|\phi_{k_f\sigma_f}\phi_{k_e\sigma_e}> - <\phi_{k_h' m_2};\phi_{k_h m_1}|V_{ee}|\phi_{k_f\sigma_f}\phi_{k_e\sigma_e}> \right] \tag{4}$$

where ϕ is a one electron Bloch function and V_{ee} is the Coulomb interaction. The two electron matrix elements in Eq. (4) can be written as

$$<\phi_{k_h m_1};\phi_{k_h' m_2}|V_{ee}|\phi_{k_f\sigma_f}\phi_{k_e\sigma_e}>$$

$$= \sum_{GG'} U_{k_h m_1;k_f\sigma_f}(G)\, U_{k_h' m_2;k_e\sigma_e}(G')\, \frac{e^2(2\pi)^3\, \delta(\underset{\sim}{k}_f+\underset{\sim}{k}_e-\underset{\sim}{k}_h-\underset{\sim}{k}_h'+\underset{\sim}{G}-\underset{\sim}{G}')}{\epsilon(\underset{\sim}{k}_f-\underset{\sim}{k}_h+\underset{\sim}{G})\, |k_f-k_h+G|^2} \tag{5}$$

Here ϵ is the dielectric function, G and G' are reciprocal lattice vectors and

$$U_{k_h m;k\sigma}(G) = \frac{1}{\Omega}\int d^3 r e^{-i\underset{\sim}{G}\cdot\underset{\sim}{r}} u^*_{k_h m}(r) u_{k\sigma}(r) \tag{6}$$

where u is the periodic part of the Bloch function and Ω is the sample volume.

The maximum contribution to the matrix element comes from terms with G = 0 so that the denominator can be small. The delta function in Eq. (5) requires that

$$\underset{\sim}{k}_f + \underset{\sim}{k}_e - \underset{\sim}{k}_h - \underset{\sim}{k}'_h + \underset{\sim}{G}' = 0 \tag{7}$$

for G = 0. The amplitude function, A, will be peaked at

$$k_h \sim k'_h \sim 0 \text{ and } k_e \sim k_{eo}$$

where k_{eo} is the conduction band minimum. The wavevector k_f lies on a constant energy surface. For Si, k_{eo} is about 82% of the way out in the Brillouin zone in the (100) direction [12] and k_f is approximately 25% of the way out in the zone with the value varying somewhat with the direction of k_f. Under these conditions, the most important term in the sum over G' will be with G' = 0. For Ge, k_{eo} is at the zone edge in the (111) direction so that there is a non-zero G' that puts k_{eo} + G' at the zone edge in the $(\bar{1}\bar{1}\bar{1})$ direction. Both this term and the one with G' = 0 will be significant in the sum on G'. These two terms are important for different values of k_f so there is no interference between them, and they give the same contribution to the Auger rate. Thus, we

evaluate the contribution to one of the terms and multiply this by a factor of two. (Since our conclusion will be that the BE Auger rate in Ge is several orders of magnitude smaller than the measured free exciton lifetime, this factor of two is not important.) Thus, for Si and Ge we need only consider the term G = G' = 0 in Eq. (5).

The wavefunction amplitude function is taken to have the form

$$A^{JM}_{m_1 m_2}(k_h, k_h', k_e) = C^{JM}_{m_1 m_2} f_h(k_h) f_h(k_h') f_e(k_e) \tag{8}$$

where the coefficients, C, are chosen to give wavefunctions that are eigenstates of the total spin of the two holes. In particular, we have

$$C^{22}_{\frac{3}{2}\frac{1}{2}} = C^{21}_{\frac{3}{2}-\frac{1}{2}} = C^{2-1}_{\frac{1}{2}-\frac{3}{2}} = C^{2-2}_{-\frac{1}{2}-\frac{3}{2}} = 1 \tag{9a}$$

and

$$C^{20}_{\frac{3}{2}-\frac{3}{2}} = C^{20}_{\frac{1}{2}-\frac{1}{2}} = C^{00}_{\frac{3}{2}-\frac{3}{2}} = -C^{00}_{\frac{1}{2}-\frac{1}{2}} = \frac{1}{\sqrt{2}} \tag{9b}$$

and all others are zero. The BE wavefunction is properly normalized so long as the one electron functions f_h and f_e are. Using this notation, Eq. (4) becomes

$$\langle F|H|I\rangle = \sum_{k_h k_h' k_e m_1 m_2} f_h(k_h)\ f_h(k_h')\ f_e(k_e)$$

$$U_{k_h m_1; k_f \sigma_f}\ U_{k_h m_2; k_e \sigma_e}\ \frac{e^2 (2\pi)^3\ \delta(\underset{\sim}{k}_f + \underset{\sim}{k}_e - \underset{\sim}{k}_h - \underset{\sim}{k}_h')}{\varepsilon(k_f - k_h)\ |k_f - k_h|^2} \left[C^{JM}_{m_1 m_2} - C^{JM}_{m_2 m_1}\right] \tag{10}$$

We next consider the overlap integrals U. Both k_f and k_h are toward the zone center and in the upper valence band. From the k • P calculations of Cardona and Pollak [13], we see that overlap integrals of the form $U_{k_h m_1;k_f\sigma_f}$ are not strongly dependent on the magnitude of k_f or k_h in Si and Ge, and we make the approximation

$$U_{k_h m_1;k_f\sigma_f} \approx \lim_{k_f \to o} U_{om_1;k_f\sigma_f} \tag{11}$$

The value depends on m_1, σ_f, and the final state hole band index b_f. An analogous approximation cannot be used for $U_{k_h' m_2;k_e\sigma_e}$ in Si because it is zero at $k_h' = 0$ and $k_e = k_{eo}$. Since the spreading in K-space of the holes in the BE is much greater than that for the electron, we set $k_e = k_{eo}$ and expand in k • P perturbation theory for k_h' away from the zone center. Using the k • P perturbation theory, the periodic part of the hole Bloch function is

$$u_{k_h' m_2}(r) = u_{om_2}(r) + \frac{\hbar}{m} \sum_{b\sigma''} u_{o\beta\sigma''}(r) \frac{\langle u_{ob\sigma''}|k_h' \cdot P|u_{om_2}\rangle}{E_o - E_b} \tag{12}$$

where b labels bands and σ' spins. Then we have

$$u_{k_h' m_2;k_e\sigma_e} \approx \underset{\sim}{k}_h' \cdot \underset{\sim}{M}_{om_2;k_{eo}\sigma_e} \tag{13a}$$

where

$$\underset{\sim}{M}_{om_2;k_{eo}\sigma_e} = \frac{\hbar}{m} \sum_{b\sigma''} U_{ob\sigma'';k_{eo}\sigma_e} \frac{\langle u_{ob\sigma''}|P|u_{om_2}\rangle}{E_o - E_b} \tag{13b}$$

The only band which makes a significant contribution to the sum in Eq. (13b) for Si is the Γ_{15} conduction band. If k_{eo} is taken to define the Z direction, the Z component of $\underset{\sim}{M}$ is zero.

In Ge, $U_{om_2;k_{eo}\sigma_e}$ is not zero as it is in Si. However, the $k \cdot P$ calculations of Cardona and Pollak [13] show that this overlap integral is small. We have computed the Auger rates in Ge both approximating $U_{k_h m_2;k_e\sigma_e}$ by $U_{om_2;k_{eo}\sigma_e}$ and using the $k \cdot P$ expansion similar to Si (that is, setting $U_{om_2;k_{eo}\sigma_e}$ equal to zero). The second result gave almost an order of magnitude larger Auger rates. It is the one we report [14]. For Ge, the Γ_2' conduction band makes the dominant contribution to the sum in Eq. (13b).

With these approximations, the transition matrix element becomes

$$\langle F|H|I\rangle = \sum_{m_1 m_2} (C^{JM}_{m_1 m_2} - C^{JM}_{m_2 m_1})\, U_{om_1;b_f\sigma_f}\, \underset{\sim}{M}_{om_2;k_{eo}\sigma_e} \cdot \underset{\sim}{\beta}(k_f) \qquad (14a)$$

where

$$\underset{\sim}{\beta}(k_f) = \left(\frac{1}{2\pi}\right)^3 \frac{1}{2\pi^2} \int d^3k_h d^3k_h' \, f_h(\underset{\sim}{k}_h)\, f_h(\underset{\sim}{k}_h')$$
$$f_e(\underset{\sim}{k}_h + \underset{\sim}{k}_h' - \underset{\sim}{k}_f) \frac{e^2 \, \underset{\sim}{k}_h'}{\varepsilon(\underset{\sim}{k}_h - \underset{\sim}{k}_f)\, |\underset{\sim}{k}_h - \underset{\sim}{k}_f|^2} \qquad (14b)$$

To obtain the transition rate, the matrix element is squared, averaged over the initial BE states and summed over final states. The most important final hole states are in the two upper valence bands; these two bands are degenerate in the [100] and [111] directions. We

include only these two bands in the summation and neglect the fact that they are not degenerate in all directions [15]. The remaining summations on discrete indices can be performed in a straightforward but tedious way. The result becomes

$$\frac{1}{\tau} = |D|^2 B \qquad (15a)$$

where

$$D = [2] \left(\frac{2}{3}\right)^2 |\langle u_\Gamma | u_c \rangle|^2 \left(\frac{\hbar}{m}\right)^2 \frac{|\langle u_\Gamma | P_x | u_{\Gamma_{25'}} \rangle|^2}{(E_\Gamma)^2} \qquad (15b)$$

and

$$B = \frac{2\pi}{\hbar} \frac{1}{(2\pi)^3} \int d^3k_f \; \beta_x^2(k_f) \; \delta(E_I - E_F) \qquad (15c)$$

The factor of two in square brackets is to be included for Ge but not for Si. In Eq. (15), Γ refers to the Γ_{15} conduction band state for Si and the Γ_2' conduction band state for Ge; c refers to the conduction band minimum (Δ_1 in Si and L_1 in Ge) and P_x is the x component of the momentum operator. (The minimum of the conduction band is taken to define the Z axis; the x and y components which appear in the product $\underset{\sim}{M} \cdot \underset{\sim}{\beta}$ give equal contributions to the transition rate.)

To evaluate $\underset{\sim}{\beta}(k_f)$, it is necessary to obtain the envelope functions $f_h(k_f)$ and $f_e(k_e)$. As a first approximation, we use effective mass theory with a simplified model for the band structure. The electron effective mass is taken to be spherical with a value [16]

$$\frac{1}{m_e} = \frac{1}{3}\left(\frac{2}{m_t} + \frac{1}{m_e}\right) \tag{16}$$

where m_t is the transverse electron effective mass and m_e is the longitudinal electron effective mass. The interaction between the holes and the charged acceptor is taken to be a Coulomb part, screened by the static dielectric function, plus a short range square well. The radius of the square well is taken to be the covalent radius of the host. For Si:Al and Ge:Ga (the impurity with the same core structure as the host), the square well is taken to be due only to the dielectric function. In Appendix I, we obtain an expression for the depth of the square well for Si:Al and Ge:Ga based on this assumption. The hole effective mass is taken to be spherical. We chose a value for the hole effective mass by making a variational calculation for the Si:Al and Ge:Ga acceptors, using a 1s hydrogenic wavefunction and fitting the measured binding energy. For impurities other than Al in Si and Ga in Ge, we determine the depth of the square well by making a variational calculation for the acceptor using a 1s hydrogenic wavefunction and fitting the measured binding energy. The interaction between the electron and the charged acceptor was taken to be the same as for holes but with the sign changed.

As a first approximation, f_h and f_e are assumed to have a 1s hydrogenic form

$$f_h(k) = \sqrt{\frac{\pi}{a^5}} \frac{8}{(k^2 + (1/a)^2)^2} \tag{17a}$$

$$f_e(k) = \sqrt{\frac{\pi}{b^5}} \frac{8}{(k^2 + (1/b)^2)^2} \tag{17b}$$

The Bohr radii for the holes and electron are determined from a variational calculation.

There are corrections to the effective mass approximation for wavevectors far from the band extrema because the hole dispersion curves are not parabolic at large $\underset{\sim}{k}$. We take these corrections into account by substituting the hydrogenic form into the Hartree equation for the holes in the BE

$$f_h(k) = \frac{1}{E(k) + E_B} \sum_{k'} V_{kk'} f_h^H(k') \tag{18}$$

Here $E(k)$ is the hole dispersion curve, E_B is the one hole Hartree energy, f_h^H is the hydrogenic form for the hole wavefunction (Eq. (17a)) and V is the Hartree potential seen by the hole computed taking the hydrogenic forms for the envelope function

$$V(r) = \frac{-e^2}{\varepsilon(o)r} + \frac{e^2}{\varepsilon(o)} \int \frac{|f_h^H(r')|^2}{|r-r'|} d^3r'$$

$$\frac{-e^2}{\varepsilon(o)} \int \frac{|f_e^H(r')|^2}{|r-r'|} d^3r' \frac{-4\pi}{3} V_o R^3 \delta(r) \tag{19}$$

Here the short range square well of radius R and depth V_0 has been replaced by a delta function for convenience. (The Fourier transform of the square well is effectively constant for the range of wave-vectors of interest.) Evaluating the integrals using the hydrogenic functions and using the fact that the hole Bohr radius is much smaller than the electron Bohr radius gives

$$V(r) \simeq \frac{-e^2}{\varepsilon(o)} e^{-2r/a}\left(\frac{1}{r} + \frac{1}{a}\right) \frac{-4\pi}{3} V_o R^3 \delta(r) \tag{20}$$

Using this form for the potential, the iterated wavefunction is

$$f_h(k) = \frac{e^2}{\varepsilon(o)} \frac{4\pi}{\sqrt{\pi a^3}} \frac{1}{(E(k) + E_B)} \left\{ \frac{1}{k^2 + 9/a^2} + \frac{6}{a^2(k^2 + 9/a^2)^2} + \frac{V_o R^3}{6\, e^2/\varepsilon(o)} \right\} \tag{21}$$

Although this function appears to be quite different than the hydrogenic form, they are numerically rather close at small k. At large k, where both functions are small, the iterated function dies off more slowly with increasing k than the hydrogenic form. We compare the two functions for k in the (111) direction for Si:Ga in Fig. (1) [17]. (Si:Ga represents a case with an intermediate value for the strength of the short range potential. The (111) direction is the one of greatest interest because the hole dispersion curves for Si and Ge drop off most slowly in this direction so that the hole wavefunction is spread most effectively in this

Fig. 1. Hole envelope function for the BE in Si:Ga vs wavevector in units of the hole Bohr radius. The dashed line is the hydrogenic form for the envelope function (see Eq. (17a)) and the solid line is the iterated form (see Eq. (21)). The wavevector is in the [111] direction; $|K|a$ equal twelve corresponds to the zone edge.

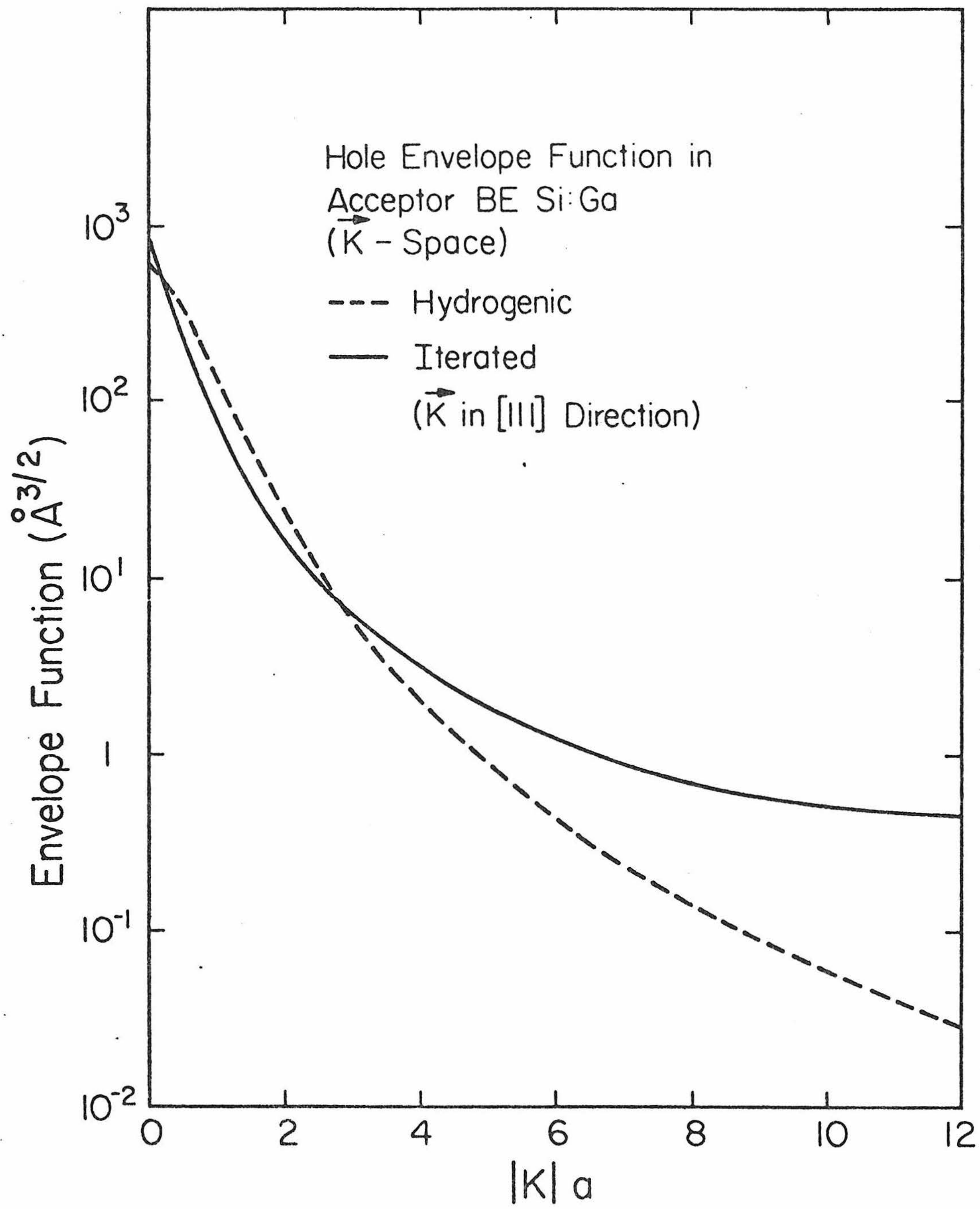
Hole Envelope Function in
Acceptor BE Si:Ga
(K - Space)
Hydrogenic
Iterated
(K in [111] Direction)
Envelope Function (Å^3/2)
10^3
10^2
10^1
1
10^-1
10^-2
0
2
4
6
8
10
12
|K| a

direction.) In the calculations of Auger rates and no-phonon oscillator strengths, we will only need the iterated form of the hole wavefunction in the tail region.

With the approximate expressions for the envelope functions, f_h and f_e, we can perform the integral in Eq. (14b). First, we notice that the function f_e is much more sharply peaked than the other functions (the electron Bohr radius is large) and replace it by a normalized delta function,

$$f_e(\underset{\sim}{k}_e) \approx \frac{(2\pi)^3}{\sqrt{\pi b^3}} \delta(\underset{\sim}{k}_e - \underset{\sim}{k}_{eo}) \tag{22}$$

Then we have

$$\underset{\sim}{\beta}(\underset{\sim}{k}_f) = \frac{1}{2\pi^2} e^2 \frac{1}{\sqrt{\pi b^3}} \int d^3k_h f_h(\underset{\sim}{k}_h) \frac{f_h(\underset{\sim}{k}_{eo} + \underset{\sim}{k}_f - \underset{\sim}{k}_h)\ (\underset{\sim}{k}_f + \underset{\sim}{k}_{eo} - \underset{\sim}{k}_h)}{\varepsilon(k_h - k_f)\ |k_h - k_f|^2} \tag{23}$$

The calculation would still be very lengthy if it was done without further simplification because both the integration in $\beta(\underset{\sim}{k}_f)$ and the final state integration $\underset{\sim}{k}_f$ involve evaluation of valence band energies at every point. We have examined the integration in Eq. (23) numerically and found that nearly all the contribution to the integral comes from the region near $\underset{\sim}{k}_h = 0$. This occurs because the function $f_h(\underset{\sim}{k}_h)$ is peaked at $k_h = 0$. There is no corresponding contribution at $(\underset{\sim}{k}_{eo} + \underset{\sim}{k}_f = \underset{\sim}{k}_h)$ because of the factor $(k_f + k_{eo} - k_h)$

and because the denominator $|k_h - k_f|^2$ is large in this region. As long as $a|k_{eo} + k_f|$ is much larger than unity, the integral in Eq. (23) is that of a sharply peaked function times a smoothly varying one in the region which contributes. In this case, the sharply peaked function can be reasonably approximated by a normalized delta function. Since we are only concerned with the part of $f_h(\underset{\sim}{k}_h)$ where the function is large (i.e., near $k_h = 0$) we use the hydrogenic form to determine the normalization,

$$f_h(k_h) \approx \frac{(2\pi)^3}{\sqrt{\pi a^3}} \delta(k_h) \tag{24}$$

To check the validity of this approximation, we have used it for the integral with $f_h(k_{eo} + k_f - k_h)$ being hydrogenic. For the hole Bohr radius parameters used here, the approximate result was within 50% of the exact value determined by numerical integration for all cases except Si:In. For Si:In the approximate result was within a factor of two of the exact result. When Eq. (21) is used for $f_h(k_{eo} + k_f - k_h)$, the approximation should be better than for the hydrogenic form because $f_h(k_{eo} + k_f - k_h)$ is more slowly varying near $k_h = 0$ in this case. With this approximation, we have

$$\underset{\sim}{\beta}(\underset{\sim}{k}_f) = \left(\frac{e^2}{2\varepsilon(o)a}\right)^2 \frac{64\sqrt{\pi a}}{ak_f} \left(\frac{a}{b}\right)^{3/2}$$

$$(\underset{\sim}{k}_{eo} + \underset{\sim}{k}_f) \left[\frac{1}{E(k_{eo}+k_f) + E_B} \frac{\varepsilon(o)}{\varepsilon(k_h-k_f)}\right] \frac{\varepsilon(o)}{\varepsilon(k_h-k_f)}$$

$$\left\{ \frac{1}{|k_{eo}+k_f|^2 a^2+9} + \frac{6}{(|k_{eo}+k_f|^2 a^2+9)^2} + \frac{V_o R^3}{6 \frac{e^2}{2\varepsilon(o)a} a^3} \right\} \quad (25)$$

Here E_B is negligible compared to $E(k_{eo} + k_f)$; thus, it plays no role in the calculation of Auger rates.

The final state integral in Eq. (15c) is performed numerically. The valence band structure was obtained from a tight binding band structure calculation using essentially the parameters of Chadi and Cohen [20]. We have changed the second nearest neighbor interaction parameter (u_{xx} in the notation of Ref. (20)) by 0.21 eV in Si and 0.16 eV in Ge in order to produce the known energies at the L_3 valence band points [21]. It is desirable to get this point as accurately as possible because the largest contribution to the density of final hole states for the Auger transition in Si and Ge come with k in the (111) directions. In Table III, we list parameters used in the calculation.

In order to obtain BE no phonon radiative decay and absorption rates, it is convenient to compute the no-phonon oscillator strengths. From the oscillator strength f, the radiative transition can be obtained using the relation

$$\frac{1}{\tau_R} = \left(\frac{g_{BE}}{g_A}\right) \frac{e^2 2\omega^2 n\ f}{mc^3} \quad (26)$$

where g_{BE} is the degeneracy of the BE, g_A is the degeneracy of the acceptor, $\hbar\omega$ is the photon energy, and n is the index of refraction.

The oscillator strength is defined as

$$f = \frac{2}{\hbar\omega m} |\langle I|P_y|F\rangle|^2 \tag{27}$$

Here $|F\rangle$ is the final state acceptor BE, $|I\rangle$ is the initial acceptor state, P is the momentum operator and $\hbar\omega$ is the photon energy required in the optical transition; Eq. (28) is to be averaged over the initial acceptor states and summed over the final BE states. Using the BE wavefunction in Eq. (8) and an acceptor wavefunction of the form

$$|I\rangle = \sum_k F_m(k)\ \Psi(km) \tag{28}$$

The matrix element can be written as

$$\langle I|P_y|F\rangle = \sum_{k_h k_h'} \sum_{m_1 m_2 \sigma_e} f_h(k_h)\ f_h(k_h') \\ f_e(k_h)\ F_{m_2}(k_h')\ \langle u_{k_h m_1}|P_y|u_{k_h\sigma_e}\rangle \left[C^{JM}_{m_1 m_2} - C^{JM}_{m_2 m_1}\right] \tag{29}$$

Here $u_{k_h\sigma_e}$ is the periodic part of the electron Bloch function and $u_{k_h m_1}$ is the periodic part of the hole Bloch function. We assume that the acceptor envelope function $F(k_h')$ does not depend on the hole spin state m_2 and that near $k_h = 0$ where $F(k_h)$ and $f_h(k_h)$ are large, they may be reasonably approximated by hydrogenic functions with Bohr radii a_A and a, respectively. In this case we have

$$\sum_{k_h'} f_h(k_h')\ F_{m_2}(k_h') = \frac{8}{(1 + \frac{a_A}{a})^3} \left(\frac{a_A}{a}\right)^{3/2} \tag{30}$$

Next we use the fact that the spread of the electron envelope function in K-space is very small compared to that for holes and replace $f_e(k_h)$ with the normalized delta function given in Eq. (22). The matrix element becomes

$$<I|P_y|F> = f_h(k_{eo})\frac{1}{\sqrt{\pi b^3}}\frac{8}{(1+\frac{a_A}{a})^3}\left(\frac{a_A}{a}\right)^{3/2}$$

$$\sum_{m_1 m_2 \sigma} <u_{k_{eo}m_1}|P_y|u_{k_{eo}\sigma_e}> \left[C^{JM}_{m_1 m_2} - C^{JM}_{m_2 m_1}\right] \tag{31}$$

The spin sums in Eq. (32), initial state averages and final state sum can be performed in a straightforward but tedious way. In Si, the result is

$$f = \frac{2}{\hbar\omega m} \left|<u_{\Delta_5}|P_y|u_{\Delta_1}>\right|^2$$

$$4\left(\frac{8}{(1+\frac{a_A}{a})^3}\left(\frac{a_A}{a}\right)^{3/2}\right)^2\left[\frac{f_h(k_{eo})}{\sqrt{\pi b^3}}\right]^2 \tag{32}$$

Here u_{Δ_5} is the periodic part of the hole Bloch function in the Δ_5 valence band at k_{eo} and u_{Δ_1} is the periodic part of the electron Bloch function at this point. The conduction band minimum is in the z direction (a [100] direction).

For Ge, the result is

$$f = \frac{2}{\hbar\omega m} \left| \langle u_{\Lambda_3} | P_y | u_{\Lambda_1} \rangle \right|^2$$

$$\frac{8}{3} \left[\frac{8}{\left(1 + \frac{a_A}{a}\right)^3} \left(\frac{a_A}{a}\right)^{3/2} \right]^2 \left| \frac{f_h(k_{eo})}{\sqrt{\pi b^3}} \right|^2 \qquad (33)$$

Here u_{Λ_3} and u_{Λ_1} are periodic parts of the hole and electron Bloch functions at the conduction band minimum. The conduction band minimum is in the z direction (a [111] direction).

IV. RESULTS OF CALCULATION

In order to test the validity of the BE wavefunction, we have used this function to compute no-phonon oscillator strengths for acceptor BE in Si and Ge. The radiative oscillator strength (rather than the radiative transition rate) is the quantity of interest because it is directly accessible to experimental measurement. The radiative rates are simply related to the oscillator strengths and will not be presented. In Ge acceptor BE no-phonon optical transitions are too weak to observe [18]. Our calculation produces very small oscillator strengths [19]; this is consistent with experiment, but not very helpful. In Si, the acceptor BE no-phonon oscillator strengths have been measured [10]. In Table I, we list the measured oscillator strengths and the computed values for Si. For Si:Al, Si:Ga and Si:In, the results are within about a factor of two of the measured values; for Si:B, the calculated oscillator strength is about a factor of four too large. Si:B is different than the other cases because the square well potential is repulsive for holes in this case. The binding energy for the acceptor is not very sensitive to the strength of this potential; the no-phonon oscillator strength is rather sensitive to it. In addition, the no-phonon oscillator strength is sensitive to the tail (in K-space) of the hole wavefunction in much the same way as the Auger transition rate. We adjust the depth of the square well

TABLE I: NO-PHONON OSCILLATOR STRENGTHS FOR ACCEPTOR BE IN SI

	MEASURED	CALCULATED
Si:B	$\sim 2 \cdot 10^{-6}$ a,b	$8.7 \cdot 10^{-6}$
Si:Al	$7 \cdot 10^{-6}$ a	$3.5 \cdot 10^{-6}$
Si:Ga	$1 \cdot 10^{-5}$ a	$9.0 \cdot 10^{-6}$
Si:In	$9 \cdot 10^{-5}$ a	$9.3 \cdot 10^{-5}$

a. Ref. (8).

b. Estimated from the measured TO phonon oscillator strength of Ref. (8) and the ratio of TO to NP emission intensity given by R. Sauer and J. Weber, Phys. Rev. Lett. 36, 48 (1976).

potential to produce the measured oscillator strength. This adjustment is most significant for Si:B; if we had not made the adjustment, the calculated Auger rate for Si:B would be about a factor of three larger than that which we report.

In Table II, we list the square well parameters and resulting Bohr radii determined by the acceptor binding energy and by the no-phonon oscillator strengths. We also list the acceptor binding energies produced by the square wells determined by the no-phonon oscillator strengths. In Si:B, the strength of the repulsive square well is reduced to produce the measured oscillator strengths, and as a result the corresponding acceptor binding energy is greater than the measured value.

In Fig. (2) we show the result of the calculation for Si along with experimental bound exciton lifetimes for the four common shallow acceptors [3,23]. The calculated lifetimes show the same dependence on acceptor type as the observed lifetimes and have numerical values that differ by about a factor of three from the experimental lifetimes. Considering the simplified BE wavefunctions used in the calculation, we consider this agreement between the calculated Auger rates and measured lifetimes to be quite reasonable. The results indicate that the BE lifetimes are limited by phononless Auger transitions for acceptors in Si.

In Ge, it is difficult to determine the appropriate square well parameters because the no phonon acceptor BE oscillator strengths

TABLE II: Square well parameters and Bohr radii for acceptor BE in Si. The diameter of the square well is taken as the covalent radius of Si (1.11 Å). The unprimed numbers are determined by fitting acceptor binding energies and the primed numbers are determined by fitting no-phonon oscillator strengths

	V_oR^3	E_A	a	b	V'_oR^3	E'_A	a'	b'
Si:B	-27.1 eV Å^3	46 meV	18.7 Å	51.5 Å	-12.0 eV Å^3	53 meV	16.4 Å	48.2 Å
Si:Al	2.8 eV Å^3	67 meV	13.0 Å	43.3 Å	4.9 eV Å^3	70 meV	12.4 Å	42.5 Å
Si:Ga	5.7 eV Å^3	71 meV	12.2 Å	42.1 Å	6.2 eV Å^3	72 meV	12.0 Å	41.9 Å
Si:In	14.8 eV Å^3	154 meV	7.7 Å	34.9 Å	14.8 eV Å^3	154 meV	7.7 Å	34.9 Å

TABLE III: PARAMETERS USED IN THE CALCULATION. ALL SYMBOLS ARE DEFINED IN THE TEXT.

	Si	Ge
R	1.11 Å	1.22 Å
m_e	0.26 m	0.12 m
m_h	0.60 m	0.19 m
$\langle u_\Gamma \| u_c \rangle$	0.8 [a]	0.6 [a]
$\| \langle u_\Gamma \| P_x \| u_{\Gamma'_{25}} \rangle \|$	0.53 a.u. [a]	0.68 a.u. [a]
E_Γ	3.4 eV [a]	1.0 eV [a]
$\| \langle u_{\Delta_5} \| P_y \| u_{\Delta_1} \rangle \|$	0.57 a.u. [a]	-
$\| \langle u_{\Lambda_3} \| P_y \| u_{\Lambda_1} \rangle \|$	-	0.65 a.u. [a]

a) Ref. (10)

are so weak that these optical transitions have not been observed. In addition, the acceptor binding energies for the different acceptors are nearly the same in Ge, and they are not very sensitive to a short range potential (due to the large Bohr radii of the acceptors in Ge). In Fig. (3), we plot calculated Auger rates for acceptor BE in Ge versus the square well parameter V_0R^3. In the lower panel of the figure, we show the electron and hole Bohr radii. The range of the square well parameter shown in the figure is over four times that used for Si:In. (The binding energy of the Ge:In acceptor is produced by a well parameter of 37 eV $\mathring{A}^3$.) Over the entire range of the square well parameters, the calculated Auger rate is almost two orders of magnitude (or more) slower than the measured FE recombination rate in Ge. (The measured FE lifetime in undoped Ge is about 8 μsec [23].) Since it seems unreasonable that the appropriate square well depth for the shallow acceptors in Ge should be many times larger than that for Si:In, the calculation indicates that the phononless Auger rate for acceptor BE in Ge is too slow to significantly influence the BE lifetime [24]. The slow Auger rates in Ge follow from the large Bohr radii.

Fig. 2. Bound exciton lifetimes vs impurity binding energy for the four common acceptors in Si. The hollow squares are our calculation of the Auger lifetime and the solid circles are the measure values from Ref. (3). Only an upper bound of 5 nsec (indicated by the top of the arrow) was set on the BE lifetime for Si:In in Ref. (3). Subsequent measurements from Ref. (27) produced a Si:In BE lifetime of 2.7 nsec.

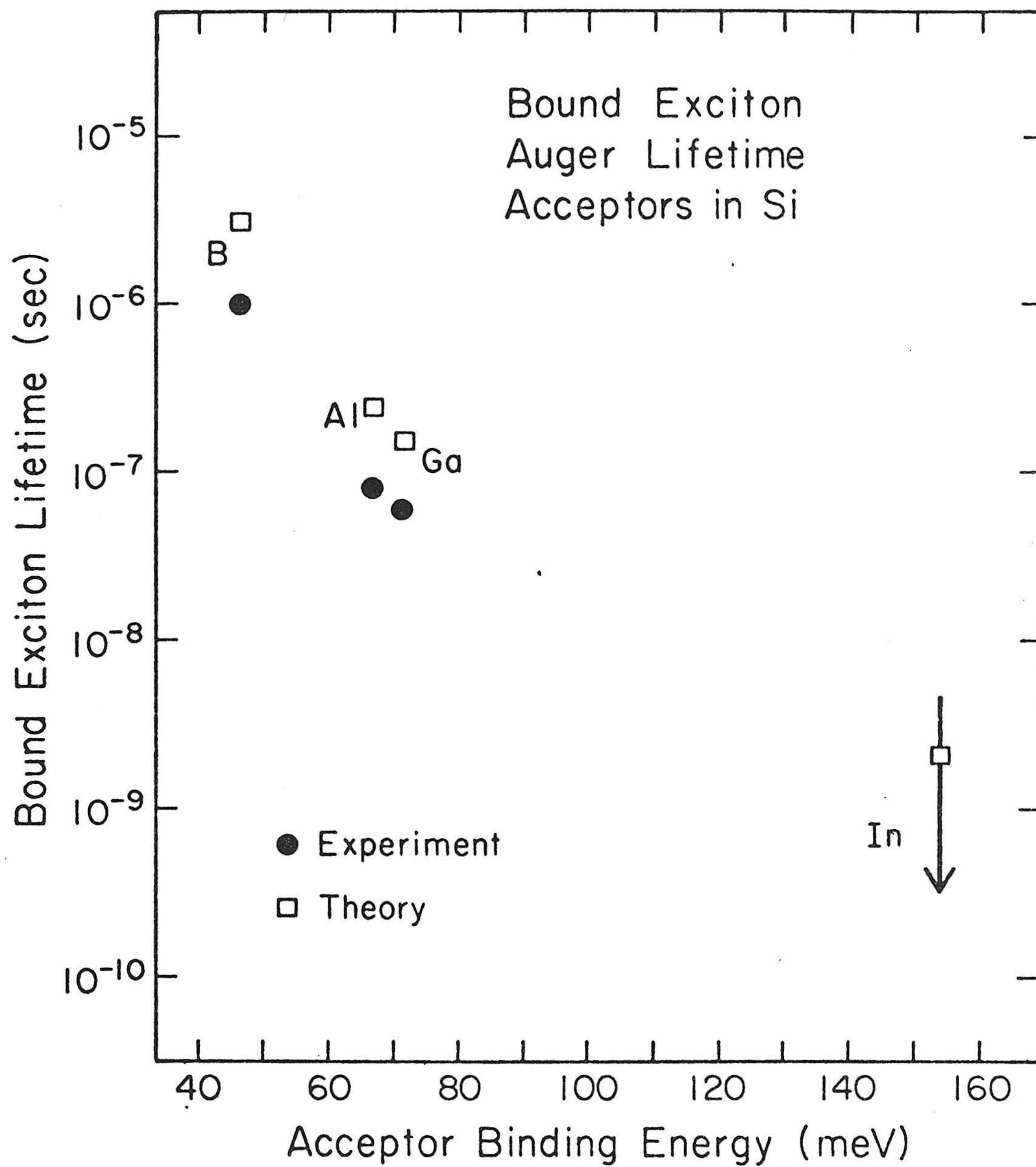
Bound Exciton
Auger Lifetime
Acceptors in Si
B
Al
Ga
In
Experiment
Theory
Bound Exciton Lifetime (sec)
Acceptor Binding Energy (meV)
10^{-5}
10^{-6}
10^{-7}
10^{-8}
10^{-9}
10^{-10}
40
60
80
100
120
140
160

Fig. 3. Calculated Auger lifetimes for acceptor BE in Ge vs the square well parameter V_0R^3. The range of square well parameter is over four times that appropriate for Si:In. Even for this unrealistically large value, the calculated no-phonon Auger lifetime is almost two orders of magnitude greater than the measured FE lifetime in Ge indicating that the phononless Auger transition is not an important process for acceptor BE in Ge. In the lower panel, the hole and electron Bohr radii are shown.

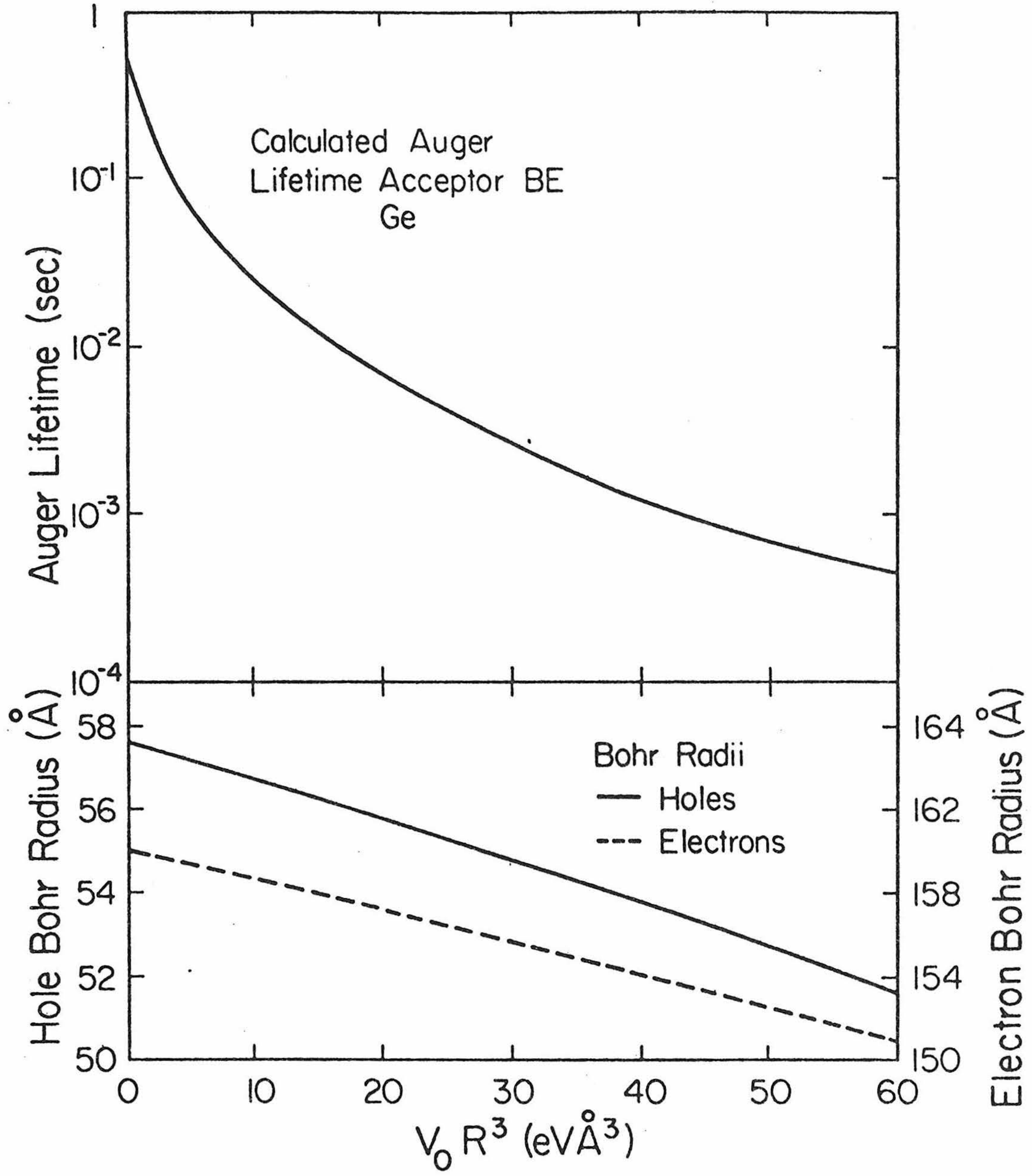
Calculated Auger
Lifetime Acceptor BE
Ge
Auger Lifetime (sec)
1
10⁻¹
10⁻²
10⁻³
10⁻⁴
Hole Bohr Radius (Å)
58
56
54
52
50
Bohr Radii
Holes
Electrons
164
162
158
154
150
Electron Bohr Radius (Å)
0
10
20
30
40
50
60
$V_o R^3$ (eVÅ³)

V. SUMMARY AND CONCLUSION

We have presented a calculation of phononless Auger and radiative transition rates for excitons bound to shallow acceptors in Si and Ge. We used a simplified model for the BE wavefunction and did not expect to produce numerically precise results. (It would be a very formidable task to calculate a high precision BE wavefunction. It would be necessary to include the degenerate valence band structure, conduction band anisotropies and a realistic impurity-carrier potential in a three body problem.) The purpose of the calculation was to understand the very large (almost three orders of magnitude) dependence of acceptor BE lifetimes observed in Si [(3)] and the fact that shallow acceptors do not significantly effect the lifetime of photoexcited carriers in Ge at low temperature [(8)] (qualitatively different behavior than in Si). These are large effects and qualitative differences which can be accounted for in an approximate calculation.

The results of the calculation produced the strong dependence of the Auger rate on acceptor type for BE in Si. The calculated results deviated from the measured BE lifetimes by about a factor of three. For Ge, the calculation gave Auger rates at least two orders of magnitude slower than the observed FE recombination rate in undoped Ge. We conclude that phononless Auger transitions limit the acceptor BE lifetime in Si but are ineffective in Ge. The principal

difference between the two materials is that the holes are much more tightly bound to the charged acceptor in Si than in Ge. Because the holes are more tightly bound in the Si BE, the hole wavefunction is more strongly spread in K-space and the Auger rates are faster. This effect enters the calculation primarily through the Bohr radii which are much smaller in Si than in Ge. The increased spreading in K-space for more tightly bound acceptors also accounts for the dependence of the Auger rate on acceptor type observed in Si.

APPENDIX: DIELECTRIC FUNCTION CONTRIBUTION TO SHORT RANGE POTENTIAL

In this appendix, we estimate the contribution to the short range potential due to the frequency dependence of the dielectric function. We set the integrated value of the short range potential equal to that for a square well,

$$\frac{4\pi}{3} V_o R^3 = \int V_s(r)\, d^3r$$

$$= V_s(q=0) \qquad (26)$$

For the short range potential, we take

$$V_s(q) = \frac{4\pi e^2}{q^2}\left(\frac{1}{\varepsilon(q)} - \frac{1}{\varepsilon(o)}\right) \qquad (27)$$

We use the form of $\varepsilon(q)$ suggested by Nara and Morita [25] for Si; this gives 2.83 eV Å for $V_o R^3$.

For Ge, we use the same form for the dielectric function as in Si but replace $\varepsilon(o)$ with the measured value for Ge, 15.36. This form is a reasonable parameterization of the dielectric function calculation in Ge by Brust [26]. For Ge, we have $V_o R^3$ equals 2.89 eV Å [3].

REFERENCES

1. D. F. Nelson, J. D. Cuthbert, P. J. Dean, and G. D. Thomas, Phys. Rev. Lett. 17, 1262 (1962).
2. P. J. Dean, R. A. Faulkner, S. Kimura, and M. Ilegems, Phys. Rev. B4, 1926 (1971).
3. S. A. Lyon, G. C. Osbourn, D. L. Smith, and T. C. McGill, Solid State Commun. 23, 425 (1977).
4. P. T. Landsberg, Phys. Status Solidi 41, 457 (1970).
5. P. T. Landsberg and M. J. Adams, J. Lumin. 7, 3 (1973).
6. J. D. Cuthbert, Phys. Rev. B1, 1552 (1970).
7. K. R. Elliott, D. L. Smith, and T. C. McGill (to be published).
8. M. Chen, D. L. Smith, and T. C. McGill, Phys. Rev. B10, 4983 (1977).
9. At temperatures and excitation conditions for which electron-hole drops are formed, the decay of the drops is slower in lightly doped Ge than in undoped Ge. This effect can be understood as due to a reduction in the exciton diffusion away from the drops resulting in slower net evaporation of carriers (M. Chen, S. A. Lyon, K. R. Elliott, D. L. Smith, and T. C. McGill in Proceedings of the Taormina Research Conference on the Structure of Matter: Recent Developments in Optical Spectroscopy of Solids, Taormina, Italy, 1976 (to be published)). At doping levels of $10^{16}cm^{-3}$ or greater, the luminescence spectrum of Ge at low temperatures is complicated and shows complicated decay transients (see Ref. (8)); however, the decay is slower than in pure Ge. This behavior is

qualitatively different than in Si.

10. P. J. Dean, W. F. Flood, and G. Kaminsky, Phys. Rev. 163, 721 (1967).

11. We have dropped a term in Eq. (4) which corresponds to interband scattering by the impurity potential. This term makes a negligible contribution to the Auger transition rate for two reasons: first, it depends on the small expansion of a hole orbital going from the acceptor to the BE; second, the lowest order term in the k•p expansion (see Eq. (12)) does not contribute to this term.

12. W. P. Dumke, Phys. Rev. 118, 938 (1960).

13. M. Cardona and F. H. Pollak, Phys. Rev. 142, 530 (1966).

14. In Ref. (13), $\langle u_{\Gamma'_{25}} | u_{L_1} \rangle$ is found to be about 0.1; whereas, $\langle u_{\Gamma_{15}} | u_{L_1} \rangle$ is about 0.6. These overlap integrals are squared in the Auger rates. Because the overlap which appears in the first order k p expansion is considerably larger than that which appears in the zeroth order term, the first order term dominates. If these two overlap integrals were comparable, the zeroth order term would be the more important.

15. When performing the final state integration over k_f, we integrated over both bands and averaged the result. The integrations for the two bands differed by about 50%.

16. W. F. Brinkman and T. M. Rice, Phys. Rev. B7, 1508 (1973).

17. In Fig. (1), we estimate the hole Hartree energy by the BE dis-

sociation energy. This energy only affects the iterated wavefunction illustrated in Fig. (1) for $|K|\alpha \lesssim 0.5$ and does not come into the actual Auger calculation at all since we use the hydrogenic form in the $|K|$ small region.

18. E. F. Gross, B. V. Nokikov, and N. S. Sokolov, Fiz. Tverd. Tela. 14, 443 (1972) [Sov. Phys. Solid State 14, 368 (1972)].

19. We compute a no-phonon oscillator strength of $2 \cdot 10^{-7}$ for a square well parameter $(V_0 R^3)$ of 37 eV $\mathring{A}^{(3)}$ which produces the Ge:In acceptor binding energy. This is about an order of magnitude smaller than the weak no-phonon oscillator strength in Si:B. The calculated oscillator strengths for square well parameters which produce the binding energies for the other acceptors in Ge are much less than that for Ge:In. The calculated no-phonon oscillator strengths in Ge are small because the hole Bohr radii are large.

20. D. J. Chadi and M. L. Cohen, Phys. Stat. Sol.(b) 68, 405 (1975).

21. See, for example, J. C. Phillips, Solid State Physics 18, 55 (1966).

22. In Ref. (3), the measured lifetime for the BE in Si:Al was reported to be 104 nsec. Following discussions with M. H. Pilkuhn and W. Schmid, the BE lifetime in Si:Al was remeasured using lower excitation intensity. The lifetime decreased slightly to 80 nsec suggesting that there was saturation of the Al impurities in the earlier measurement. Lifetimes for the other impurities showed no change (higher doping levels were

used for the other impurities). (Private communication S. A. Lyon).

23. Ya. Pokrovskii, Phys. Stat. Solidi (a) 11, 385 (1972).
24. Except at very low temperatures, excitons probably ionize rapidly from shallow acceptors in Ge because the dissociation energy is only about 1 meV (see Ref. (18)). Thus, unless the acceptor BE has decay channels available to it (such as an Auger transition) which are rapid compared to the processes responsible for FE decay both the BE and FE densities will decay at a rate governed by the processes responsible for FE decay. At temperatures low enough that dissociation of the BE in Ge is slow compared to the FE lifetime (probably less than 2°K) photoexcited carriers in Ge form electron-hole drops.
25. H. Nara and A. Morita, J. Phys. Soc. Japan 21, 1852 (1966).
26. D. Brust, Phys. Rev. B5, 435 (1972).
27. W. Schmid, Phys. Status Solidi (b), 84, 529 (1977).

CHAPTER 3

I. INTRODUCTION

In direct band gap materials, there are two main decay mechanisms available to an exciton bound to a shallow neutral impurity: Auger [1-6] recombination and radiative recombination [7-11]. The relative importance of these two decay processes depends on the semiconductor and on the impurity. In indirect band gap materials, radiative recombination is rather slow and the Auger mechanism usually dominates the recombination [3-6]. In direct band gap materials, radiative recombination is quite fast and may dominate the recombination [9-11].

In this chapter, we present a theoretical study of Auger and radiative recombination of excitons bound to shallow neutral acceptors in direct band gap semiconductors. We consider the dependence of these two transition rates on the band gap of the semiconductor and on the binding energy of the impurity. We concentrate on the alloy system $Hg_{1-x}Cd_xTe$. This is a particularly interesting system because the band gap can be varied by changing alloy composition. We also present calculations for GaAs. We find that radiative recombination dominates Auger recombination for shallow acceptors except in rather small band gap materials ($E_g \lesssim 0.35$ eV). In these small band gap materials, the Auger rate is dominant. Radiative recombination for bound excitons in direct band gap materials has been previously studied theoretically by Rashba and Gurgenishvili [7,8]. We use a different model for the BE wavefunction than used by these authors, but our results are qualitatively similar to theirs.

II. QUALITATIVE BEHAVIOR OF AUGER AND RADIATIVE TRANSITIONS

In the acceptor BE there are two holes and one electron bound to a charged acceptor. In direct band gap materials, the electron effective mass is generally considerably smaller than the hole effective mass. As a result, the two holes are bound relatively close to the acceptor and the electron is not as localized as the holes. In a k-space picture the holes are relatively spread out about the k=0 valence band maximum and the electron is relatively well localized near the k=0 conduction band minimum. In the HgCdTe alloy system, the electron effective mass is a sensitive function of the material band gap (alloy composition). From $\underset{\sim}{k} \cdot \underset{\sim}{P}$ perturbation theory, the electron effective mass decreases with decreasing band gap [12]:

$$\frac{m}{m_e^*} = 1 + \frac{p^2}{3}\left[\frac{2}{Eg} + \frac{1}{Eg+\Delta}\right] \qquad (1a)$$

where

$$p^2 = \frac{2}{m}|\langle S|P_X|X\rangle|^2 \qquad (1b)$$

Here m_e^* is the electron effective mass, Eg is the band gap, Δ is the spin orbit splitting, m is the free electron mass, S and X refer to periodic parts of the Bloch functions at the conduction band minimum and valence band maximum (without spin-orbit splitting) and P is the momentum operator. The hole effective mass and the static dielectric function of the material are only weakly dependent on band

gap. Thus the acceptor binding energy and hole wavefunction in both the acceptor and the BE are not strongly dependent on the alloy composition [13].

In the Auger transition, the initial state is the BE and the final state is a free hole in an accessible valence band. The heavy and light hole bands are always accessible. If the band gap is greater than the spin orbit splitting of the valence band, the split off valence band is also accessible. Energy conservation requires that the energy of the final state hole measured from the valence band maximum is approximately the band gap. The dominant interaction responsible for the Auger transition is carrier-carrier scattering which conserves total wavevector [14]. Thus the transition rate depends on the amplitude for the BE to have wavevectors which are accessible to the final state hole. This amplitude depends on the strength of the impurity potential and on the band structure of the semiconductor.

In direct gap materials, the k-space BE wavefunction is peaked at the zone center and falls off with increasing $|k|$. The possible values of the final state hole wavevector (k_f) depends on the band gap of the material and on the valence band structure. For materials with a very small band gap, the final state hole will be in the heavy or light hole band near the zone center. For these very small gap materials, the amplitude of the BE wavefunction to contain wavevectors accessible to the final state hole will be large. However, for very

small gap materials the density of final hole states is small and the electron effective mass is small. Because of the small electron effective mass, the electron is weakly bound to the BE and is not well localized near the holes. As a result of the small density of final states and the small electron-hole overlap, the Auger transition is slow for very small gap materials. As Eg increases from zero, the density of final states and the electron-hole overlap increase so the Auger transition rate increases. As Eg continues to increase, the possible values of k_f become large enough that the amplitude for the BE wavefunction to contain k_f becomes small. As a result the transition matrix element begins to decrease rapidly, overcoming the effects of the increasing density of final states and increasing electron hole overlap, and the transition rate decreases. We find that this change in slope of the transition rate occurs at about 0.2 eV for hydrogenic acceptors in the HgCdTe system. When Eg first exceeds the spin orbit splitting of the valence band ($\Delta \simeq 0.9$ eV in HgCdTe), final states in the split off band with k_f near the zone center become available. There is a rapid increase in the Auger transition rate when this new set of final states becomes accessible. As Eg continues to increase, the possible values of k_f become large and the transition matrix element and hence the transition rate decreases.

The extent of the spread in k-space of the BE wavefunction depends on the strength of the impurity potential. Stronger impurity poten-

tials (resulting in larger acceptor binding energies) lead to an increased localization of the holes in the BE in position space and hence an increased spread of the BE wavefunction in k-space. For those values of the band gap that have final states with large k_f, an impurity with a stronger attractive potential (hence larger acceptor binding energy) will have a faster Auger rate than an impurity with a weaker potential. For those values of the band gap that have final states with small k_f, the Auger transition rate does not depend strongly on the impurity potential.

For radiative transitions, the BE is the initial state and the neutral acceptor is the final state. Radiative transition rates decrease monotonically as the band gap is decreased. There are two reasons for this decrease in the radiative transition rate with band gap: first, the density of final photon states is smaller for the lower energy photons emitted from the small band gap material; second, because the electron effective mass is small in small gap materials, the electron-hole overlap is small. The radiative rate also depends on the strength of the impurity potential. The holes in the acceptor BE are bound close to the impurity and their wavefunctions are sensitive to the short range part of the impurity potential. The electron is bound relatively loosely about the impurity (held in the complex by its interaction with the holes) and its wavefunction is relatively insensitive to short range parts of the impurity potential. As the impurity potential becomes increasingly

attractive to holes, the hole wavefunction will be more closely bound to the impurity. As a result, the electron-hole overlap will decrease and the radiative transition rate will decrease.

The radiative lifetime is a monotonically decreasing function of band gap. The Auger lifetime is a more complicated function of band gap, but for most values of the band gap it is an increasing function. As a result, radiative recombination tends to dominate in large gap materials and Auger recombination tends to dominate in small gap materials. The radiative lifetime is an increasing function of acceptor binding energy; whereas, the Auger lifetime is a decreasing function of acceptor binding energy. Thus, in large band gap materials (where radiative recombination is dominant), the lifetime increases with acceptor binding energy and in small gap materials (where Auger recombination is dominant), the lifetime decreases with acceptor binding energy.

III. CALCULATION OF AUGER AND RADIATIVE TRANSITION RATES

From time dependent perturbation theory, the recombination rate of a BE due to a perturbation v is given by

$$\frac{1}{\tau} = \frac{2\pi}{\hbar} \sum_{\text{AVE } I;F} |\langle F|v|I\rangle|^2 \, \delta(E_I - E_F) \tag{2}$$

where $|I\rangle$ is the initial BE state and $|F\rangle$ is the final state (free hole for Auger transition, neutral acceptor and photon in the radiative transition). We take the BE wavefunction to have the form

$$|I\rangle = \sum_{k_h k_h' k_e m_1 m_2} C^{JM}_{m_1 m_2} \, f_h(k_h) \, f_h(h_h') \, f_e(k_e)$$

$$\Psi(k_h m_1;k_h' m_2;k_e \sigma_e) \qquad (3)$$

where $\Psi(k_h m_1;k_h' m_2;k_e \sigma_e)$ is a Slater determinant with the valence band states (k_h,m_1) and $(k_h' m_2)$ empty and the conduction band state $(k_e \sigma_e)$ occupied. Here m_1 and m_2 label the four hole states degenerate at the valence-band maximum, σ_e labels electron spin, J is the total hole spin with projection M in the BE, the coefficients C are given in Eq. (9) of Chapter 2 and f_h and f_e are the amplitudes that a given hole and electron state are contained in the BE wavefunction.

For Auger decay of the BE, the final state contains a free hole and an ionized acceptor. The Coulomb interaction between carriers is responsible for the Auger transition. The transition matrix element has the same structure in direct band gap materials as for indirect band gap materials. From Chapter 2

$$\langle F|V|I\rangle = \sum_{k_h k_h' k_e m_1 m_2} f_h(\vec{k}_h)\, f_h(\vec{k}_h')\, f_e(\vec{k}_e)$$

$$U_{k_h m_1;k_f \sigma_f}\, U'_{k_h m_2;k_e \sigma_e}\, \frac{e^2(2\pi)^3\, \delta(\vec{k}_f+\vec{k}_e-\vec{k}_h-\vec{k}_h')}{\varepsilon|k_f-k_h|^2}$$

$$\left(C^{JM}_{m_1 m_2} - C^{JM}_{m_2 m_1}\right) \qquad (4)$$

Here ε is the dielectric function and the overlap integrals U have the form [15]

$$U_{k_h m_1;k\sigma} = \frac{1}{\Omega}\int d^3r\, u^*_{k_1 m_1}(r)\, u_{k\sigma}(r) \qquad (5)$$

where Ω is the sample volume and $u_{k\sigma}$ is the periodic part of the Bloch function.

We use the same approximations for the envelope functions f here as in Chapter 2 for the indirect case. The impurity potential is taken to be that of a negative point charge screened by the static dielectric function plus a short range square well of variable strength. The square well is used to account for short range differences in the potential of different impurities. As a first approximation, the envelope functions f_h and f_e are assumed to have a 1S hydrogenic form with the electron and hole Bohr radii determined by a variational calculation. Corrections to the hole envelope functions, due primarily to nonparabolic valence band structure at large k, are taken into account by iterating the Hartree equation for the holes in the acceptor BE. As discussed in Chapter 2, the iterated envelope function is close to the hydrogenic one at small k, but drops off more slowly at large k. The integral in Eq. (4) is simplified by the fact that the function $f_e(k_e)$ is sharply peaked at the zone center. We replace $f_e(k_e)$ by a normalized delta function

$$f_e(k_e) \approx \frac{(2\pi)^3}{\sqrt{\pi b^3}} \delta(k_e) \tag{6}$$

where b is the electron Bohr radius.

For the overlap integrals U, we use the results of Kane obtained from degenerate k•p perturbation theory [12]. The discrete

sums in the matrix element (m_1 and m_2), the sum over final hole spins and bands and the average over initial states (labeled by J, M and σ_e) can be performed in a straightforward but tedious fashion; the result becomes

$$\frac{1}{\tau_A} = \frac{2\pi}{\hbar} \sum_{k_f} \left[\frac{1}{3} I_h(k_f)\, \delta(E_I - E_h(k_f)) + \frac{1}{6} I_\ell(k_f)\, \delta(E_I - E_\ell(k_f)) + \frac{1}{6} I_S(k_f)\, \delta(E_I - E_S(k_f)) \right] \quad (7)$$

where h, ℓ and S refer to transitions in which this final state hole is in the heavy hole, light hole and split-off bands, respectively.

The integrals I are given by

$$I_h(k_f) = \left(\frac{1}{\pi b^3}\right) \left| \sum_{k'} \frac{f_h(k_f - k')\, f_h(k')}{\varepsilon |k'|^2}\, a_{v_2}(k')\, (\hat{k}_f \cdot \hat{k}') \right|^2 \quad (8a)$$

$$I_\ell(k_f) = \left(\frac{1}{\pi b^3}\right) \left| \sum_{k'} \frac{f_h(k_f - k')\, f_h(k')}{\varepsilon |k'|^2}\, a_{v_2}(k')\, (\hat{k}_f \cdot \hat{k}') \right. \quad (8b)$$

$$\left. \left[a_{v_2}(k_f - k')\, a_{v_2}(k_f) + b_{v_2}(k_f - k')\, b_{v_2}(k_f) + c_{v_2}(k_f - k')\, c_{v_2}(k_f) \right] \right|^2$$

$$I_S(k_f) = \left(\frac{1}{\pi b^3}\right) \left| \sum_{k'} \frac{f_h(k_f-k')\, f_h(k')}{\varepsilon |k'|^2} a_{v_2}(k') \left(\hat{k}_f \cdot \hat{k}'\right) \right.$$

$$\left. \left[a_{v_2}(k_f-k')\, a_{v_3}(k_f) + b_{v_2}(k_f-k')\, b_{v_3}(k_f) + c_{v_2}(k_f-k')\, c_{v_3}(k_f)\right] \right|^2 \tag{8c}$$

Here $\hat{k}_f$ and $\hat{k}'$ are unit vectors, and the functions a_{v_i}, b_{v_i} and c_{v_i} are those defined by Kane [(12)].

The form for the iterated hole envelope function is the same as that used in Chapter 2 for the Auger transitions in indirect band gap materials

$$f_h(k) = \frac{e^2}{\varepsilon} \frac{4\pi}{\sqrt{\pi a^3}} \left(\frac{1}{E(k) + E_B}\right)$$

$$\left[\frac{1}{k^2+9/a^2} + \frac{6}{a^2(k^2+9/a^2)^2} + \frac{V R^3}{6\, e^2/\varepsilon}\right] \tag{9}$$

where a is the hole Bohr radius, E_B is the BE localization energy, V is the depth of the short range square well and R is the radius of the short range square well (taken to be half the nearest neighbor distance). The one hole energy (E(k)) was taken as a spherical average of the heavy hole band from a tight binding band structure calculation joined continuously to the parabolic effective mass

result at small k. The tight binding parameters for HgTe and CdTe were taken from Ref. (16); those for GaAs are from Ref. (17). The band structure for the HgCdTe alloy was calculated in a virtual crystal approximation. The integrations in the matrix elements of Eq. (8) were evaluated numerically. The final state integral in Eq. (7) was evaluated numerically; the final state hole energies were taken from a tight binding band structure calculation. The input parameters used in the calculation are summarized in Table I.

In radiative recombination of the acceptor BE, the final state is the neutral acceptor with a wavefunction of the form

$$|F> = \sum_{k} F\ (k)\ \Psi(kn) \tag{10}$$

where $\Psi(kn)$ is a Slater determinant with the hole state labeled by (k,n) empty and F(k) is the hole envelope function. The radiative decay rate can be expressed in terms of oscillator strengths by

$$\frac{1}{\tau_R} = \left(\frac{g_{BE}}{g_A}\right) \frac{e^2 2\omega^2 n}{c^3 m}\ f \tag{11}$$

where g_{BE} is the degeneracy of the BE (12), g_A is the degeneracy of the acceptor (4) $\hbar\omega$ is the photon energy, n is the index of refraction and the oscillator strength is given as

$$f - \frac{2}{\hbar\omega m}\ |<I|P_Z|F>|^2 \tag{12}$$

Here Eq. (12) is to be summed over the 12 degenerate BE states and

TABLE I. Parameters used in the calculation. All symbols are defined in the text.

	$Hg_{1-x}Cd_xTe$	GaAs
P^2	(18+3X) eV [+a]	25.7 eV [a]
ε	15.1 - 4.5X [b]	12.53 [c]
m_h	0.45 m [d]	0.36 m [g]
m_e		0.067 m [a]
Δ	(1.00-0.24X) eV [+e]	0.35 eV [f]
Eg	(1.79X-0.26) eV [+e]	1.51 eV [f]

+ Linearly interpolated between the HgTe and CdTe values

a P. Lawaetz, Phys. Rev. B4, 3460 (1971).

b J. J. Dubowski, Phys. Stat. Sol.(b) 85, 663 (1978).

c K. G. Hambleton, C. Hilson, and B. R. Holeman, Proc. Phys. Soc. 77, 1147 (1961).

d A. Jedrzejczak and T. Kietl, Phys. Stat. Sol. (b) 79, 691 (1977).

e Ref. 16.

f J. R. Chelikowsky and M. L. Cohen, Phys. Rev. B14, 556 (1976).

g Fit to Zn acceptor binding energy E_A = 31 meV.

averaged over the 4 degenerate acceptor states. To evaluate the oscillator strength we use hydrogenic envelope functions

$$F(k) = \left(\frac{\pi}{a_A}\right)^{1/2} \frac{8}{\left[k^2 + 1/a_A{}^2\right]^2} \qquad (13)$$

where a_A is the acceptor Bohr radius and similar forms with Bohr radii b and a, for the electron and the holes in the BE. The radiative rate is not sensitive to the large k part of the hole envelope function so it is not necessary to use the iterated form for the hole envelope function to calculate radiative rates. The calculation of the oscillator strength from Eq. (12) is straightforward and the result is

$$f = \frac{2}{\hbar\omega m} |<S|P_Z|Z>|^2 \left[\frac{8}{(1 + a_{A/a})^3} \left(\frac{a_A}{a}\right)^{3/2}\right]^2$$

$$\times \left[\frac{8}{(1 + b/a)^3} \left(\frac{b}{a}\right)^{3/2}\right]^2 \qquad (14)$$

IV. RESULTS

The results of the calculation for Auger and radiative lifetimes in HgCdTe as a function of band gap (composition) are shown in Fig. (1). The solid curves correspond to hydrogenic acceptors ($VR^3=0$) and the dashed curve to a deeper acceptor modeled by $VR^3 = 16.5$ eV $\mathring{A}^3$. The binding energy of the acceptors depends somewhat on the composition because of the compositional dependence of ε. For the hydrogenic acceptor the binding energy goes from $E_B = 31$ meV in the smallest gap case considered to $E_B = 46$ meV in the largest gap case; the binding energy of the deeper acceptor varies between $E_B = 38$ meV and $E_B = 59$ meV. The Auger lifetime has a local minimum at $Eg \approx 0.2$ eV; it increases for smaller Eg because the density of final hole states and the electron-hole overlap in space becomes small. The increase in the Auger lifetime for $Eg \approx 0.2$ eV is due to the larger values of k_f and the decreased amplitude for the BE wavefunction to contain these larger wavevectors. The sudden decrease in the Auger lifetime at $Eg \approx 0.9$ eV is due to the fact that transitions in which the final state hole is in the split-off band first become possible at this point. The Auger lifetime for the deeper acceptor is shorter than that for the hydrogenic acceptor because of the greater spread of the BE wavefunction in k-space for the deeper acceptor. The results for the radiative lifetimes in the

HgCdTe case are also shown in Fig. (1). The radiative lifetime decreases monotonically as the band gap is increased because of the larger density of photon states and increased electron-hole overlap in the larger gap material. The radiative lifetime is larger for the deeper acceptor than the hydrogenic acceptor because the electron-hole overlap is greater for the shallow acceptor. For band gap greater than about 0.35 eV for the hydrogenic acceptor and greater than about 0.43 eV for the deeper acceptor, the lifetime is dominated by radiative recombination; for smaller gaps, the lifetime is dominated by Auger recombination.

The results for the Auger and radiative lifetimes in GaAs as a function of impurity binding energy are shown in Fig. (2). The hydrogenic acceptor in this case has a binding energy of 31 meV (corresponding to the experimental value for the Zn acceptor in GaAs [18]). The radiative lifetime increases as the acceptor binding energy increases because the electron-hole overlap is decreased with increasing acceptor binding energy. The Auger lifetime decreases with increasing acceptor binding energy because of an increased spread of the BE wavefunction in k-space for the deeper impurities. The radiative transition rate is much faster than the Auger rate for reasonably shallow impurities. The calculated value of the acceptor BE radiative lifetime for the hydrogenic acceptor is 3.1 nsec; experimentally a value of 1.6 ± 0.6 nsec [11] is found for an exciton bound to a shallow acceptor in GaAs.

Fig. 1. Auger and radiative acceptor bound exciton lifetimes as a function of band gap (composition) in the HgCdTe alloy system. The solid curves are for hydrogenic acceptors and the dashed curves are for a deeper acceptor where the impurity potential is taken to be that of a screened point charge plus a short range attractive (for holes) square well. The radius of the square well (R) was taken to be half the nearest neighbor distance and V is the depth of the square well.

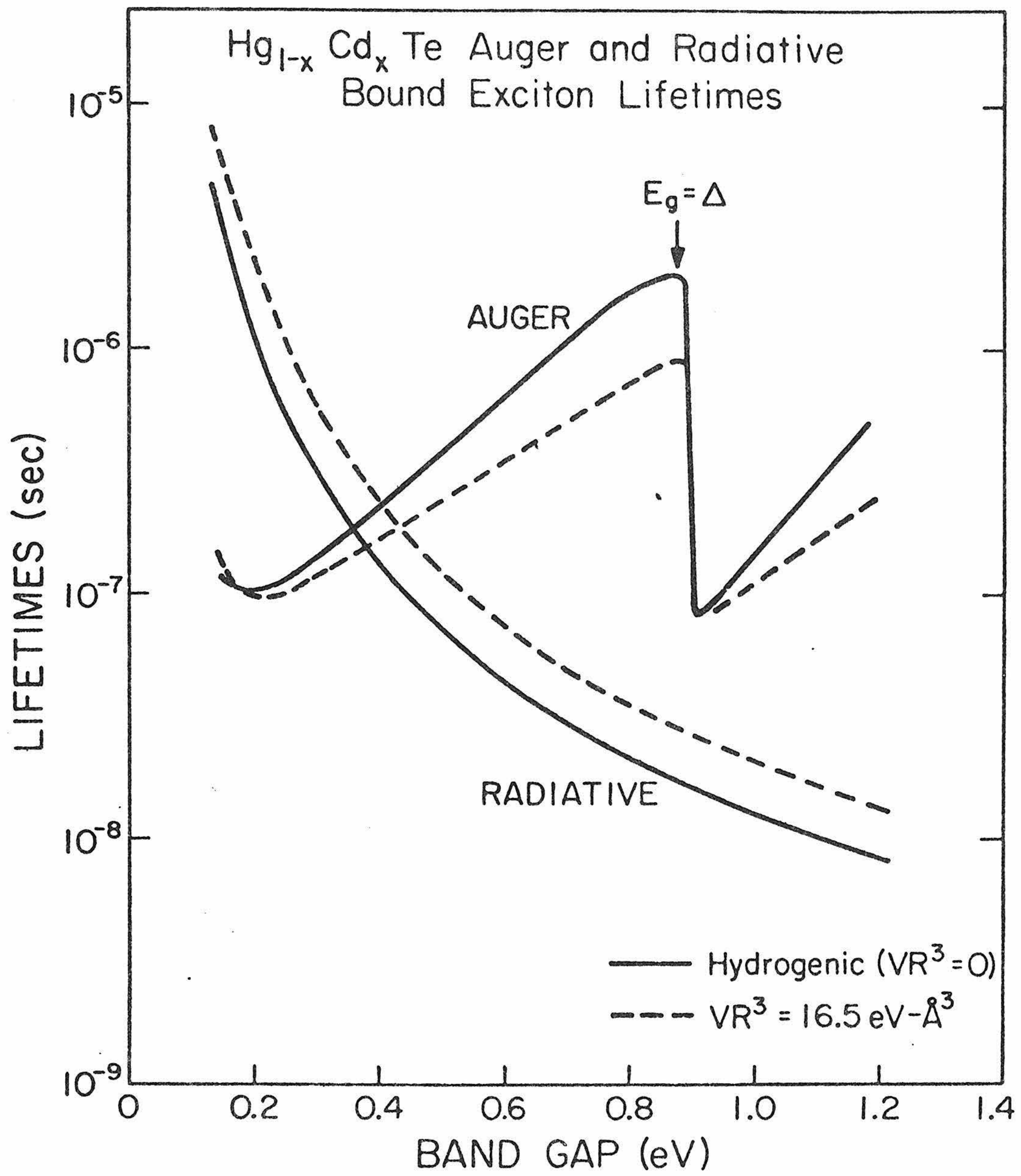
Hg1-x Cdx Te Auger and Radiative
Bound Exciton Lifetimes
Eg = Δ
AUGER
RADIATIVE
LIFETIMES (sec)
BAND GAP (eV)
Hydrogenic (VR3 = 0)
VR3 = 16.5 eV-Å3
10-5
10-6
10-7
10-8
10-9
0
0.2
0.4
0.6
0.8
1.0
1.2
1.4

Fig. 2. Auger and radiative acceptor bound exciton lifetimes as a function of acceptor binding energy in GaAs. The acceptor binding energy was varied by adjusting the strength of a short range square well added to a screened point charge to form the acceptor potential. A binding energy of 31 meV corresponds to a hydrogenic acceptor (no square well).

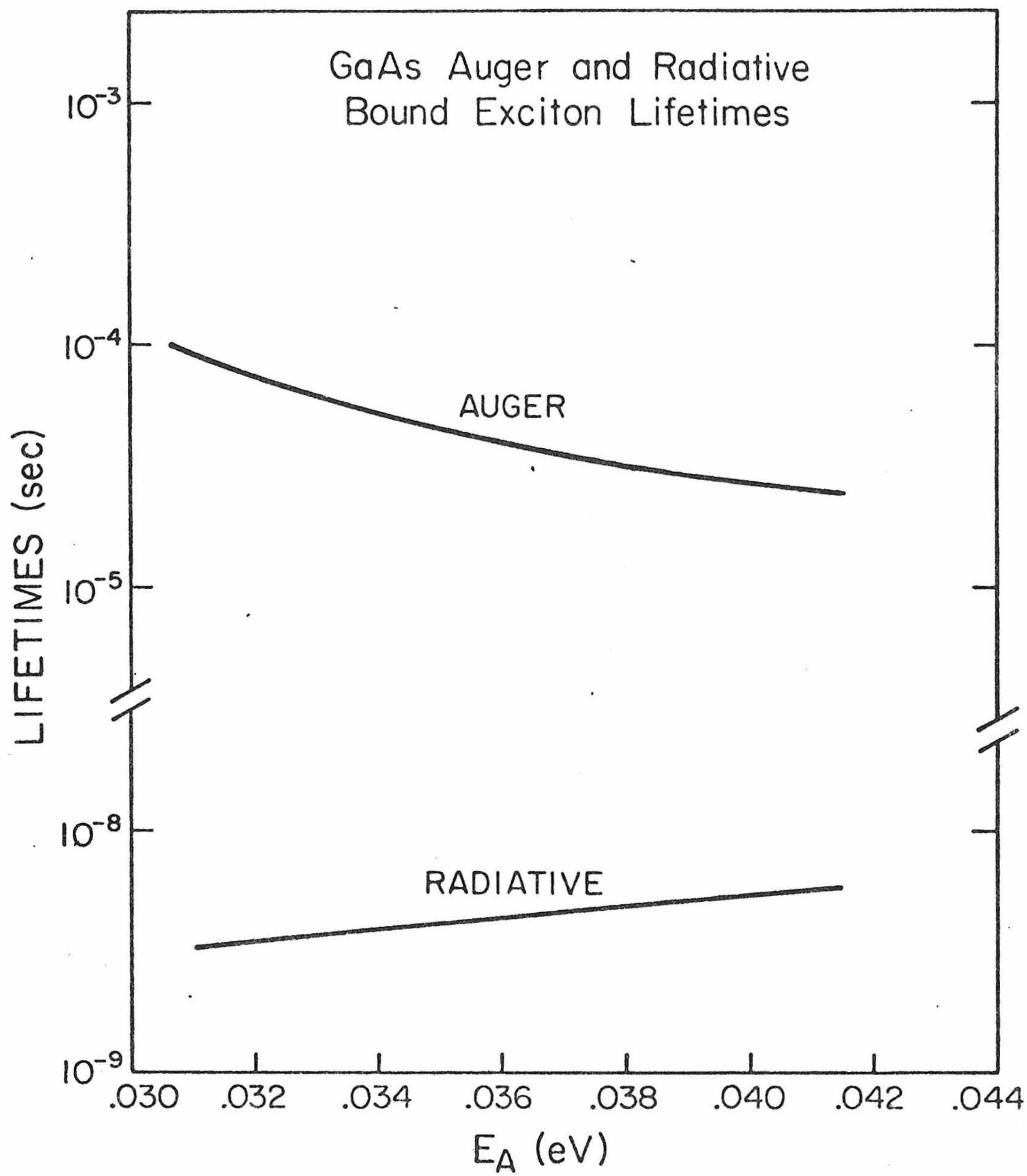
GaAs Auger and Radiative
Bound Exciton Lifetimes
10^{-3}
10^{-4}
10^{-5}
10^{-8}
10^{-9}
LIFETIMES (sec)
AUGER
RADIATIVE
.030
.032
.034
.036
.038
.040
.042
.044
E_A (eV)

V. SUMMARY AND CONCLUSIONS

We have presented a calculation of Auger and radiative transition rates for acceptor BE in HgCdTe and GaAs. The purpose of the work was to investigate the dependence of the Auger and radiative transition rates of acceptor BE in direct gap materials on acceptor binding energy and semiconductor band gap. For HgCdTe we find that the radiative lifetimes decrease with increasing energy gap, while the Auger lifetimes increase with energy gap except for: $Eg \gtrsim \Delta$, where the split-off band first becomes accessible to the final state hole; and at $Eg \lesssim 0.2$ eV where the electron-hole overlap and density of final states becomes small. The Auger and radiative lifetimes cross for hydrogenic acceptors in HgCdTe at Eg - 0.35 eV; radiative decay dominates for larger band gaps and Auger decay dominates for smaller gaps. As the acceptor binding energy increases, the cross over point between the two rates moves to higher band gaps. For GaAs, the radiative rate is much faster than the Auger rate. As the acceptor binding energy is increased, the radiative rate decreases and the Auger rate increases. It is possible that the Auger rate could become dominant for very deep acceptors, but for reasonably shallow acceptors the Auger rate makes a negligible contribution to the BE lifetime in GaAs.

REFERENCES

1. P. T. Landsberg, Phys. Status Solidi 41, 457 (1970).
2. P. T. Landsberg and M. J. Adams, J. Lumin. 7, 3 (1973).
3. D. F. Nelson, J. D. Cuthbert, P. J. Dean, and G. D. Thomas, Phys. Rev Lett. 17, 1262 (1962).
4. P. J. Dean, R. A. Faulkner, S. Kimura, and M. Ilegems, Phys. Rev. B4, 1926 (1971).
5. S. A. Lyon, G. C. Osbourn, D. L. Smith, and T. C. McGill, Solid State Commun. 23, 425 (1977).
6. W. Schmid, Phys. Status Solidi (b), 84, 529 (1977).
7. E. I. Rashba and G. E. Gurgenishvili, Fiz. Tverd. Tela, 4, 1029 (1962) [Sov. Phys. Solid State, 4, 759 (1962)].
8. E. I. Rashba, Fiz. Tekh. Poluprovodn., 8, 1241 (1974) [Sov. Phys. Semicond. 8, 807 (1974)].
9. C. H. Henry and K. Nassau, Phys. Rev. B1, 1628 (1970).
10. C. J. Hwang and L. R. Dawson, Solid State Commun. 10, 443 (1972).
11. C. J. Hwang, Phys. Rev. B8, 646 (1973).
12. E. O. Kane, J. Phys. Chem. Solids 1, 249 (1975).
13. C. T. Elliott, I. Melngailis, T. C. Harmon, and A. G. Foyt, J. Phys. Chem. Sol. 33, 1527 (1972).
14. We treat the alloy in the virtual crystal approximation and neglect phonon assisted Auger recombination.
15. We neglect umklapp terms in Eq. (4). Such terms will give a

negligible contribution to the Auger rate because the wave-vector match ups will be very unfavorable.

16. J. N. Schulman and T. C. McGill (to be published).
17. D. J. Chadi, Phys. Rev. B16, 790 (1977).
18. W. Schairer and T. O. Yep, Solid State Commun. 9, 421 (1971).

CHAPTER 4

I. INTRODUCTION

At a sharp semiconductor-semiconductor interface, there is an abrupt change in the crystal potential. Carriers (electrons and holes) can be quantum mechanically reflected by this change in crystal potential even if they have enough energy to cross the interface. The possibility of quantum mechanical reflection at the interface was recognized in the earliest work on semiconductor heterojunctions [2]. However, there have been few attempts to calculate the transmission and reflection coefficients in these systems. If the interface is graded over a distance of several hundred angstroms, effective mass theory can be used [3-4]. However, effective mass theory is not appropriate for a rapidly changing potential such as occurs at an abrupt interface. To the author's knowledge, only one calculation has been made of quantum mechanical reflection and transmission coefficients at an abrupt semiconductor-semiconductor interface and this calculation was performed using a simple one-dimensional model [5].

In this chapter, we present a calculation of electron and hole transmission and reflection coefficients for abrupt and compositionally graded (100) $GaAs-Ga_{1-x}Al_xAs$ interfaces. We consider semi-infinite crystals of the two semi-conductors joined at a perfect, atomically abrupt and graded interface. The empirical tight binding method was used to perform the calculation. We solve

the tight binding equations to find the one electron eigenstate near the interface. An eigenstate consists of an incoming Bloch function in one material, reflected and transmitted Bloch functions and evanescent states [6,7] which decay exponentially away from the interface. The transmission and reflection coefficients are determined from the amplitudes of the transmitted and reflected Bloch states and the group velocity of carriers in these states.

II. THEORETICAL APPROACH

We consider, as a model for our calculations, an abrupt or graded interface between two semi-infinite crystals of materials with the same crystal structure and a perfect lattice match. We assume that there is no structural rearrangement at the interface. This model is fairly realistic for GaAs-$Ga_{1-x}Al_xAs$ interfaces fabricated by molecular beam epitaxy, since GaAs and AlAs have a small lattice mismatch and are chemically similar. Transfer of charge density across the interface and any band bending in the two materials have not been included in our calculations. However, slab calculations for the GaAs-AlAs system show that charge transfer is small and occurs only at the interface layer [8,9]. Band bending in lightly doped materials can be accounted for using the effective mass approximation; it affects the carriers on a distance scale which is large compared to the one we are considering and does not

modify the processes that we discuss. As an input to the calculations, we include empirical valence band offsets for the GaAs-$Ga_{1-x}Al_xAs$ system equal to 15% of the direct gap differences between $Ga_{1-x}Al_xAs$ and GaAs [1]. Because the dielectric constants of GaAs and AlAs are similar, we have neglected the effects of induced image charges on the free carriers.

Our problem is to construct eigenstates of the interface system which represent the transmission and reflection of an incoming free carrier at the interface. While this problem is somewhat analogous to the 3-dimensional scattering of a free particle at a 2-dimensional (plane) step potential, it contains the interesting feature that the incoming carrier can in some cases reflect and/or transmit at the interface into more than one Bloch state. For example, an electron approaching the interface from the AlAs side and located near the conduction band minimum at X (for the minimum which is normal to the interface) can be transmitted into a Bloch state near the Γ conduction band minimum or the X conduction band relative minimum in GaAs [10]. We would like to construct the eigenstates on each side of the interface out of linear combinations of eigenstates of the bulk materials with the same energy E. Because the periodicity of the crystal in the plane parallel to the interface remains intact, k parallel to the interface ($\vec{k}^{||}$) remains a good quantum number. Since $\vec{k}^{||}$ is conserved, we need include only those bulk states that have the same component $\vec{k}^{||}$ as the incoming state, but any component

of k normal to the interface ($k^{\perp}$) that corresponds to a state of energy E. In general, these $k^{\perp}$ can take on both real and complex values, with the real $k^{\perp}$ producing Bloch states and the complex $k^{\perp}$ producing evanescent states [6,7]. The evanescent states are bulk eigenstates that exponentially decay in one direction parallel to $k^{\perp}$ and exponentially grow in the opposite direction. In the bulk material these states are not allowed because they do not satisfy the bulk boundary conditions. In the interface system, the evanescent states that exponentially decay in the normal direction away from the interface are allowed and must be included in the solution. However, evanescent states do not carry flux in the direction normal to the interface, and so only the Bloch states can contribute to reflection or transmission. Our general solution takes the form

$$\Psi = \begin{cases} \phi^{E}_{k_I^{||},k_I^{\perp}} + \sum_{\alpha} A_{\alpha}\, \phi^{E}_{k_I^{||},k_{1\alpha}^{\perp}} & \text{side 1} \\ \\ \sum_{\alpha} B_{\alpha}\, \phi^{E}_{k_I^{||},k_{2\alpha}^{\perp}} & \text{side 2} \end{cases} \tag{1}$$

where $\phi^{E}_{k_I^{||},k_I^{\perp}}$ is the incident Bloch state (which carries flux towards the interface) with energy E and $\vec{k}_I = \vec{k}_I^{||} + \vec{k}_I^{\perp}$, $\phi^{E}_{k_I^{||},k_{1\alpha}^{\perp}}$ and $\phi^{E}_{k_I^{||},k_{2\alpha}^{\perp}}$ are the outgoing Bloch states which carry flux away from

the interface (real $k_{1\alpha}^{\perp}$ or $k_{2\alpha}^{\perp}$) or decaying evanescent states (complex $k_{1\alpha}^{\perp}$ or $k_{2\alpha}^{\perp}$) for sides 1 and 2, and A_α and B_α are expansion coefficients. The eigenstate is determined by solving the Schrodinger Equation for the expansion coefficients A_α and B_α.

To proceed further it is necessary to have explicit forms for the Bloch and evanescent states in the two bulk materials. We obtain these in a tight binding form, using one s and three p (p_x, p_y, p_z) type atomic orbitals per atomic site. In particular we take (11)

$$\phi^E_{k^{||},k^{\perp}}(\vec{r}) = \sum_{n,i} C_n^{\vec{k}}(\vec{R}_i)\, e^{i\vec{k}\cdot\vec{R}_i}\, F_n(\vec{r}-\vec{R}_i) \qquad (2)$$

where $\phi^E_{k^{||},k^{\perp}}(\vec{r})$ is the Bloch or evanescent state of energy E and $\vec{k} = \vec{k}^{||} + \vec{k}^{\perp}$, $F_n(\vec{r}-\vec{R}_i)$ is the atomic orbital of type $n=(s,p_x,p_y,p_z)$ at site $\vec{R}_i$, and the $C_n^k(\vec{R}_i)$ are atomic expansion coefficients. The $C_n^k(\vec{R}_i)$ are found by solving the one electron Schrodinger equation with the tight binding Hamiltonian:

$$\sum_{n,i} C_n^{\vec{k}}(\vec{R}_i)\, e^{i\vec{k}\cdot\vec{R}_i} \left[\langle F_p(\vec{r}\ \vec{R}_o)|H|F_n(\vec{r}-\vec{R}_i)\rangle - E\ \delta_{pn}\delta_{\vec{R}_o,\vec{R}_i} \right] = 0 \qquad (3)$$

The tight binding parameters $\langle F_p(\vec{r}-\vec{R}_o)|H|F_n(\vec{r}-\vec{R}_i)\rangle$ characterize the bulk materials and are inputs to the calculation. We discuss the details of our treatment of these parameters for GaAs, AlAs, and $Ga_{1-x}Al_xAs$ at the end of this section. Once the $C_n^{\vec{k}}(\vec{R}_i)$ are determined from Eq. (3), Eq. (2) can be substituted into Eq. (1), producing

$$\psi = \begin{cases} \sum_{n,i} C_n^{k_I^{||},k_I^{\perp}}(R_i)\, e^{i\vec{k}_I\cdot\vec{R}_i} F_n^1(r-R_i) \\ + \sum_\alpha A_\alpha \sum_{n,i} C_n^{k_I^{||},k_{1\alpha}^{\perp}}(R_i)\, e^{i\vec{k}_{1\alpha}\cdot\vec{R}_i} F_n^1(r-R_i) & \text{side 1} \\ \sum_\alpha B_\alpha \sum_{n,i} C_n^{k_I^{||},k_{2\alpha}^{\perp}}(R_i)\, e^{i\vec{k}_{2\alpha}\cdot\vec{R}_i} F_n^2(r-R_i) & \text{side 2} \end{cases} \tag{4}$$

Taking the overlap of the one electron Schrodinger equation with all of the atomic orbitals in the crystal produces an infinite set of equations:

$$\sum_{n,i}\left(C_n^{k_I^{||},k_I^{\perp}}(R_i)e^{ik_I\cdot\vec{R}_i}+\sum_\alpha A_\alpha C_n^{k_I^{||},k_I^{\perp}}(R_i)e^{ik_{1\alpha}\cdot\vec{R}_i}+\sum_\alpha B_\alpha C_n^{k_I^{||},k_{2\alpha}^{\perp}}(R_i)e^{ik_{2\alpha}\cdot\vec{R}_i}\right)$$

$$\times\left(\langle F_p(r-R_j)|H|F_n(r-R_i)\rangle - E\,\delta_{pn}\delta_{R_jR_i}\right) = 0 \tag{5}$$

where it is understood that the atomic functions $F_n(r-R_i)$ for side 1(2) go with the bulk states on side 1(2). Although Eqs. (5) are an infinite set, all but a finite number of distinct equations in the set are automatically satisfied. In particular, for any atomic

site $\vec{R}_j$ that is far enough from the interface that it does not interact with the atoms on the other side, the equation becomes a bulk equation which each bulk function in Ψ already satisfies (by Eq. (3)). This simply means that far enough from the interface, each material has a potential equal to that in the bulk eigenstates with the same energy is also an eigenstate in this region. The remaining equations are for the coefficients of $F_p(\vec{r}-\vec{R}_j)$ at sites $\vec{R}_j$ on either side of the interface close enough to interact with atomic functions on the other side. There are still infinitely many such equations, but the periodicity of the crystal in the plane parallel to the interface results in only a finite number of these being distinct.

The number of distinct nontrivial equations in Eqs. (5) as well as the number of bulk solutions with a given E and $\vec{k}^{||}$ depends on (i) the orientation of the interface plane (i.e., the direction of $k^{\perp}$) and (ii) the number of nearest neighbor groups of atoms that are allowed to interact with a given atom. In the next section we show that if m is the number of parallel planes of atoms normal to $k^{\perp}$ that can interact with a chosen plane of atoms normal to $k^{\perp}$ not counting the chosen plane itself (m is even), then the number of states that have a particular E and $k^{\perp}$ is equal to $(m \cdot n)$ where n is the number of orbitals per atom. For GaAs and AlAs, there are 4m such states. If we include up to 2nd nearest neighbor interactions, and we take the interface to be a (100) plane, then m=4

and there are 16 states with a given E and $k^{||}$. The evanescent states come in pairs ($k^{\perp}$ and $k^{\perp *}$), and therefore there are an even number of Bloch states. Assuming all of the Bloch states carry non-zero flux, half of them carry flux in the wrong direction and are discarded. Of the remaining evanescent states, half of these exponentially grow away from the interface and are also discarded. This leaves 8 (2m in general) states for each material, so that there are 16 coefficients (4m in general) to determine. For the case we have been considering, we assume that an imaginary plane bisects the crystal so that all atoms are on either side of the plane (but not on it). Then the number of distinct equations is also 16 (4m in general). For the case of a graded interface in which a number of planes of atoms between the two bulk materials are not considered to be part of either of the bulk materials, but have the same lattice structure, then Eq. (1) must be generalized to read

$$\psi = \begin{cases} \phi^{E}_{k_I^{||},k_I^{\perp}} + \sum\limits_{\alpha} A_\alpha \phi^{E}_{k_I^{||},k_{1\alpha}^{\perp}} & \text{side 1} \\ \sum\limits_{n,i} b_n(R_i) F_n(\vec{r}-\vec{R}_i)\, e^{i\vec{k}_I^{||}\cdot\vec{R}_i} & \text{compositionally graded region} \\ \sum\limits_{\alpha} B_\alpha \phi^{E}_{k_I^{||},k_{2\alpha}^{\perp}} & \text{side 2} \end{cases} \tag{6}$$

For this case the number of parameters to determine and the number of equations is 4m + 4r, where r is the number of planes of atoms in the graded region. In either case the result is a NxN set of linear inhomogeneous equations. The inhomogeneous terms are just the parts of Eq. (5) due to the incoming state. Since such a system of equations will have a non-trivial solution if the determinant of the coefficient matrix is nonzero and the inhomogeneous terms are not all zero, scattering eigenstates are guaranteed to exist for any energy at which incoming Bloch states exist and for which the coefficient matrix determinant is non-zero.

At this point we note that the formalism we have described can be applied to the case of interface states. An interface state of particular interest would be one that has an energy in the gap of both materials, so that it contains only evanescent states. The set of equations to solve for this case are the same as Eq. (5) except that there is no incoming Bloch state, and the NxN set of equations is homogeneous. Interface states can therefore exist only for E and $k^{||}$ such that the determinant of the coefficient matrix in Eq. (5) is zero. We have carried out a search for interface states in the gap of the GaAs-AlAs system and have found that there are none. This lack of interface states in the gap for the (100) interface of GaAs-AlAs is consistent with the results of previous calculations [8].

Once Eq. (5) has been solved for the A_α and B_α for a given

incoming Bloch state, the transport coefficients for the various reflection and transmission Bloch states are computed using the expressions

$$R_\alpha = |A_\alpha|^2 \left|\frac{\partial E_\alpha}{\partial k\perp}\right| \Big/ \left|\frac{\partial E_I}{\partial k\perp}\right|$$
$$T_\beta = |B_\beta|^2 \left|\frac{\partial E_\beta}{\partial k\perp}\right| \Big/ \left|\frac{\partial E_I}{\partial k\perp}\right| \qquad (7)$$

where $\left|\frac{\partial E_\alpha}{\partial k\perp}\right|$ is the group velocity for the Bloch state α normal to the interface. The transport coefficients satisfy the conservation of flux relation

$$\sum_\alpha R_\alpha + \sum_\beta T_\beta = 1 \qquad (8)$$

To carry out the calculation of transmission and reflection coefficients it is necessary to have tight binding matrix elements that represent the bulk materials GaAs and $Ga_{1-x}Al_xAs$. The parameters for GaAs and AlAs are chosen to fit the bulk band structures to pseudopotential results [12,13]. The parameters obtained from fitting are presented in Table I and the resulting band structures are presented in Fig. (1). The alloy $Ga_{1-x}Al_xAs$ is treated in a virtual

TABLE I. Tight-binding parameters for GaAs and AlAs determined by fitting to bulk pseudopotential calculations. The notation is that of Ref. (11). The subscripts 0 and 1 designate anion and cation, respectively. All parameters are in units of eV.

	GaAs	AlAs
$E_{SS}(000)$.	-6.953	-6.150
$E_{SS}(000)_1$	-2.254	-1.274
$E_{XX}(000)_0$	1.338	2.168
$E_{XX}(000)_1$	1.839	1.588
$E_{SS}(\frac{1}{2}\frac{1}{2}\frac{1}{2})$	-1.774	-1.817
$E_{SX}(\frac{1}{2}\frac{1}{2}\frac{1}{2})_{01}$	1.304	1.326
$E_{SX}(\frac{1}{2}\frac{1}{2}\frac{1}{2})_{10}$	1.121	1.001
$E_{XX}(\frac{1}{2}\frac{1}{2}\frac{1}{2})$	0.479	0.515
$E_{XY}(\frac{1}{2}\frac{1}{2}\frac{1}{2})$	1.447	1.237
$E_{XY}(110)_0$	0.295	0.321
$E_{XY}(110)_1$	0.195	0.264
$E_{XX}(110)_0$	0.200	0.189
$E_{XX}(110)_1$	0.207	0.220
$E_{XX}(011)_0$	-0.347	-0.492
$E_{XX}(011)_1$	-0.282	-0.218
$E_{SX}(110)_0$	0.001	0.026
$E_{SX}(110)_1$	0.018	0.059
$E_{SS}(110)_0$	-0.002	-0.007
$E_{SS}(110)_1$	-0.178	-0.144

Fig. 1. Bulk band structures of GaAs and AlAs obtained using tight binding parameters given in Table I.

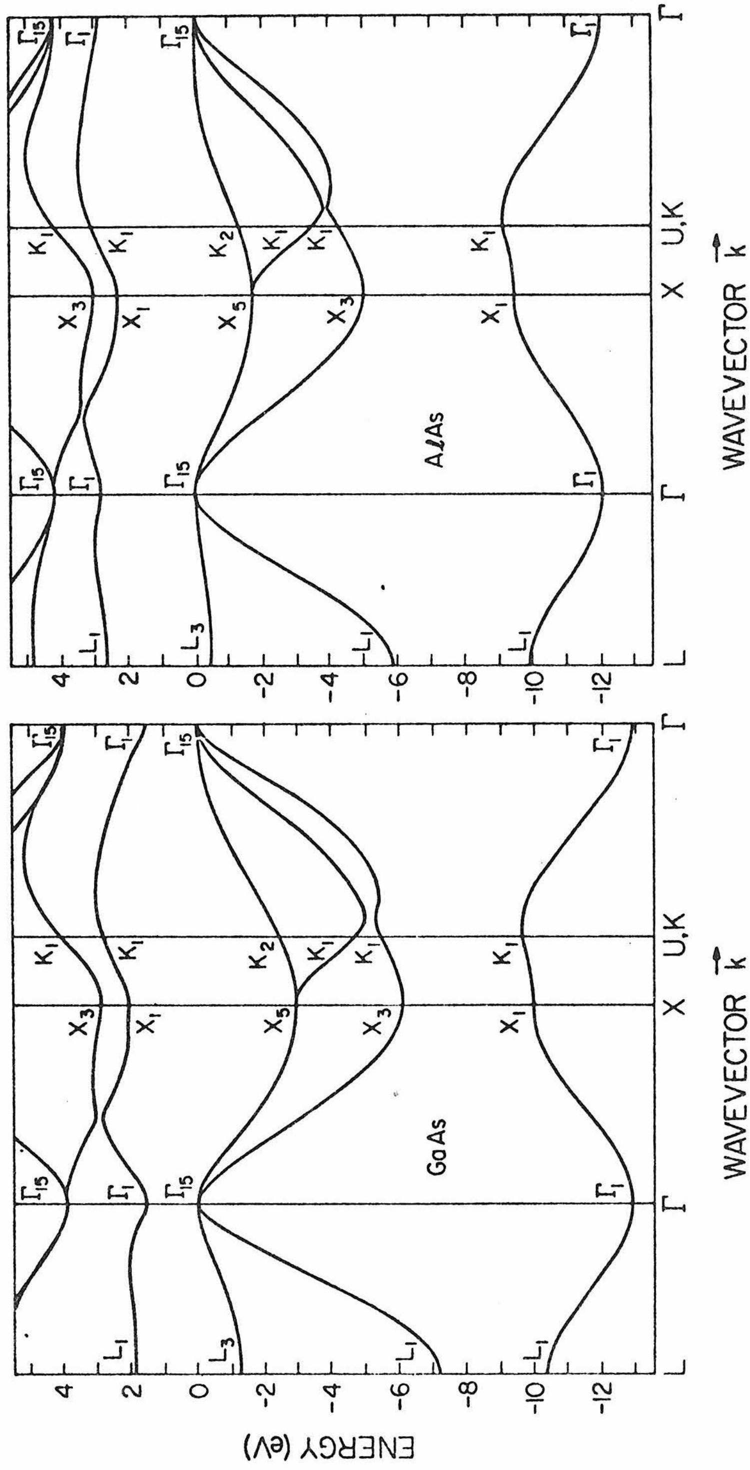
ENERGY (eV)
WAVEVECTOR k
GaAs
AℓAs
L
Γ
X
U,K
L_1
L_3
Γ_1
Γ_{15}
X_1
X_3
X_5
K_1
K_2
4
2
0
-2
-4
-6
-8
-10
-12

crystal type approximation in the sense that the alloy parameters are taken to be weighted averages of the GaAs and AlAs parameters. These alloy parameters yield band structures that vary linearly with alloy concentration x from GaAs to AlAs.

For the abrupt case, the central plane of As atoms (those with Ga neighbors on one side and $Ga_{1-x}Al_x$ neighbors on the other) are treated as As in an $Ga_{(1-x/2)}Al_{x/2}As$ alloy. The atomic planes in the compositionally graded region between the GaAs and $Ga_{1-x}Al_xAs$ bulk regions are treated as alloys of composition x', where x' varies linearly from zero at the GaAs side to x at the $Ga_{1-x}Al_xAs$ side. The overlaps of $Ga_{1-x'}Al_{x'}$ orbitals with second nearest neighbor $Ga_{1-x''}Al_{x''}$ orbitals are taken as a weighted average of Ga-Ga, Al-Al and Ga-Al overlaps. We take the Ga-Al second nearest neighbor parameters to be the average of Ga-Ga and Al-Al bulk second nearest neighbor parameter. Since we treat the central plane of As atoms differently than the bulk in the abrupt interface case, Eq. (6) was used to compute the coefficients A_α and B_α for both the abrupt and compositionally graded interfaces.

Although the parameters we use to characterize GaAs, AlAs, and the alloy $Ga_{1-x}Al_xAs$ are not necessarily the only ones possible, they are reasonable sets that give satisfactory fits to the bulk pseudopotential results for the bands of interest. Since the bulk Bloch states of interest are all near critical points (X, Γ) at which the symmetry is both known and properly represented by the tight

binding states, the tight binding form of these states will be qualitatively correct. For this reason, we expect that the results we obtain are qualitatively independent of our particular sets of parameters.

III. EVANESCENT STATES

Because we require explicit forms for the evanescent states in our calculations, and because these states are of some intrinsic interest of themselves, we have included in this section a discussion of the properties of these states and the way in which we obtain them. The evanescent states are assumed to be made up of linear combinations of atomic orbitals of the form in Eq. (2) where $k^{\perp}$ is complex. For a given E and $k^{||}$, we must first find the possible values of $k^{\perp}$ for which a state of the form in Eq. (2) satisfies the Schrodinger equation. To do this we set

$$\det(H_{p;\ell}(\vec{k}) - \delta_{p\ell}E) = 0 \qquad (9)$$

where $H_{p;\ell}(\vec{k})$ is the usual tight binding matrix

$$H_{p;\ell}(\vec{k}) = \sum_j e^{i\vec{k}\cdot(\vec{R}_j+\vec{\tau}_\ell-\vec{\tau}_p)} \langle F_p(\vec{r}-\vec{\tau}_p)|H|F_\ell(\vec{r}-\vec{\tau}_\ell-\vec{R}_j)\rangle \qquad (10)$$

Here p and ℓ label atomic orbitals (orbital symmetry and atomic type),

$\vec{\tau}_p$ is the position of the atom in the unit cell and R_j is a translation vector. For fixed $\vec{k}^{||}$ and E, Eq. (9) is a polynonimial equation for the variable $\exp(ik^{\perp}R_0)$ where R_0 is the distance along the $k^{\perp}$ direction between the nearest planes of atoms. The order of the polynomial equation is (m•n) where m is the number of parallel planes of atoms normal to $k^{\perp}$ that interact with any chosen plane of atoms normal to $k^{\perp}$ (not including the chosen plane) and n is the number of orbitals per atom. In our case of first and second nearest neighbor interactions, $k^{\perp}$ normal to a (100) plane and four orbitals per atom, we have n and m both equal to four. Thus, there are sixteen possible values of $k^{\perp}$. From Eq. (9) we see that if $k^{\perp}$ is a solution, so is $k^{\perp *}$. Thus, there are an even number of evanescent states (half growing and half decaying) and an even number of Bloch states for any given E and $k^{||}$. Once the possible values of $k^{\perp}$ have been determined, the coefficients $C_n^{\vec{k}}(R_i)$ in Eq. (2) are found from Eq. (3) in the usual way.

We have generated evanescent states in the energy range of interest for $k^{||} = 0$ and $k^{\perp}$ along the Δ direction for GaAs and AlAs and show them in Fig. (2). The dashed and dotted lines plot the real part of $k^{\perp}$ as a function of energy for the evanescent states; the solid lines correspond to the usual Bloch states. The states in the figure belong to one of two symmetry types Δ_1 or Δ_5; for any energy there are 8 states of each symmetry type.

Fig. 2. Dispersion curves for Bloch and evanescent states for GaAs and AlAs along the Δ direction. The solid lines refer to the Bloch states. The other lines refer to the real part of k for the evanescent states. These other lines are extended in the directions indicated by the arrows.

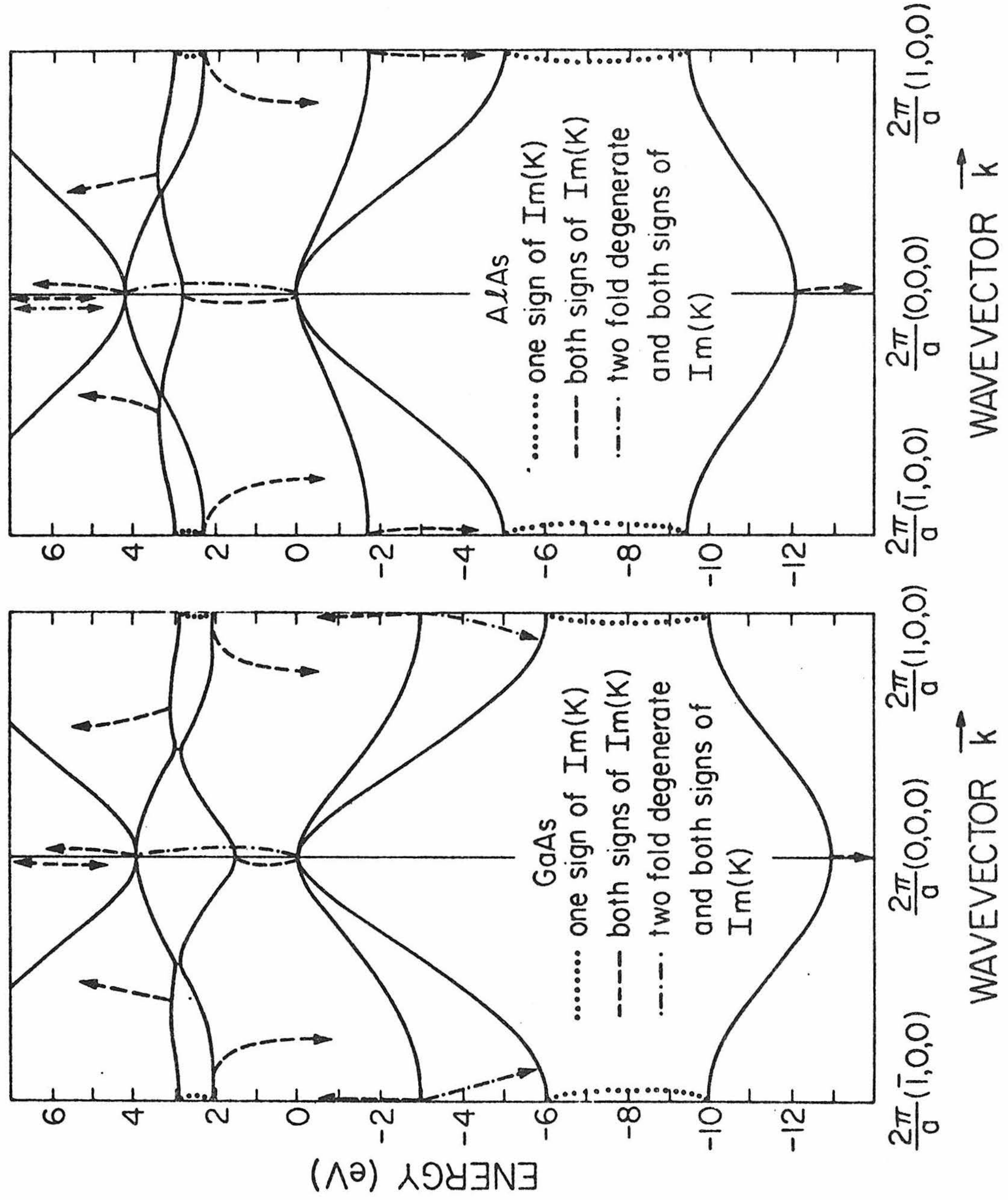
ENERGY (eV)
GaAs
one sign of Im(K)
both signs of Im(K)
two fold degenerate and both signs of Im(K)
AℓAs
one sign of Im(K)
both signs of Im(K)
two fold degenerate and both signs of Im(K)
WAVEVECTOR k
$\frac{2\pi}{a}(\bar{1},0,0)$
$\frac{2\pi}{a}(0,0,0)$
$\frac{2\pi}{a}(1,0,0)$
6
4
2
0
-2
-4
-6
-8
-10
-12

As discussed by Heine [6], the evanescent state energies as a function of k connect up to the Bloch state energies at the critical points of the Bloch state energies. The evanescent state energies approach Bloch state energies from below for minima and from above for maxima of the Bloch state energies. Only Bloch and evanescent states of the same symmetry can connect. This behavior is seen in Fig. (2). The imaginary part of $k^{\perp}$ goes to zero at the point where evanescent and Bloch state energies connect. For evanescent state energies more than about 1 eV from the energy at which the state connects with a Bloch state, the value of $\mathrm{Im}(k^{\perp})$ is rather large (greater than $1\mathrm{\AA}^{-1}$) and the state decays rapidly.

There are actually infinitely many evanescent states with a given E and $\vec{k}^{||}$ [6]. By constructing these states out of a restricted basis set, we produce only a finite number of them. Some of these are ones that connect up to the 8 energy bands produced by the tight binding basis set. The others have large values of $\mathrm{Im}(k^{\perp})$ and do not play an important role in our calculation [14].

IV. QUALITATIVE FEATURES OF CARRIER TRANSPORT COEFFICIENTS

The case of interest is one in which the incoming Bloch state is near a band extrema point (conduction band minimum for electrons, valence band maximum for holes). The outgoing flux carrying states consist of one or more reflected Bloch states and from zero to

several transmitted Bloch states, depending on the alloy concentration x and the incoming state considered. The transmission and reflection coefficients for these Bloch states will depend on the alloy concentration x, the distance over which the interface is graded, and the $k_I^{\perp}$ of the incoming state, for fixed $k^{||}$. The qualitative dependence of the transport coefficients on these parameters has simple and general features which we will now discuss.

We first notice that it is not necessary to consider transmission coefficients for carriers approaching the interface from both sides because these two processes are related by a theorem analogous to the reciprocity theorem of scattering theory. Consider a carrier approaching the interface from the left in a Bloch state of wave vector $\vec{k}_I$. Suppose that transmission into a Bloch state on the right with wavevector $\vec{k}_0$ is possible and that the transmission amplitude (see Eq. (4)) for the state on the right is $B(k_I;k_0)$. Then if we consider the process in which a carrier in the Bloch state of wavevector $-\vec{k}_0$ approaches the interface from the right, the transmission amplitude for the state $-\vec{k}_I$ on the left is given by (see appendix)

$$B(k_I;k_0) \left|\frac{\partial E_0}{\partial k^{\perp}}\right|_{k_0} = B(-k_0;-k_I) \left|\frac{\partial E_I}{\partial k^{\perp}}\right|_{k_I} \tag{11a}$$

Therefore, the transmission coefficients for the two processes are equal,

$$T(k_I;k_0) = T(-k_0;-k_I) \tag{11b}$$

We have a similar result for the reflection amplitudes and coefficients

$$A(k_I;k_o)\left|\frac{\partial E_0}{\partial k^{\perp}}\right|_{k_o} = A(-k_o;-k_I)\left|\frac{\partial E_I}{\partial k^{\perp}}\right|_{k_I} \tag{12a}$$

and

$$R(k_I;k_o) = R(-k_o;-k_I) \tag{12b}$$

We next consider the threshold behavior of the reflection and transmission coefficients. For fixed $\vec{k}^{||}$, there is a critical point $k^{\perp}$ such that $\partial E_I/\partial k^{\perp}_{IC}$ is zero. As $k^{\perp}_I$ approaches $k^{\perp}_{IC}$, there is a possible reflected state whose wavevector, $k^{\perp}_0$, also approaches $k^{\perp}_{IC}$. At $k^{\perp}_{IC}$, the "incoming state" carries no flux and the "reflected state" becomes identical with the "incoming state". In this case, the transport coefficients are not well defined. However, the expansion coefficients A_α and B_α are well defined. It is clear from Eq. (5) that $A_{k^{\perp}_{0C}}$ equals minus one and the other coefficients equal zero in this case. Thus the reflection coefficient for the state $k^{\perp}_0$ approaches unity as $k^{\perp}_I$ approaches $k^{\perp}_{IC}$. Indeed, transmission or reflection into other states is not possible since the "incoming

state" carries no flux and the other Bloch states of the necessary energy and $k^{||}$ would, in general, not have zero group velocity normal to the interface.

As $k_I^{\perp}$ moves away from $k_{IC}^{\perp}$, transmission (and reflection into states other than $k_0^{\perp}$) may become possible. To be specific consider electrons near the Γ minimum in $Ga_{1-x}Al_xAs$. The Γ minimum in GaAs is at lower energy than the Γ minimum in $Ga_{1-x}Al_xAs$. As $k_I^{\perp}$ approaches zero ($k^{||} = 0$), the group velocity of the electron state in $Ga_{1-x}Al_xAs$ approaches zero linearly with $k_I^{\perp}$. To lowest order the group velocity of the transmitted stated near the Γ minimum in GaAs is constant. From Eq. (11a), we see that $B(k_I,k_0)$ increases linearly from zero as $k_I^{\perp}$ increases from zero. (Here we assume that $B(-k_0;-k_I)$ does not go to zero with $k_I^{\perp}$. There is no reason for this amplitude to vanish at $k_I^{\perp} = 0$ and our calculations indicate that it does not.) Thus, the transmission coefficient $T(k_I,k_0)$ increases from zero linearly with $k_I^{\perp}$. Likewise the transmission coefficient $T(-k_0,-k_I)$ increases linearly from zero with $k_I^{\perp}$, but in this case the amplitude is approximately constant and the $k_I^{\perp}$ dependence is from the group velocity of the transmitted state. Analogous arguments show that when a new reflection channel becomes possible, the reflection coefficient increases from zero linearly with $k^{\perp}$.

When more than one transmission channel is possible, the relative importance of the channels depends on the nature of the states. Consider, for example, an electron approaching the interface from the

$Ga_{1-x}Al_xAs$ side and located near the conduction band minimum at X (for the minimum which is normal to the interface). It can be transmitted into a Bloch state near the Γ conduction band minimum or the X conduction band relative minimum of GaAs. (Both minima are lower in energy than the X point in $Ga_{1-x}Al_xAs$). The states at the X point of GaAs are similar to those at the X point in the alloy and energies of the band minima at the X point are close. In this case, we find that the transmission into the state near the X point is much larger than that for the state near the Γ point.

Next, consider the x dependence of the transport coefficients. The alloy parameter x determines how different the material $Ga_{1-x}Al_xAs$ is from GaAs. The two materials are the same for x = 0 and become increasingly different as x increases. As the two materials are made increasingly different, the incoming carrier will experience in the interface region a correspondingly larger change in crystal potentials. This results in a larger probability for the incoming carrier to be reflected into one of the accessible reflection Bloch states. So, as x increases, for a fixed $\vec{k}_I$ the total probability for reflection will increase, with a corresponding decrease occurring for transmission. This is analogous to the 1-D potential step problem for a free particle, with increasing x corresponding to increasing the height of the potential step.

Finally, the number of atomic layers over which the interface is graded determines (for larger number of layers) how smoothly the

crystal potential changes from GaAs to $Ga_{1-x}Al_xAs$. Smoother transitions lead to less reflection for fixed incident states, so that for sufficiently many layers, increasing the layer number increases transmission.

V. NUMERICAL RESULTS

In this section, we present our numerical results for the transport coefficients. These coefficients were computed using Eq. (7). The total flux was conserved within the numerical precision of the calculation (about 1%) in all cases.

In Figs. (3) and (4) we present the transport coefficients for incoming $Ga_{1-x}Al_xAs$ conduction band states as a function of $\vec{k}_I^{\,|}$ and $x(k^{||}=0)$ for the (100) interface. In Fig. (3), the incoming state is near the X minimum which is normal to the interface and in Fig. (4) the incoming state is near the Γ minimum. For the range of x in Fig. (3), the $Ga_{1-x}Al_xAs$ conduction band minimum is at the X point, and for Fig. (4) it is at the Γ point. The curves in the central part of Fig. (3) are for reflection and transmission into states near the X minimum. Transmission into the Γ minimum of GaAs is shown in the inset of Fig. (3). As discussed in Sec. IV, the reflection coefficient goes to unity as the incident state wavevector approaches the band minimum. The transmission coefficients increase from zero linearly in wavevector near threshold. For fixed

Fig. 3. Transport coefficients as a function of incident wavevector normal to the interface for different alloy compositions. In our calculation the alloy is indirect for the range of compositions in the figure. The incident states are in the alloy near the X conduction band minimum along the Δ direction normal to the interface. The central portion of the figure shows the transport coefficients into states near the corresponding X minima. The inset shows the transmission coefficients into states near the Γ minimum of GaAs.

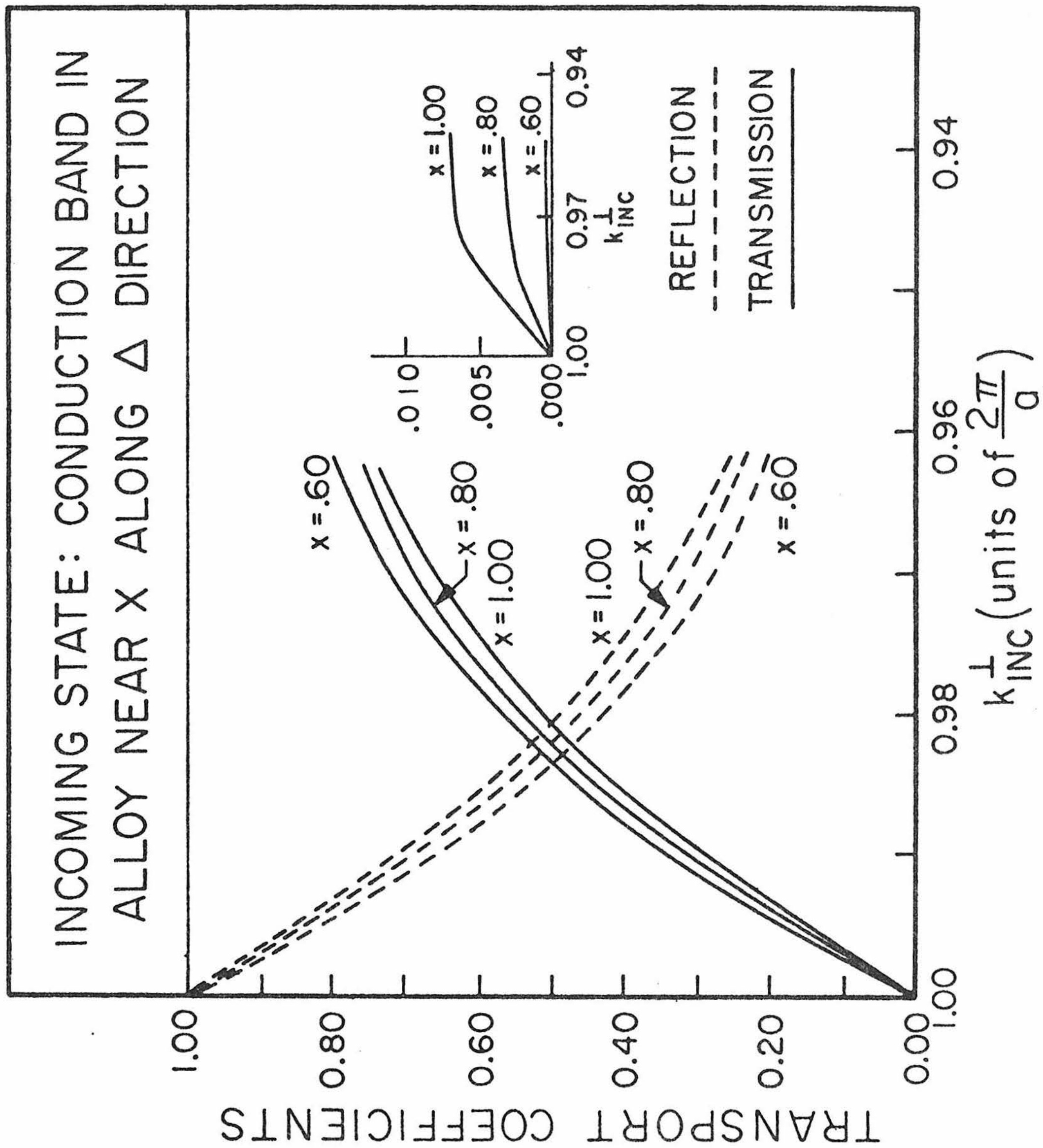
INCOMING STATE: CONDUCTION BAND IN
ALLOY NEAR X ALONG Δ DIRECTION
TRANSPORT COEFFICIENTS
1.00
0.80
0.60
0.40
0.20
0.00
1.00
0.98
0.96
0.94
$k^{\perp}_{INC}$ (units of $\frac{2\pi}{a}$)
x = .60
x = .80
x = 1.00
x = 1.00
x = .80
x = .60
.010
.005
.000
1.00
0.97
0.94
$k^{\perp}_{INC}$
x = 1.00
x = .80
x = .60
REFLECTION
TRANSMISSION

Fig. 4. Transport coefficients as a function of incident wave-vector normal to the interface for different alloy compositions. In our calculation the alloy is direct for the range of compositions in the figure. The incident states are in the alloy near the Γ conduction band minimum along the Δ direction normal to the interface.

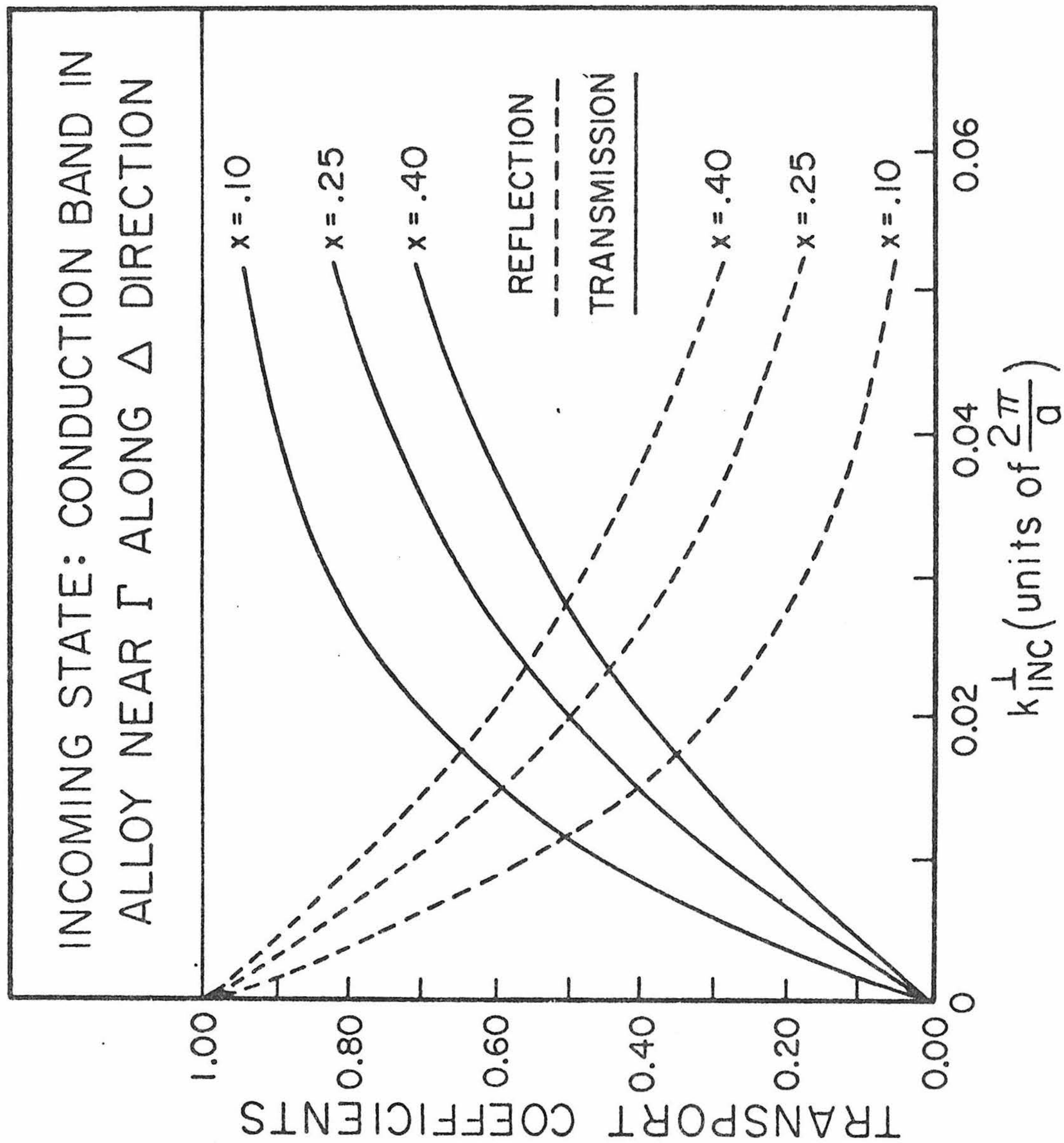

INCOMING STATE: CONDUCTION BAND IN
ALLOY NEAR Γ ALONG Δ DIRECTION
REFLECTION
TRANSMISSION
x = .10
x = .25
x = .40
x = .40
x = .25
x = .10
TRANSPORT COEFFICIENTS
0.00
0.20
0.40
0.60
0.80
1.00
0
0.02
0.04
0.06
$k^{\perp}_{INC}$ (units of $\frac{2\pi}{a}$)

wavevector, the transmission increases with decreasing AlAs concentration of the alloy. From Fig. (3), we see that transmission from the X valley of the alloy to the X valley of GaAs is much greater than the transmission from the X valley of the alloy to the Γ minimum of GaAs. Thus, from Eq. (11), we see that the transmission coefficient for incident electrons near the Γ minimum of GaAs with enough energy to transmit into the X valley in an indirect $Ga_{1-x}Al_xAs$ alloy will be small. Most likely electron transmission from GaAs into large x $Ga_{1-x}Al_xAs$ occurs via the X valley in GaAs.

In Fig. (5), we present the transport coefficients for an incoming $Ga_{1-x}Al_xAs$ conduction band state near an X minimum which is parallel to the interface as a function of $k_I^{\perp}$ and x with $k^{||} = \frac{2\pi}{a}$ (0,.95,0). The range of x is the same as Fig. (3). The curves in the central part of the figure are for transmission and reflection into the same valley as $\vec{k}_I$. When $k_I^{\perp}$ becomes large enough, new outgoing channels become accessible in which $\vec{k}_0$ lies outside of the zone. There are no equivalent states in the zone with the same $k^{||}$ as k_0 (i.e., $k_I^{||}$). When mapped back into the zone by a reciprocal lattice vector, these outgoing states have $\vec{k}^{||}$ lying near one of the zone edge faces rotated 90° from the zone edge face near the incident state (i.e., from the Y valley to the Z valley if the interface is in the Y-Z plane). The threshold for these outgoing channels is determined by E and $k^{||}$ conservation. This transmission threshold depends on the alloy composition because the energy separation of the

Fig. 5. Transport coefficients as a function of the incident wave-vector component normal to the interface for different alloy compositions. In our calculation, the alloy is indirect for the range of compositions in the figure. The incident states are in the alloy near the parallel X conduction band minimum. The states have fixed $k_{||}$ equal to $2\pi/a$ (0,.95,0). The central portion of the figure shows the transport coefficients into states near the corresponding X minima. For $k_{\perp INC}$ sufficiently large it becomes possible to transmit and reflect into states near the parallel X minima rotated 90° from the incident valley (see text). The inset shows the transmission coefficients into these states.

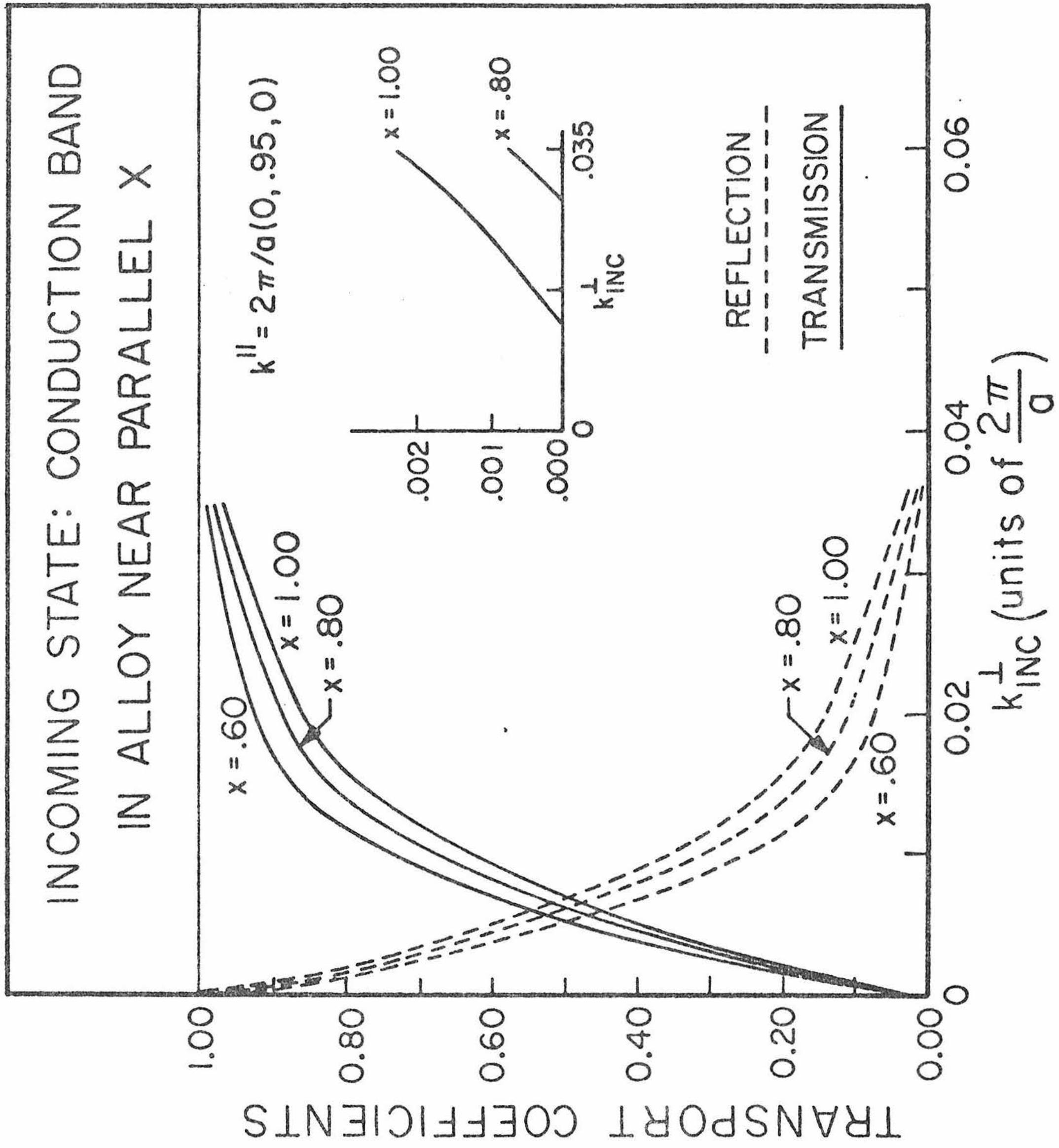
INCOMING STATE: CONDUCTION BAND
IN ALLOY NEAR PARALLEL X
$k^{\parallel} = 2\pi/a(0,.95,0)$
x = .60
x = 1.00
x = .80
x = 1.00
x = .80
x = .60
x = 1.00
x = .80
.002
.001
.000
0
.035
$k^{\perp}_{INC}$
REFLECTION
TRANSMISSION
TRANSPORT COEFFICIENTS
1.00
0.80
0.60
0.40
0.20
0.00
0
0.02
0.04
0.06
$k^{\perp}_{INC}$ (units of $\frac{2\pi}{a}$)

X points in the two materials depends on the alloy composition. The transmission coefficients for these states are shown in the inset of Fig. (5). Because these states are rather different in character than the incoming state, these transmission coefficients are quite small. The threshold for this reflection process occurs near $k_I^{\perp} = \frac{2\pi}{a}$ (0.05, 0,0) for $k_I^{||} = \frac{2\pi}{a}$ (0, .95,0). Near threshold, the reflection coefficients for this process are small and we do not display them here.

In Fig. (6), we show the dependence of the transport coefficients for incoming AlAs conduction band states near the X minimum normal to the interface on $\vec{k}_I^{||}$ for fixed k_I. Here $k_I^{\perp}$ is in a (100) direction (i.e., along V). The results show that the transmission increases as $\vec{k}_I^{||}$ increases, but the dependence of the transport coefficients on $\vec{k}_I^{||}$ is much weaker than on k_I. We have also calculated the transport coefficients as a function of $k_I^{||}$ for incoming states near the parallel X valley and the Γ valley. In these cases, the dependence on $\vec{k}_I^{||}$ was not as strong as for the case shown in Fig. (6). For the free particle problem, the transmission and reflection coefficients are independent of $k_I^{||}$!

In Figs. (7) and (8), we present the transport coefficients for incoming $Ga_{1-x}Al_xAs$ hole states near the Γ valence band maximum as a function of $k_I^{\perp}$ and x with $k_I^{||} = 0$. We note that a detailed treatment of the hole transport coefficients should include spin orbit splitting. However, the qualitative features of the dependence of

Fig. 6. Transport coefficients as a function of the incident wavevector component parallel to the interface. The incident states are in AlAs near the perpendicular X conduction band minimum. The states have fixed k_{INC} equal to $2\pi/a$ (.983,0,0). The parallel component of the incident wavevector is in the V direction.

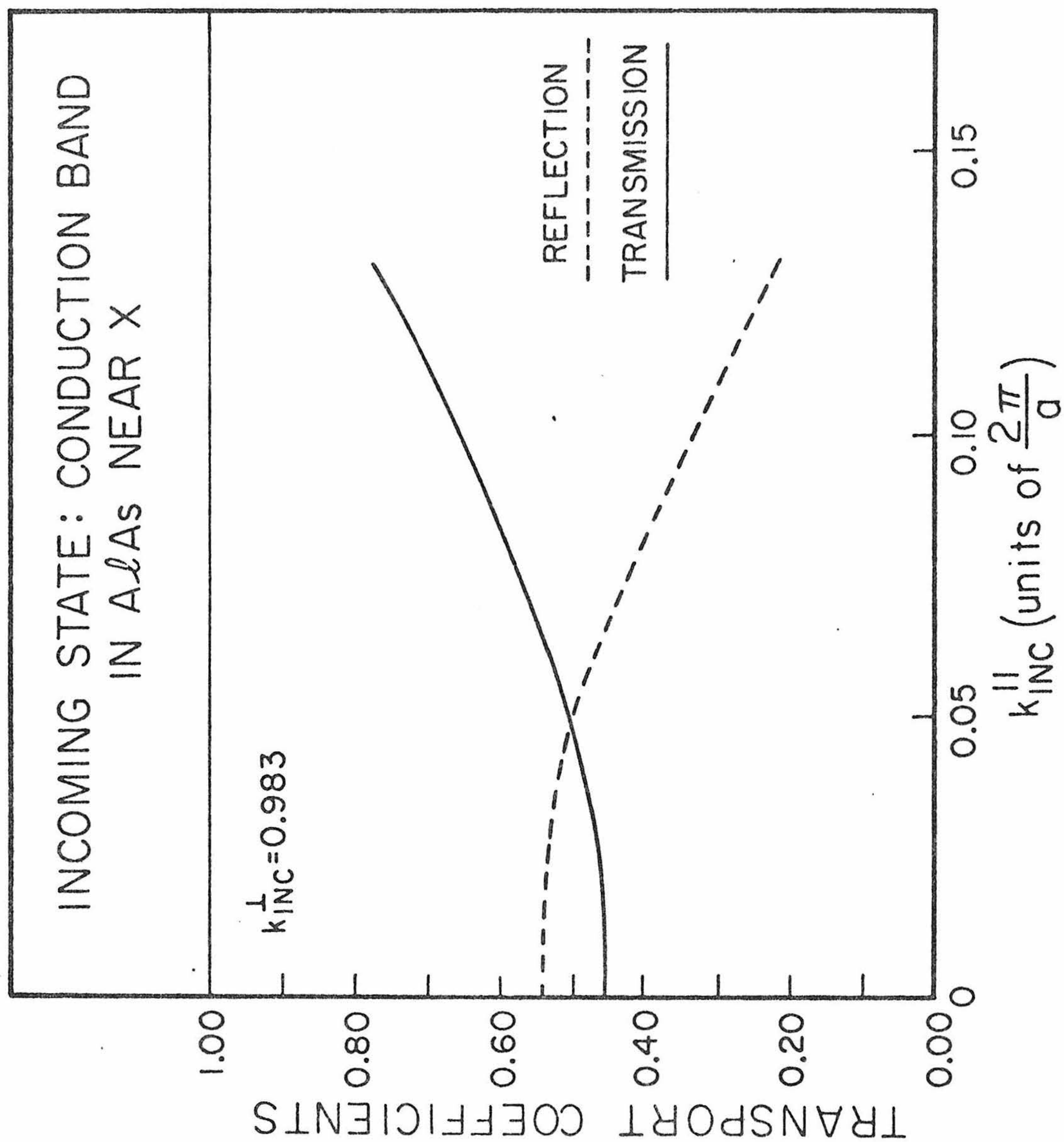
INCOMING STATE: CONDUCTION BAND
IN AℓAs NEAR X
$k^{\perp}_{INC}$=0.983
REFLECTION
TRANSMISSION
TRANSPORT COEFFICIENTS
1.00
0.80
0.60
0.40
0.20
0.00
0
0.05
0.10
0.15
$k^{\parallel}_{INC}$ (units of $\frac{2\pi}{a}$)

Fig. 7. Transport coefficients as a function of incident wave-vector normal to the interface for different alloy compositions. The incident states are in the alloy near the Γ valence band maxima along the Δ direction normal to the interface. All states involved have Δ_5 symmetry.

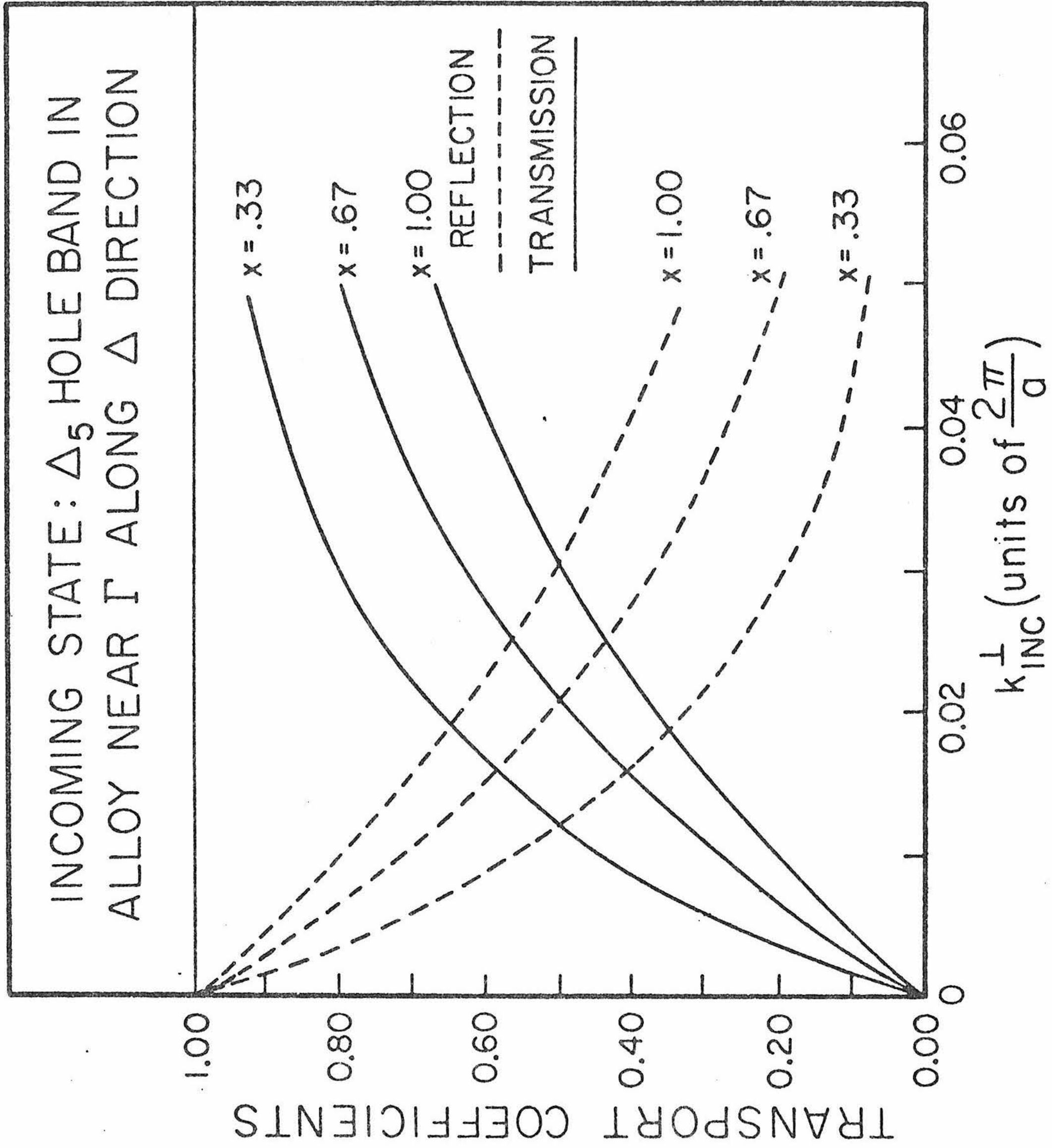

INCOMING STATE: Δ_5 HOLE BAND IN
ALLOY NEAR Γ ALONG Δ DIRECTION
x = .33
x = .67
x = 1.00
REFLECTION
TRANSMISSION
x = 1.00
x = .67
x = .33
TRANSPORT COEFFICIENTS
1.00
0.80
0.60
0.40
0.20
0.00
0
0.02
0.04
0.06
$k_{INC}^{\perp}$ (units of $\frac{2\pi}{a}$)

Fig. 8. Transport coefficients as a function of incident wave-vector normal to the interface for different alloy compositions. The incident states are in the alloy near the Γ valence band maxima along the Δ direction normal to the interface. All states involved have Δ_1 symmetry.

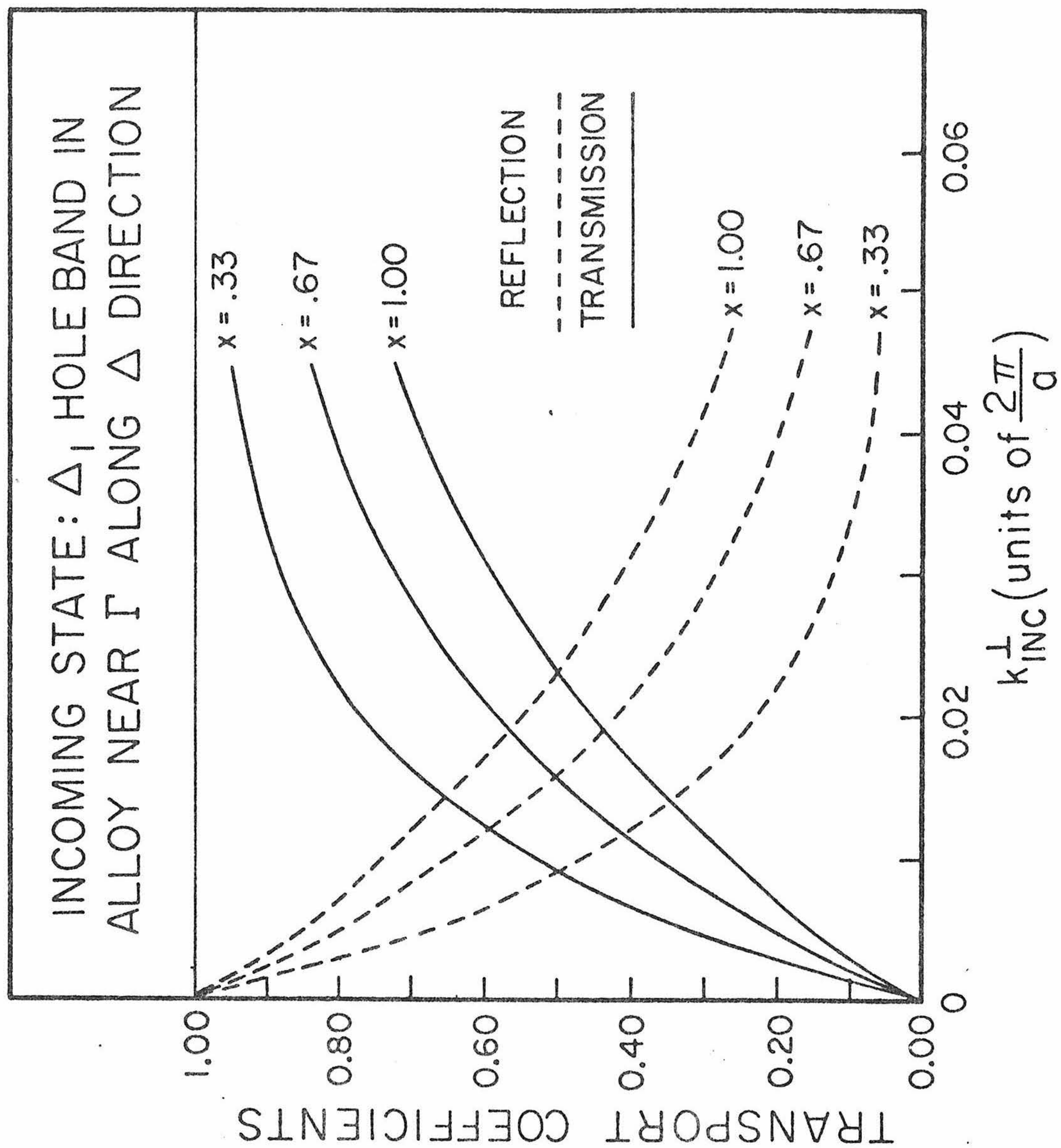
INCOMING STATE: Δ1 HOLE BAND IN
ALLOY NEAR Γ ALONG Δ DIRECTION
REFLECTION
TRANSMISSION
x = .33
x = .67
x = 1.00
x = 1.00
x = .67
x = .33
TRANSPORT COEFFICIENTS
1.00
0.80
0.60
0.40
0.20
0.00
0
0.02
0.04
0.06
k⊥INC (units of 2π/a)

the transport coefficients on $k_I^{\perp}$ and x will not be altered by the spin orbit interaction. In Fig. (7), we show the transport coefficients for the Δ_5 hole states and in Fig. (8) for the Δ_1 hole states. There is no coupling between the Δ_5 states and the Δ_1 states because of symmetry. The qualitative features of the transport coefficients are similar to that for electrons.

In Fig. (9), we present the transmission coefficients for incoming AlAs conduction band states near the X minimum as a function of $k_I^{\perp}$ ($k_I^{||}=0$) and the number of atomic planes in the graded interface. Results are presented for the cases of an abrupt interface and interfaces graded over 17 and 27 atomic planes. As the number of atomic planes in the graded region is increased, the transmission coefficients for a given incident state increase.

VI. SUMMARY AND CONCLUSIONS

We have computed quantum mechanical reflection and transmission coefficients for electrons and holes at abrupt and compositionally graded (100) GaAs-$Ga_{1-x}Al_xAs$ interfaces. To the best of our knowledge, this is the first calculation of these transport coefficients for abrupt and nearly abrupt interfaces between two semiconductors using a three-dimensional model. We have determined the threshold behavior of the transmission and reflection coefficients. We have found that transmission into states with qualitatively similar char-

Fig. 9. Transmission coefficients as a function of incident wavevector normal to the interface for abrupt and compositionally graded interfaces. The incident states are in AlAs near the X conduction band minimum along the Δ direction normal to the interface. The graded interface transmission coefficients are shown for interfaces graded over 17 and 27 atomic layers.

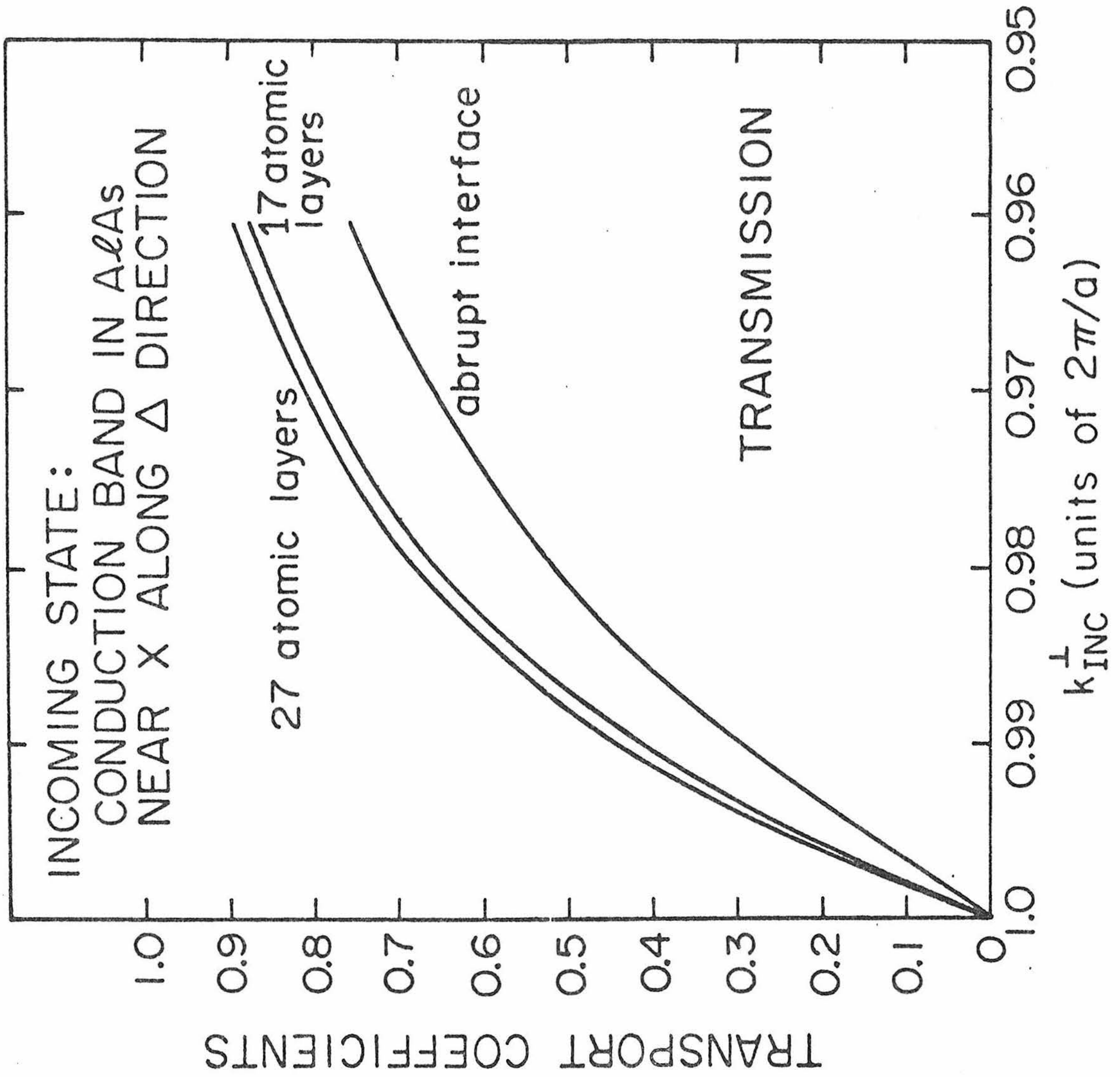

INCOMING STATE:
CONDUCTION BAND IN AℓAs
NEAR X ALONG Δ DIRECTION
27 atomic layers
17 atomic layers
abrupt interface
TRANSMISSION
TRANSPORT COEFFICIENTS
0
0.1
0.2
0.3
0.4
0.5
0.6
0.7
0.8
0.9
1.0
1.0
0.99
0.98
0.97
0.96
0.95
$k^{\perp}_{INC}$ (units of $2\pi/a$)

acter to the incident state is much greater than transmission into states of different character. In particular an electron near the perpendicular X valley in $Ga_{1-x}Al_xAs$ transmits into the perpendicular X valley of GaAs with much greater probability than it transmits into the Γ minimum of GaAs. For electrons in a particular valley, the transport coefficients have been found to depend less sensitively on $k_I^{||}$ than on $k_I^{\perp}$. Decreasing the alloy composition x and increasing the distance over which the interface is graded both increase the transmission coefficients of incident carriers.

APPENDIX: Reciprocity Theorem

In this appendix, we establish Eqs. (11) and (12). They are the analogue of the reciprocity theorem of scattering theory and are established in a similar way. Since we have been unable to find a demonstration of these results for this particular problem in the literature, we include a brief demonstration here.

Let ψ_L be a state specified by a Bloch state incident on the interface from the left. Far to the left of the interface (where the evanescent states have negligible amplitude), this state will consist of the incident state and one or more reflected Bloch states,

$$\psi_{L_{Z\to-\infty}} = \phi_{k_I^L} + \sum_i A(-k_i^L)\ \phi_{-k_i^L} \tag{A1}$$

Far to the right of the interface, it will consist of one (say) or more transmitted Bloch states

$$\psi_{L_{Z\to\infty}} \sum_j B(k_j^R)\ \phi_{k_j^R} \tag{A2}$$

Let ψ_R be a state specified by having $\phi_{-k_0^R}$ (the complex conjugate of one of the transmitted states in Eq. (A2)) approach the interface from the right. We have

$$\psi_{R_{Z\to\infty}} \phi_{-k_0^R} + \sum_i \alpha(k_i^R)\ \phi_{k_i^R} \tag{A3}$$

and

$$\psi_{R_{Z\to-\infty}} = \sum_j \beta(-k_j^L) \; \phi_{-k_j^L} \tag{A4}$$

The state $\phi^*_{k_I}$ will be included in the set $\{\phi_{-k_j^L}\}$.

Because ψ_L and ψ_R solve the same Schrodinger equation with the same energy, we have

$$0 = \psi_L \nabla^2 \psi_R - \psi_R \nabla^2 \psi_L \tag{A5}$$

Integrate Eq. (A5) over a rectangular volume which contains the interface (X-Y plane), extends to infinity in the X and Y directions, and extends far enough in the Z direction that the amplitudes of the evanescent states at the surface of the volume (X-Y planes) in the bulk of the two materials is negligible Green's theorem then gives

$$\begin{aligned} 0 = &\int dx\, dy\, \left(\psi_L \frac{\partial}{\partial Z} \psi_R - \psi_R \frac{\partial}{\partial Z} \psi_L\right)\Big|_Z \\ &- \int dx\, dy\, \left(\psi_L \frac{\partial}{\partial Z} \psi_R - \psi_R \frac{\partial}{\partial Z} \psi_L\right)\Big|_{-Z} \end{aligned} \tag{A6}$$

Substituting the asymptotic forms for the wavefunctions and integrating Eq. (A6) over Z gives

$$B(k_0^R)\ \Big(-2i\ k_0^{\perp R} + \big(\langle u_{k_0^R}|\tfrac{\partial}{\partial Z}|u_{k_0^R}\rangle^*$$

$$- \langle u_{k_0^R}|\tfrac{\partial}{\partial Z}|u_{k_0^R}\rangle\big)\Big) \tag{A7}$$

$$= \beta(-k_I^L)(-2ik_I^{\perp L} + (\langle u_{k_I^L}|\tfrac{\partial}{\partial Z}|u_{k_I^L}\rangle)^*$$

$$- \langle u_{k_I^L}|\tfrac{\partial}{\partial Z}|u_{k_I^L}\rangle))$$

where u_k is the periodic part of the Bloch function ϕ_k. Since,

$$\frac{\partial \varepsilon}{\partial \vec{k}} = \frac{h^2}{2m}(2\vec{k} + 2\langle u_k|-i\nabla|u_k\rangle) \tag{A8}$$

and $\langle u_k|-i\nabla|u_k\rangle$ is real, Eq. (A7) is the same as Eq. (11).

One can establish Eq. (12) in the same way as above; simply replace ψ_R with the state specified by having $\phi^*_{-k_0^L}$ (the complex conjugate of one of the reflected Bloch states in Eq. (A1)) approach the interface from the left.

REFERENCES

1. R. Dingle, W. Weigmann, and C. H. Henry, Phys. Rev. Lett. 33, 827 (1974).
2. R. L. Anderson, Solid State Electron. 5, 341 (1962).
3. P. J. Ben Daniel and C. B. Duke, Phys. Rev. 152, 683 (1966).
4. L. Leibler, Phys. Rev. B12, 4443 (1975).
5. P. J. Price, in Proceedings of the International Conference on the Physics of Semiconductors, Exeter, 1962, edited by A. C. Stickland, (The Institute of Physics and the Physical Society, London) p. 99.
6. V. Heine, Proc. Phys. Soc. 81, 300 (1963).
7. E. I. Blount, Solid State Phys. 13, 305 (1962).
8. J. N. Schulman and T. C. McGill, Phys. Rev. Lett. 39, 1680 (1977).
9. W. E. Pickett, S. G. Louie and M. L. Cohen, Phys. Rev. B17, 815 (1978).
10. After the band offsets have been included, the X conduction band minimum in GaAs is slightly lower in energy than the X conduction band minimum in AlAs.
11. J. C. Slater and G. F. Koster, Phys. Rev. 94, 1498 (1954).
12. J. R. Chelikowsky and M. L. Cohen, Phys. Rev. B14, 556 (1976).
13. F. Hess, I. Topol, K. R. Schulze, H. Newmann, and K. Unger, Phys. Stat. Sol. (b) 55, 187 (1973).
14. It is necessary to include all 16 Bloch and evanescent states in the calculation in order to have a well defined algebraic problem. However, we find that evanescent states with large values of

$Im(k^{\perp})$ make a small contribution to the atomic amplitudes.

CHAPTER 5

I. INTRODUCTION

Impact ionization is the process in which a free carrier in a state of high energy relaxes to a state of lower energy in the same band by producing an electron hole pair. This process is the inverse of a free carrier Auger decay [1-3], and so requires conservation of total wavevector. In bulk materials this process has often been studied because it usually leads to avalanche breakdown of reverse biased diodes [3]. Impact ionization can also be an important process in heterojunction systems [4]. For heterojunctions made of a large gap material (with conduction band minimum E_{c_1}) and a small gap material (with conduction band minimum E_{c_2} and band gap E_{g_2}), and if $E_{c_1} \geq E_{c_2} + E_{g_2}$, all electrons near the conduction band minimum E_{c_1} in the large gap material have enough energy to excite an electron hole pair in the smaller gap material. An example of such a heterojunction system is the CdTe-HgCdTe interface. CdTe and HgCdTe have the same lattice structure and a mismatch in lattice constants that is less than .3%. The CdTe material has a band gap of 1.5 eV and the HgCdTe alloy has a band gap that can be varied from 1.5 eV to 0 eV by increasing the HgTe content. From the common anion rule [5], the difference in band gaps of the two materials is expected to appear primarily as a conduction band offset. Thus, for HgCdTe alloy compositions such that the alloy band gap is less than half of the CdTe gap, all the CdTe electrons in the conduction band have enough energy to impact ionize an electron

hole pair in the alloy. In heterojunction systems k is not conserved in the direction normal to the interface, so that the wavevector conservation condition required for impact ionization in bulk is relaxed in this case. Consequently, impact ionization can occur in the heterojunction system in two ways: the electron can cross the interface and undergo essentially bulk impact ionization in the small gap material; the electron can impact ionize at the interface. In this chapter we present a theoretical study of impact ionization in heterojunction systems. We have concentrated on the case of impact ionization by electrons as they cross the interface, because this process has not been previously studied..

II. THEORETICAL CALCULATION

In a bulk semiconductor crystal, the Hartree Fock wavefunction for a conduction electron is represented by a Slater determinant with all the one electron valence band orbitals occupied and an additional one electron conduction band orbital labelled by $\hbar k$, σ, and E. The one electron valence and conduction band states are the familiar Bloch states. In the interface system, the Hartree Fock wavefunction for a conduction electron is also represented by a Slater determinant with the valence states occupied and an additional one electron conduction state labelled by $\hbar k_{INCIDENT}$, σ, and E. As discussed in Chapter 4, in the interface system the one electron states are made up of incident and reflection Bloch states on one side of the inter-

face, transmission Bloch states (if they exist) on the other side of the interface, and exponentially decaying evanescent states on both sides of the interface. The interface wavefunction for a hole consists of a Slater determinant that is missing an interface valence band state.

The initial state of the impact ionization process is

$$|I\rangle = \Psi(k_{e_o}, \sigma_o) \qquad (1)$$

where Ψ is a Slater determinant of interface wavefunctions with an additional electron state representing an electron incident on the interface from the large gap material with incident wavevector k_{e_o} and spin σ_o. The final state is

$$|F\rangle = \Psi(k_e, \sigma_e; k_e' \sigma_e'; k_h, m) \qquad (2)$$

where Ψ is a Slater determinant of interface wavefunctions with: an absent valence state representing a hole confined in the small gap material labelled by the wavevector k_h and the spin m of one of its Bloch states; an additional pair of electron states (not necessarily both confined in the small gap material) labelled by the wavevectors k_e and k_e' and the spins σ_e and σ_e' of Bloch states of each in the small gap material. The interaction that produces impact ionization is the carrier-carrier Coulomb interaction [1,2]. The first order impact ionization transition rate is given by

$$\frac{1}{\tau} = \frac{2\pi}{\hbar} \sum_{\substack{\text{ave I;}\\ F}} \left|\langle F|\frac{e^2}{\varepsilon_0|r-r'|}|I\rangle\right|^2 \delta(E_I-E_F) \tag{3}$$

The matrix element is

$$\langle F|\frac{e^2}{\varepsilon_0|\vec{r}-\vec{r}'|}|I\rangle = \langle\phi^I_{k_e\sigma_e}(\bar{r})\ \phi^I_{k'_e\sigma'_e}(\bar{r}')|\frac{e^2}{\varepsilon_0|\vec{r}-\vec{r}'|}|\phi^I_{k_h m}(\vec{r})\ \phi^I_{k_{e_0}\sigma_0}(\vec{r}')\rangle$$

$$-\text{ exchange term} \tag{4}$$

where the ϕ^I_k are the one electron interface eigenfunctions. The ϕ^I_k have the form presented in Chapter 4

$$\phi^I_{k\sigma}(r) = \begin{cases} \dfrac{D_k}{\sqrt{V}}\left[\phi^\alpha_{k\sigma} + \sum_i A_{k_i}\ \phi^\alpha_{k_i\sigma}\right] & \text{side } \alpha \\ \dfrac{D_k}{\sqrt{V}}\sum_j B_{k_j}\ \phi^\beta_{k_j\sigma} & \text{side } \beta \end{cases} \tag{5}$$

where V is the volume of the crystal, ϕ_k is the incident Bloch state on side α, the ϕ^α are the reflection Bloch orevanescent states on side α, the ϕ^β are the transmission Bloch or evanescent states on side β, the A and B are expansion coefficients, and D_k is the normalization constant. The normalization constant is

$$D_k = \left[\frac{1}{2}(1 + \sum_i|A_{k_i}|^2 + \sum_j|B_{k_j}|^2)\right]^{-1/2} \tag{6}$$

where the summations are over Bloch coefficients only. The direct term in Eq. 4 can be expressed as [6]

$$4\pi\frac{e^2}{\varepsilon_o}\int\frac{d^3k}{k^2}\left[\int d^3r\phi^{I*}_{k_e\sigma_e}(\vec{r})\phi^{I}_{k_h m}(\vec{r})e^{i\kappa\cdot\vec{r}}\right]\left[\int d^3r'\phi^{I*}_{k'_e\sigma'_e}(\vec{r})\phi^{I}_{k_{e_o}\sigma_o}(\vec{r})e^{-i\kappa\cdot\vec{r}'}\right] \tag{7}$$

The $\phi^{I*}\phi^{I}$ can be expressed in the form

$$\phi^{I*}_{k\sigma}(r)\phi^{I}_{k'\sigma'}(r) = \frac{1}{V}\sum_G\sum_i\sum_j\sum_{q=1}^{2} C^{*}_{k_iq}C_{k'_jq}U_{k_i\sigma;k'_j\sigma'}(G)e^{-i(\kappa^{*}_i-\kappa'_j-\vec{G})\cdot\vec{r}} \times\theta((-1)^{q+1}r^{\perp}) \tag{8}$$

where V is the volume of the solid, G is a reciprocal lattice vector, the indice i(j) runs over the various Bloch and evanescent states in the total interface wavefunction labelled by the incident wavevector k(k'), the index q labels side 1 and side 2 of the heterojunction and

$$C_{k_i1} \equiv A_{k_i}D_{k_j};C_{k_i2} \equiv B_{k_i}D_k \tag{9}$$

$$U_{k_i\sigma;k'_j\sigma'}(G) \equiv \int d^3r\ e^{i(\kappa^{*}_i-\kappa_j-\vec{G})\cdot\vec{r}}\phi^{1(2)*}_{k_i\sigma}(r)\phi^{1(2)}_{k'_j\sigma'}(r) \tag{10}$$

$$\theta(\pm r^{\perp}) = \begin{cases} 1 & \text{if} \quad \pm r^{\perp} \geq 0 \\ 0 & \quad\quad \pm r^{\perp} < 0 \end{cases} \tag{11}$$

Substitution of Eq. 8 into Eq. 7 produces the result

$$\langle direct \rangle = \frac{1}{V} \sum_{\vec{G}\vec{G}'} \sum_{qq'=1}^{2} \sum_{ijmn} M^{BB}_{qq'ijmn}(G,G')\,\delta_K(\bar{k}_{ei}+\bar{k}'_{em}-k_{n_j}-\bar{k}_{eon}-\vec{G}-\vec{G}')$$

$$+ \frac{1}{V^{4/3}} \sum_{\vec{G}\vec{G}'} \sum_{qq'=1} \sum_{ijmn} \left[M^{BE}_{qq'ijmn}(G,G') + M^{EE}_{qq'ijmn}(G,G') \right] \qquad (12)$$

$$\delta_K(\bar{k}^{||}_{ei}+\bar{k}'^{||}_{em}-\bar{k}^{||}_{n_j}-\bar{k}^{||}_{eon}-\vec{G}^{||}-\vec{G}'^{||})$$

where δ_k is the Kronecker delta and

$$M^{BB}_{qq'ijmn}(G,G') \equiv \left(\frac{4\pi e^2}{\varepsilon_o}\right)(2\pi)^3 \frac{S^{BB}_{ijq}(\vec{G})\; T^{BB}_{mnq'}(\vec{G}')}{|\bar{k}_{e_i}-\bar{k}_{h_j}-G|^2} \qquad (13a)$$

$$M^{BE}_{qq'ijmn}(G,G') \equiv \left(\frac{4\pi e^2}{\varepsilon_o}\right)(2\pi)^3(-i) \left[\frac{S^{BE}_{ijq}(\vec{G})\; T^{BB}_{mnq'}(\vec{G}')}{|\bar{k}'_{em}-\bar{k}_{eon}-G'|^2 (k^{\perp *}_{e_i}+k^{\perp *}_{em}-k^{\perp}_{h_j}-k^{\perp}_{eon}-G^{\perp}-G'^{\perp})} \right.$$

$$\left. + \frac{S^{BB}_{ijq}(\vec{G})\; T^{BE}_{mnq'}(\vec{G}')}{|\bar{k}_{ei}-\bar{k}_{hj}-\vec{G}|^2 (k^{\perp}_{ei}-k^{\perp}_{em}\,k^{\perp}_{hj}-k^{\perp}_{eon}-G^{\perp}-G'^{\perp})} \right] \qquad (13b)$$

$$M^{FE}_{qq'ijmn}(G,G') \equiv \left(\frac{4\pi e^2}{\varepsilon_o}\right)(2\pi)^3(i)\; S^{BE}_{ijq}(\vec{G})\; T^{BE}_{mnq'}(\vec{G}') \quad .$$

$$\left[\frac{1}{\left[|k_{ei}^{||}-k_{hj}^{||}|^2 + (k_{eon}^{\perp}-k_{em}^{'\perp *})^2\right](k_{ei}^{\perp *}-k_{em}^{'\perp *}-k_{hj}-k_{eon}^{\perp})} + \right.$$

$$\left.\frac{(-i)}{2|k_{ei}^{||}-k_{hj}^{||}|(k_{ei}^{\perp *}-k_{hj}^{\perp}-i|k_{ei}^{||}-k_{hj}^{||}|)(k_{ej}^{'\perp *}-k_{eon}^{\perp}+i|k_{ei}^{||}-k_{hj}^{||}|)}\right] \qquad (13c)$$

The quantities $k^{||}$ and $k^{\perp}$ refer to the components of k parallel and normal to the interface, respectively, and

$$S_{ijq}(\vec{G}) \equiv C^*_{k_{e_i}q}\, C_{k_{hj}\,q}\, U_{k_{ei}\sigma_e;k_{hj}\,\sigma_o}(\vec{G}) \qquad (14a)$$

$$T_{mnq'}(\vec{G}') \equiv C^*_{k'_{em}q'}\, C_{k_{eon}q'}\, U_{k'_{em}\sigma'_e;k_{eon}\sigma_o}(\vec{G}') \quad . \qquad (14b)$$

The superscripts BB and BE for S_{ijq} and $T_{mnq'}$ refer to the following two cases: for BB, both states in the overlap integral U in Eqs. 14 are Bloch states; for BE, one or both states in the overlap U in Eqs. 14 are evanescent states. The exchange term corresponding to the direct term in Eq. 12 is obtained by exchanging $k_{e_i\sigma_e}$ and $k'_{e_j\sigma_e}$ in Eq. 7.

For a given incident state, the impact ionization rate is

$$\frac{1}{\tau_{INC}} = \left[\frac{2\pi}{\hbar} \int d^3k_e' \int d^3k_h \sum_{spin} \sum_{\substack{GG' \\ HH'}} \sum_{\substack{qq'=1 \\ pp'=1}}^{2} \sum_{\substack{ijmn \\ \alpha\beta\gamma\delta}} (M^{BB}_{qq'ijmn}(G,G')\text{-exchange})^* \cdot \right.$$

$$(M^{BB}_{pp'\alpha\beta\gamma\delta}(H,H')\text{-exchange})\,\delta_D(\kappa_{ei}+\kappa'_{em}-\kappa_{nj}-\kappa_{eon})\,\delta_K(\kappa_{e\alpha}+\kappa'_{e\gamma}-\kappa_{h\beta}-\kappa_{eo\delta})$$

$$\left. \delta_D(E_I-E_F) \right]$$

$$+ \frac{1}{\ell\perp} \left[\int d^3k_e \int d^3k_e' \int d^3k_n \sum_{spin} \sum_{\substack{GG' \\ HH'}} \sum_{\substack{qq'=1 \\ pp'=1}}^{2} \sum_{\substack{ijmn \\ \alpha\beta\gamma\delta}} (M^{BE}_{qq'ijmn}(G,G')+M^{EE}_{qq'ijmn}(G,G') \right.$$

$$\text{-exchange})^* \cdot$$

$$(M^{BE}_{pp'\alpha\beta\gamma\delta}(H,H')+M^{EE}_{pp'\alpha\beta\gamma\delta}(H,H')\text{-exchange})\;\delta_D(\kappa^{||}_{ei}+\kappa'^{||}_{em}-\kappa^{||}_{nj}-\kappa^{||}_{eon}) \cdot$$

$$\left. \delta_k(\kappa^{||}_{e\alpha}+\kappa'^{||}_{e\gamma}-\kappa^{||}_{h\beta}-\kappa^{||}_{eo\delta})\;\delta_D(E_I-E_F) \right] \qquad (15)$$

where $\delta_D(k)$ is the Dirac delta function, $\delta_k(k)$ is the Kronecker delta, $\ell\perp$ is the length of the crystal in the direction normal to the interface, $\{G,G',H,H'\}$ are reciprocal lattice vectors, $\{q,q',p,p'\}$ label sides one and two, and $\{i,j,m,n,\alpha,\beta,\gamma,\delta\}$ label the various Bloch

and evanescent states. The first set of terms in brackets in Eq. 15 is analogous to the usual impact ionization rate for bulk materials. The terms in the second set of brackets are due to impact ionization of carriers at the interface. Because the second set of terms is multiplied by $1/\ell^{\perp}$, it does not affect the impact ionization rate in the bulk of the small gap semiconductor. However, this part does produce a finite probability that an electron crossing the interface will impact ionize. The result of Eq. (15) can be represented by

$$\frac{1}{\tau_{INC}} = \frac{1}{\tau_{BULK}} + \frac{v_{interface}}{\ell_z} \tag{16}$$

The probability that an electron impact ionizes at the interface is

$$P = \frac{\text{No.of carriers that impact ionize at interface/(unit area-unit time)}}{\text{Incident flux of carriers}}$$

$$= \frac{\frac{N_{INC}}{A}\ \frac{v_{interface}}{\ell_z}}{\frac{N_{INC}}{(A\ell_z)}\ \frac{|\nabla_{k^{\perp}}\epsilon_{INC}(k)|}{\hbar}}$$

$$= \frac{hv_{interface}}{|\nabla_{k^{\perp}}\epsilon_{INC}(k)|} \tag{17}$$

where N_{INC}/A is the number of incident carriers incident per unit area on the interface, and $|\nabla_{k\perp}\varepsilon_{INC}(k)|$ is the group velocity of the incident carrier Bloch state.

III. QUALITATIVE DEPENDENCES

The bulk type contribution to the impact ionization process in the heterojunction system consists of sums over rates for each set of possible Bloch functions in the small gap semiconductor to undergo the usual bulk impact ionization, with each rate multiplied by the amplitudes for the carriers to be in the various Bloch states. This has the following physical interpretation: away from the interface, the only effect on the carriers in the small gap material by the interface is the possibility for the carriers to have amplitudes to be in various Bloch states with different $k^{\perp}$ (but the same $k^{||}$ and E). For each set of initial and final Bloch states, impact ionization in the semi-infinite small gap material occurs as if the interface is not present with an amplitude given by the product of the amplitudes that the carriers are in the particular set of states.

However, near the interface the carrier wavefunctions are modified by the presence of the decaying evanescent states. Their contribution produces a finite probability that electrons will impact ionize at the interface. In order to extract the general qualitative bahavior of this probability, we ignore all but the dominant terms in the expression for $v_{interface}$ given in Eq. (13). In order to

identify these terms, we make use of the following properties of the evanescent states obtained from the work in Chapter 4 and reference (7): (1) For interface eigenfunctions with E and $k^{||}$ such that Bloch states on both sides of the interface are accessible, the amplitudes of all evanescent states are small and the decay lengths of these evanescent states are quite short; (2) For interface eigenfunctions with Bloch states on the small gap side only, there will be one evanescent state on the large gap side with a large amplitude and a large decay length, and the others have small amplitudes and small decay lengths. As discussed in Chapter 4, the decay length of the large amplitude evanescent state gets larger as the energy of the state approaches the critical point where the evanescent state energy connects to the real k band structure. For the electron states, this critical point will be the conduction band minimum of the incident electron band; for hole states, this critical point will be the valence band maximum. The important terms will therefore be those involving: the incident and reflected electron Bloch states on the large gap side and the large amplitude evanescent states on the large gap side for the final state carriers; the incident and reflected electron Bloch states on the large gap side, a large amplitude electron evanescent final state on the large gap side, and the Bloch electron and hole states in the small gap side; the transmitted initial electron Bloch state and one of the final electron Bloch states in the small gap side, and the large amplitude electron and

hole evanescent states in the large gap side.

For all of the three important groups of terms described above, as the component of incident electron wavevector normal to the interface ($k_o^{\perp}$) approaches the conduction band minimum the contribution of each group of terms to $v_{interface}$ in Eq. 16 goes to zero as $(k_o^{\perp})^2$. Since the group velocity in Eq. 17 goes to zero at the conduction band minimum as $k_o^{\perp}$, the interface impact ionization probability for small $k_o^{\perp}$ is

$$P = \Lambda_o k_o^{\perp} \int d^3k_e \int d^3k_e' \int d^3k_n \; \delta(k_e^{||} + k_e'^{||} - k_n^{||} - k_o^{||}) \; \delta(E_I - E_F) \qquad (18a)$$

where

$$\Lambda_o = \frac{2\pi m_{e_1}^*}{\hbar^2} \left. \frac{d^2 \overline{|\Sigma M|^2}}{dk_o^{\perp 2}} \right|_{k_o^{\perp}=0} \qquad (18b)$$

The quantity $\overline{|\Sigma M|}^2$ is an average squared sum of the important matrix element contributions and $m_{e_i}^*$ is the incident electron effective mass. By restricting $k_o^{||}$ to be zero and assuming all bands are parabolic, the density of states integrals in Eq. 18a produce the simple result

$$P = \Lambda_1 k_o^{\perp} \left[\frac{\hbar^2 k_o^{\perp 2}}{2m_{e_i}^*} + E_{c_1} - E_{c_2} - E_{g_2} \right]^{5/2} \qquad (19a)$$

where

$$\Lambda_1 \equiv \Lambda_o \frac{\pi^3(2m_h^*)^{5/2} m_{e_2}^{*\,3}}{15\hbar^7(m_{e_2}^* + m_h^*)^2} \qquad (19b)$$

and m_n^* and $m_{e_2}^*$ are the hole and electron effective masses, respectively in the small gap material. There are a number of simple qualitative dependences that can be obtained from Eqs. 19 by taking the average squared matrix element in Eq. 18b to be a relatively slowly varying function of the conduction band offset $E_{c_1}-E_{c_2}$ and E_{g_2}

For a particular heterojunction system, so that the conduction band offset and E_{g_2} are fixed, the interface impact ionization probability is larger for incident electron states with the larger normal component of incident electron wavevector $k_o^{\perp}$. For an incident electron state with fixed $k_o^{\perp}$, the impact ionization probability is larger for heterojunctions with: large conduction band offsets for fixed E_{g_2}; small E_{g_2} for fixed conduction band offsets. For fixed incident electron energy (with $k_o^{||} = 0$), the impact ionization probability is larger for heterojunctions with: small conduction band offsets for fixed E_{g_2} and fixed or decreasing E_{c_2}; small E_{g_2} for fixed conduction band offsets and fixed or decreasing E_{c_2}. Finally, we note that in the bulk impact ionization process an incident carrier with exactly enough energy to create an electron hole pair cannot do so because the k conservation requirement cannot

be satisfied. This leads to an additional energy threshold above $E = E_{c_2} + E_{g_2}$ that the incident carrier must be above before bulk impact ionization can occur. For the case we are considering, $k^{\perp}$ conservation is not required, and $k^{||}$ conservation can be satisfied for carriers with $E = E_{c_2} + E_{g_2}$. Thus, for carrier impact ionization at an interface there is no additional energy threshold as there is in the bulk process.

IV. SUMMARY AND CONCLUSIONS

We have presented a theoretical study of impact ionization of carriers in heterojunction systems. We find that there are two mechanisms for carrier impact ionization in these systems: bulk type impact ionization occurring in the bulk of the semi-infinite small gap material; impact ionization by carriers at the interface. The second mechanism has not been suggested previously in the literature to the author's knowledge. We have presented detailed first order expressions for the bulk type impact ionization rates in heterojunctions and the probability of impact ionization at the interface. The qualitative dependences of the second process on $k^{\perp}_{INC}$, the conduction band offset, and E_{g_2} for small $k^{||}_{INC}$ have been determined. Finally we note that higher order contributions to the interface impact ionization probability can be computed. These contributions correspond to the impact ionization at the interface of more than one electron hole pair.

1. P. T. Landsberg, Phys. Status Solidi 41, 457 (1970).
2. P. T. Landsberg and M. J. Adams, J. Lumin. 7, 3 (1973).
3. See, for example, C. Todd, Zener and Avalanche Diodes (Wiley-Interscience, 1970).
4. A. G. Milnes and D. L. Feucht, Heterojunctions and Metal Semiconductor Junctions (Academic Press, New York, 1972).
5. J. O. McCaldin, T. C. McGill, and C. A.Mead, J. Vac. Sci. Tech. 13, 802 (1976).
6. We take the two semiconductors to have the same dielectric constant.
7. V. Heine, Proc. Phys. Soc. 81, 300 (1963).